Two - Particle Dispersion Models for Turbulent Flows

by

Damien Alix Albert Benveniste

A dissertation submitted to The Johns Hopkins University
in conformity with the requirements for the degree of
Doctor of Philosophy

Baltimore, Maryland
July, 2014

Abstract

This dissertation focuses on the behavior of $\langle |\mathbf{r}|^2 \rangle$ in a turbulent flow, where $\mathbf{r} = \mathbf{x}_1 - \mathbf{x}_2$ is the separation distance between particle pairs. There are three main contributions of this thesis:

- We developed a new formalism for the study of backward dispersion for both deterministic and stochastic tracers. We performed a systematic numerical study of deterministic tracers and investigated small and long time scaling laws, revealing a small time t^4 scaling and verifying the t^3 behavior at long time. This t^4 is a higher order term expansion of the dispersion after the ballistic t^2 and a short time t^3 term. We have also shown analytically how the Batchelor range persists for all times. For the stochastic tracers, we analytically computed an exact t^3 term in the separation using Ito calculus. We have shown numerically that this term is dominant at long times and that it seems to correspond to the asymptotic behavior of the deterministic tracers. These tracers are the mass-less inertia free particles following the velocity field lines.

- We solved the "inverse problem" for fluid particle pair statistics by showing that the time evolution of the probability distribution of pair separations is the exact solution of a diffusion equation with suitable diffusivity.

The "inverse problem" refers to this general framework that is used to convert observed measurements into information about a physical object or system. In contrast to common assumptions, we have shown that short time correlation is not a necessary condition for the system to be described by a diffusion equation. We have shown the assumptions necessary to arrive to the Kraichnan and Lundgren diffusion model and have studied numerically what these assumptions imply.

- We developed an analytical model for Gaussian random fields in an effort to compare it with kinematic simulation models. We have shown that our model has a very rich physics and agrees with much of the kinematic simulation physics at low Reynolds number. Unlike kinematic simulations, within our model, we can drive the system to very high Reynolds numbers and observe the asymptotic behaviors. The insights provided by our model and its asymptotic behavior can yield further arguments in the debate on the actual behavior of the kinematic simulations.

Acknowledgements

This Ph.D. has been a tumultuous ride and nothing would have been possible without the guidance of my adviser, Greg L. Eyink. This is for me the opportunity to sincerely express the intense gratitude I owe this man. I have a profound respect for Greg as a person and a scientist and it has been a honor for me to work with him. I consider Greg to be one of the smartest person I have ever encountered. I thank you professor for taking me into your research group and for giving me the opportunity to become a physicist regardless how difficult as a person I may be!

I would like to thank all the members of my research group with who it has been a pleasure to go through this adventure: Theodore D. Drivas, Yi-Kang Shi and Cristian C. Lalescu. We have had rich interactions and we even had the chance with Theodore to publish an article together.

This Ph.D. could not have been achieved without the Johns Hopkins Turbulence Database effort on which most of this work is based. This is the opportunity to thank all of the actors who participated to its creation.

I am also grateful for the guidance provided by N. Peter Armitage and Oleg Tchernyshyov when I was working with them. They truly helped me improved my understanding of physics in general and they allowed me to trace my own path as a physicist.

I would like to thank Claudia M. Ojeda Aristizabal, my fiance and talented condensed matter physicist who supported me all along this Ph.D. She has been with me in the difficult moments and helped me go through all of them.

I would like to thank the incredible support given by all the members of the physics department, including the high quality education provided by the professors, the high efficiency of the staff members and the warm comradeship of the other Ph.D. students. This is a chance for me to acknowledge Carmelita D. King as one of the most important person in this physics department for us graduate students. I want also to thank one other strong man that honored me with one the highest quality courses I have had the chance to take: Prof. Zlatko Tesanovic.

Finally I want to thank the members of my thesis committee who gave me the honor to acknowledge my work as been worthy of a Ph.D. level: Professor Gregory Eyink (my advisor), Professor Oleg Tchernyshyov, Professor Charles Meneveau, Professor Andrea Prosperetti and Professor Randal Burns. Thank you Pr. Meneveau for taking the time to review my thesis.

Table of Contents

List of Figures

Introduction

Why study particles dispersion in a Turbulent Flow?

This thesis is an endeavor to shed light on the behavior of particle separations carried by a Turbulent flow. Turbulence is actually one of the most common observed states in nature and most fluids and plasmas are in a turbulent motion. The earth atmosphere is in a constant turbulent motion as well the oceans and the interior of the planet. Turbulent state can be found in blood or engine fluids. It can e.g. characterize the dynamics of stellar interiors or interstellar media and even the motion of tangles of quantized vortices in superfluids.

The particular study of the particles separation $\mathbf{r}(t) = \mathbf{x}_1(t) - \mathbf{x}_2(t)$ between two tracers and their time evolution informs us on how a material carried by a flow in a turbulent state is spreading. The tracers "probe" the behavior of the flow and provide information on the mechanisms generating the turbulence. For example, Bodenschatz *et al.* infers that we cannot understand the evolution of a cloud without the relative dispersion of the drops and ice particles embedded within a turbulent flow [14]. This has a clear application to meteorology but also it can be critical when trying to predict the span of a radioactive cloud after a nuclear disaster or the impact of a biological attack. A more common

problem faced on daily basis by the people in urban environments is the air pollution [97]. Under sea, the living oceanic organisms undergo a proliferation driven by the turbulent motion of the seas and the biological growth is strongly influenced by the state of the flow [49, 48, 95, 31].

Relative particle dispersion is also crucial for the stellar formation mechanism [53, 96]. The stars inner part in a liquid state is constantly under extraordinary stresses (pressure, temperature, ...) and therefore highly turbulent. The turbulent flow favors the mixing of the different elements composing the stars and the homogenization of the inside temperature. Lazarian *et al.* [65] understood the fast magnetic reconnections taking place in stars as a consequence of the motion of the turbulent media. The fast magnetic reconnections can explain the occurrence of solar flares and gamma ray bursts. The intergalactic medium generated during the formation of large scale structure also exhibits a turbulent behavior [85] which holds an important role in galaxies formation.

What is turbulence?

From Da Vinci to Reynolds

Turbulence is still an imperfectly understood phenomenon. It has already been recognized 500 years ago as a distinct fluid behavior and Leonardo Da Vinci seems to be one of the first to report a scientific description (see figure 1). He called this fluid behavior "turbolenza".

The Navier-Stokes equations are universally believed to encapsulate the physics of all fluid flows in the classical regime including the turbulent one. They have been derived by Claude-Louis Navier and George Gabriel Stokes

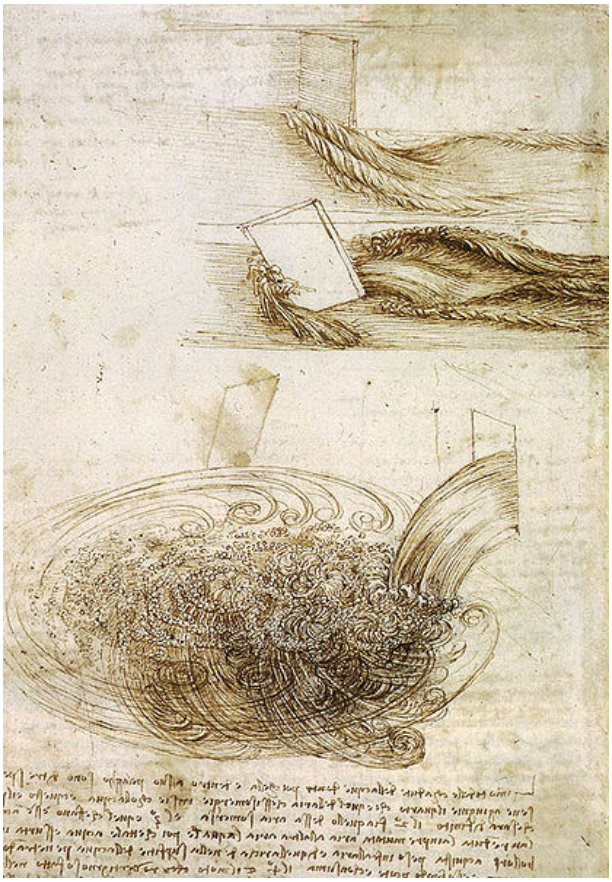

Figure 1: Sketch of a turbulent flow originating from one of Da Vinci's sketch book.

during the 19^{th} century from the second Newton's law:

$$\rho\left(\frac{\partial \mathbf{u}}{\partial t} + \mathbf{u}\cdot\nabla\mathbf{u}\right) = -\nabla p + \nabla\cdot\mathbf{T} + \mathbf{f}, \tag{1}$$

where $\mathbf{u}$ is the velocity vector of fluid elements, ρ is the fluid density, p is the pressure, $\mathbf{T}$ is the deviatoric component of the total stress tensor and $\mathbf{f}$ the body forces per unit volume acting on the fluid. In this thesis we are principally interested by incompressible flow of Newtonian fluids leading to "simplified"

equations

$$\frac{\partial \mathbf{u}}{\partial t} + \mathbf{u} \cdot \nabla \mathbf{u} = -\nabla p + \nu \nabla \mathbf{u} + \mathbf{f}, \tag{2}$$

$$\nabla \cdot \mathbf{u} = 0,$$

where we redefine $p \equiv p/\rho$, $\mathbf{f} \equiv \mathbf{f}/\rho$ and $\nu = \mu/\rho$ is the kinematic viscosity and μ is the dynamic viscosity. These equations are rather difficult to handle and few analytical solutions are known to these days. They are highly non linear and lead to strong chaotic behaviors.

Osborne Reynolds in 1851, was the first to systematically investigate the transition from laminar flow to turbulence. He introduced the concept of the dimensionless Reynolds number that characterize the state of the flow

$$Re = \frac{UL}{\nu}, \tag{3}$$

where U is a measure of the magnitude of the velocity of the flow at the length scale L. The laminar state is described by $Re \to 0$ and turbulence by $Re \to \infty$.

A modern understanding of turbulence

Defining turbulence is a difficult task. In 1922 Richardson gave this description:

> *Big whorls have little whorls,*
>
> *which feed on their velocity;*
>
> *And little whorls have lesser whorls,*
>
> *so on to viscosity.*

The concept behind these verses is that the energy is injected mechanically into the system at large scale, is transferred toward the smaller scales through the

so-called "energy cascade" process and dissipated into heat at the molecular scales. There are a few features that are generally universally accepted:

- it is a chaotic process meaning that the initial conditions fully determine the future behavior of the particles of the flow but long term prediction are difficult in practice. This concept however has been challenged by the emergence of the spontaneous stochasticity ideas that suggest that the particles forget their initial positions.

- it is a 3-dimensional process. Turbulence generates 3D vortices with non-zero rotationality for initial conditions with vorticity. This process is known as vortex stretching and is the core mechanism for the energy cascade from large scales to small scales.

- it is a dissipative process, the entropy is always increasing and it enhances mixing. The system needs an sustained energy input for the turbulent state to persist.

- it is characterized by intermittencies. The kinetic energy is dissipated in an irregular manner.

In 1941, Kolmogorov wrote one of the most influential series of papers in the field of isotropic homogeneous turbulence (K41) [57, 58, 56] and laid some fundamental concepts. He distinguished between domains of scales. The large scales at which the energy is injected characterized by the integral scale. In the inertial range, the system can be statistically described only by the energy dissipation $\epsilon = -\frac{dE}{dt}$. As a consequence the typical time scales related to particle pairs separated by a distance r is $\tau(r) = r^{2/3}/\epsilon^{1/3}$. In the dissipation range,

the system can be statistically described by the energy dissipation ϵ and the viscosity ν. It is characterized by the Kolmogorov length scale $\eta = (\nu^3/\epsilon)^{1/4}$ and the Kolmogorov time scale $\tau = (\nu/\epsilon)^{1/2}$. Although K41 is known now to not be accurate as it ignores intermittencies, it is often used as a standard to check experimental, numerical or analytical results. For example let $S(r) = \langle|\delta\mathbf{u}|^2\rangle$ (where $\delta\mathbf{u} = \mathbf{u}(\mathbf{x}+\mathbf{r}) - \mathbf{u}(\mathbf{x})$) be the second order structure function depending on r. By dimensional analysis in the inertial range we have:

$$S(r) = C(\epsilon r)^{2/3}, \tag{4}$$

where C is a dimensionless constant. This is known as the Kolmogorovs 2/3-law. This can compared to the numerical studies by Bitane et al. [10] in figure 2.

Outline of this thesis

This thesis is designed with a very simple structure in mind:

- A first expository chapter on the different research studies previously done and leading to this thesis work.
- A second chapter addressing the specific subject of backward dispersion. This chapter aims for a more "direct" study of dispersion with less modeling than for the following chapters to help familiarize the reader with the actual features and the different issues observed in real turbulence (or Navier Stokes turbulence).
- A third chapter introducing the diffusion models concept in turbulence.

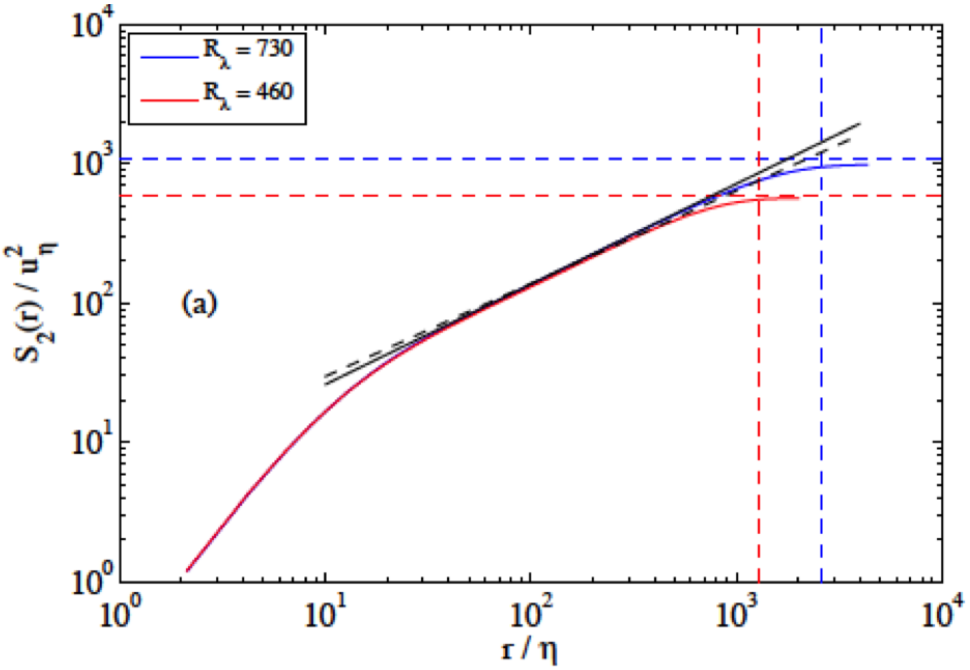

Figure 2: From Bitane et al. [10]: Second order structure function for two different Reynolds numbers.

Diffusion models are really dominating the study of dispersion in turbulence. The previous chapters help discriminate between the behavior of the models and the observed physics.

- A fourth and last chapter about an analytical diffusion model for synthetic turbulence models (non Navier-Stokes). The modeling aspect is taken to another level and we understand better from the previous chapters why there is a loss in capturing the actual physics of turbulence.

What has been done before this thesis work

In a first chapter we summarize the preceding works that led to this thesis work. This chapter exposes the different known features related to dispersion.

We introduce the Batchelor range, the t^3 range and the large scale diffusive range.

We then recapitulate the history of the most influential diffusion models that have been designed for particle pair dispersion and that are the most relevant for this thesis. It all started in 1926 with the seminal work of Richardson and additionally we will especially insist on the work of Batchelor and Kraichnan.

Finally, we introduce the kinematic simulations, a subfield of turbulence research. They have been created with the desire to simplify the study of turbulent flows by simulating a quasi-random Gaussian velocity field with a Kolmogorov spectrum. These models however have been realized to have very different behavior than that of real turbulence. In the inertial range for instance, it is not yet very well understood if the dispersion is proportional to t^3, t^6 or $t^{9/2}$.

The first chapter is an introductory chapter that strives to build the foundations and motivations for the following chapters.

Backward dispersion

The second chapter will focus on tracers labeled at the final time t_f and traveling backwards for times $t \leq t_f$. The dispersion of fluid particles backwards-in-time is critical for understanding the mixing properties of turbulent flows [87]. Mixing is a process by which scalar or vector quantities such as dye concentration, temperature or magnetic fields, are transported due to the action of an underlying flow [91, 16]. These fields are stretched and contorted, often violently, and if they have intrinsic diffusive properties (as most naturally occurring systems do), they are dissipated. If the substance is non-diffusive, its value at a point is

the initial value at the starting point of the backwards deterministic trajectory ending there. The separation of these trajectories ending at nearby points is the principal subject of study for *backward deterministic particle dispersion*. For diffusive substances, initially separate bits of material can be brought together by the action of the turbulent flow and molecular effects. Here an averaging process over backwards stochastic trajectories recovers the value at the field at any point. The reversal of the process described above – coalescence of forward perturbed trajectories – is known as *backwards stochastic particle dispersion*. Backwards particle dispersion is a key feature to understanding many physical problems.

In this chapter we investigate the properties of backwards separation for both deterministic and stochastic tracers. We perform a systematic numerical study of deterministic tracers at Taylor-scale Reynolds number $Re = 433$. We investigate small and long time scaling laws, revealing a small time t^4 scaling and verifying the t^3 behavior at long time. We also measure the observed Richardson constant for different final particle separations in addition to the corresponding probability distribution functions (PDFs) of the dispersion. For the stochastic tracers, we analytically compute an exact t^3 term in the separation using Ito calculus and show numerically that this term is dominant at long times. This t^3 term seems to correspond also to the asymptotic behavior of the deterministic tracers.

Diffusion models

The third chapter will build on the concept of diffusion models. L. F. Richardson, in a classic paper [83], initiated the study of dispersion of particle pairs

in turbulent flows, introducing a diffusion model with a scale-dependent eddy-diffusivity:

$$\frac{\partial P(r,t)}{\partial t} = \frac{1}{r^2}\frac{\partial}{\partial r}\left(r^2 K(r)\frac{\partial P(r,t)}{\partial r}\right), \tag{5}$$

where $P(r,t)$ is the probability distribution of a separation r at time t. There has since been much discussion about the accuracy of this description.

We solve an inverse problem for fluid particle pair statistics: we show that a time sequence of probability density functions (PDFs) of separations can be exactly reproduced by solving the diffusion equation with a suitable time-dependent diffusivity. The diffusivity tensor is given by a time integral of a conditional Lagrangian velocity structure function, weighted by a ratio of PDFs. Physical hypotheses for hydrodynamic turbulence (sweeping, short memory, mean-field) yield simpler integral formulas, including one of Kraichnan and Lundgren (K-L) [59, 69]. We evaluate the latter using a space-time database from a numerical Navier-Stokes solution for driven turbulence.

We also derive a similar equation for the join probability distribution of the separations and the velocity differences. This equation might provide a more accurate description of the system as the acceleration field is auto correlated with shorter time scales than the velocity field.

Dispersion and diffusion models in synthetic turbulence

In the last chapter we present an analytical model to improve the understanding of Synthetic models. Synthetic models of Eulerian turbulence like so-called kinematic simulations (KS) are often used as computational shortcuts for studying Lagrangian properties of turbulence. These models have been criticized by

Thomson and Devenish (2005) [94], who argued on physical grounds that sweeping decorrelation effects suppress pair dispersion in such models.

We derive analytical results for Eulerian turbulence modeled by Gaussian random fields, in particular for the case with zero mean velocity. Our starting point is an exact integrodifferential equation for the particle pair separation distribution obtained from the Gaussian integration-by-parts identity. When memory times of particle locations are short, a Markovian approximation leads to a Richardson-type diffusion model. We obtain a time-dependent pair diffusivity tensor of the form $K_{ij}(r,t) = S_{ij}(r)\tau(r,t)$, where $S_{ij}(r)$ is the structure-function tensor and $\tau(r,t)$ is an effective correlation time of velocity increments. Crucially, this is found to be the minimum value of three times: the intrinsic turnover time $\tau_{eddy}(r)$ at separation r, the overall evolution time t, and the sweeping time r/v_0 with v_0 the rms velocity. We study the diffusion model numerically by a Monte Carlo method. With inertial ranges like the largest achieved in most current KS (about 6 decades long), our model is found to reproduce the $t^{9/2}$ power law for pair dispersion predicted by Thomson and Devenish and observed in the KS. However, for much longer ranges, our model exhibits three distinct pair-dispersion laws in the inertial range: a Batchelor t^2 regime, followed by a Kraichnan-model-like t^1 diffusive regime, and then a t^6 regime. Finally, outside the inertial range, there is another t^1 regime with particles undergoing independent Taylor diffusion. These scalings are exactly the same as those predicted by Thomson and Devenish for KS with large mean velocities, which we argue may hold also for KS with zero mean velocity. This may, however, be an artifact of our Markovian approximation as we discuss further in this thesis. Our results support the basic conclusion of Thomson

and Devenish (2005) that sweeping effects make Lagrangian properties of KS fundamentally differ from those of hydrodynamic turbulence for very extended inertial ranges.

Chapter 1

What we know about dispersion in turbulence

1.1 Introduction

In this chapter we focus on the understanding of the physics related to turbulent dispersion previous to this thesis work. It will be an opportunity to introduce the subject for the coming chapters. We first look at different experimental and numerical results found in the literature and expose the common approaches of modeling the physics.

1.2 Features of turbulent dispersion

1.2.1 Batchelor range

Turbulent dispersion is characterized by a rich set of features that varies with the different scales (time and space) of the system. The Batchelor range relates to the small scales and was first identified by G.K. Batchelor in 1950 [4]. The position of an element of fluid within the flow is simply related to the velocity field by

$$\frac{d\mathbf{x}(t)}{dt} = \mathbf{u}(\mathbf{x}(t), t), \quad \mathbf{x}(t_0) = \mathbf{x}_0, \tag{1.1}$$

therefore the dispersion between two elements separated by a distance r at a time t is

$$\frac{d\mathbf{r}(t)}{dt} = \delta\mathbf{u}(\mathbf{r}(t), t), \quad \mathbf{r}(t_0) = \mathbf{r}_0, \tag{1.2}$$

or in the integral form

$$\mathbf{r}(t) - \mathbf{r}_0 = \int_{t_0}^{t} \delta\mathbf{u}(\mathbf{r}(s), s)ds. \tag{1.3}$$

By taking the dot product of (1.2) with (1.3) and taking the ensemble average we obtain

$$\frac{1}{2}\frac{d\langle|\mathbf{r}(t) - \mathbf{r}_0|^2\rangle}{dt} = \int_{t_0}^{t} \langle\delta\mathbf{u}(\mathbf{r}(t), t) \cdot \delta\mathbf{u}(\mathbf{r}(s), s)\rangle ds \tag{1.4}$$

Batchelor applied the K41 theory to derive a short time expansion of (1.4)

$$\frac{1}{2}\frac{d\langle|\mathbf{r}(t) - \mathbf{r}_0|^2\rangle}{dt} \simeq \langle|\delta\mathbf{u}(r_0, t_0)|^2\rangle(t - t_0) \tag{1.5}$$

$$= C(\epsilon r_0)^{2/3}(t - t_0) \tag{1.6}$$

where C is the Kolmogorov constant for the second-order velocity structure function. By integrating we get

$$\langle|\mathbf{r}(t) - \mathbf{r}_0|^2\rangle = C(\epsilon r_0)^{2/3}(t - t_0)^2 \tag{1.7}$$

Ouellette et al. in 2006 [74] were able to track hundreds of particles at $R_\lambda = 815$ with very high temporal resolution. Their results show clear evidence of the Batchelor regime at small times (figure 1.1).

1.2.2 The t^3 regime

The t^3 regime was predicted in 1926 by Richardson [83] as a consequence of his diffusion model (see next section) and has been the object of many controversies.

$$\langle|\mathbf{r}(t) - \mathbf{r}_0|^2\rangle = g\epsilon t^3 \tag{1.8}$$

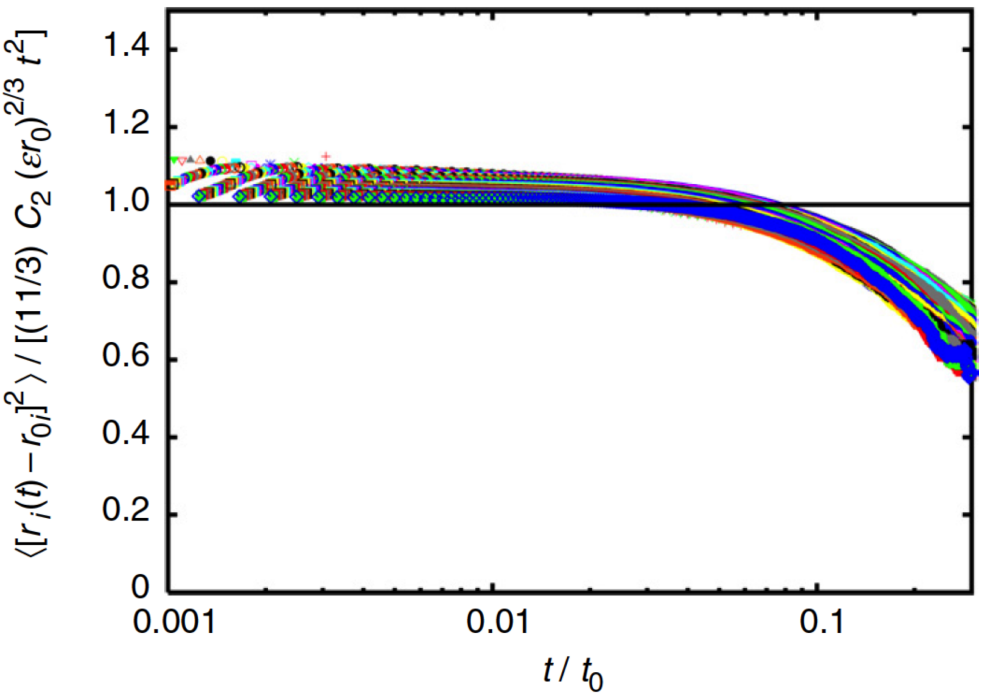

Figure 1.1: From Ouellette et al. in 2006: Mean square relative dispersion for 50 different bins of initial separations, ranging from 0-1 mm ($\approx 0 - 43\eta$) to 49-50 mm ($\approx 2107 - 2150\eta$), compensated by Batchelor scaling ($C_2 = 2.1$).

is referred as the Richardson-Obukhov law and g is the so called Richardson constant. Until recently, it has been a real experimental and numerical challenge to probe this regime as it requires very high Reynolds numbers to be observed. Although numerous experimental and numerical studies seem to indeed highlight this regime, the results are not yet fully convincing.

Despite the lack of evidence until the late 90's, there is a simple argument to expect such a regime. The Kolmogorov theory infers the velocity difference to scale as $\delta u = A\epsilon r^{1/3}$ and $\frac{dr}{dt} = \delta u$. The resulting long time dependence is therefore $r \sim g\epsilon t^3$. The transition from the Batchelor regime to the t^3 is usually characterized by the Batchelor time $t_B = \epsilon^{-1/3} r_0^{2/3}$, the time when the

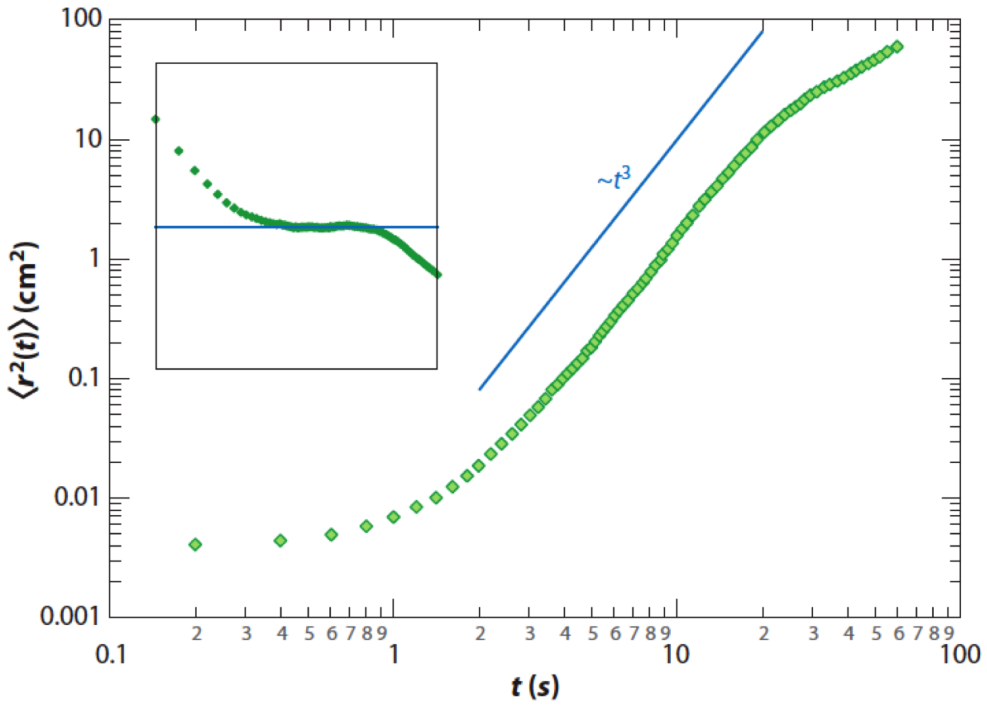

Figure 1.2: From Julien et al. in 1999: Mean square relative dispersion. (Inset) Data compensated by t^3.

two regimes equal each other

$$g\epsilon t^3 \sim C(\epsilon r_0)^{2/3} t^2 \tag{1.9}$$

In figure 1.2 we present the experimental results by Julien et al. [72] of the particles undergoing a t^3 dispersion in a 2 dimensional turbulent flow Reynolds number $Re_L \sim 5$. Figure 1.3 shows DNS results by Bitane et al. [10] for different initial separations for Reynolds number $Re_\lambda = 460$ and $Re_\lambda = 730$ (among the highest Reynolds numbers reached in DNS to this day.). Note that it is unclear even with these high Reynolds numbers if the system has reached an asymptotic regime.

Another fundamental feature is that the dispersion within the t^3 regime is

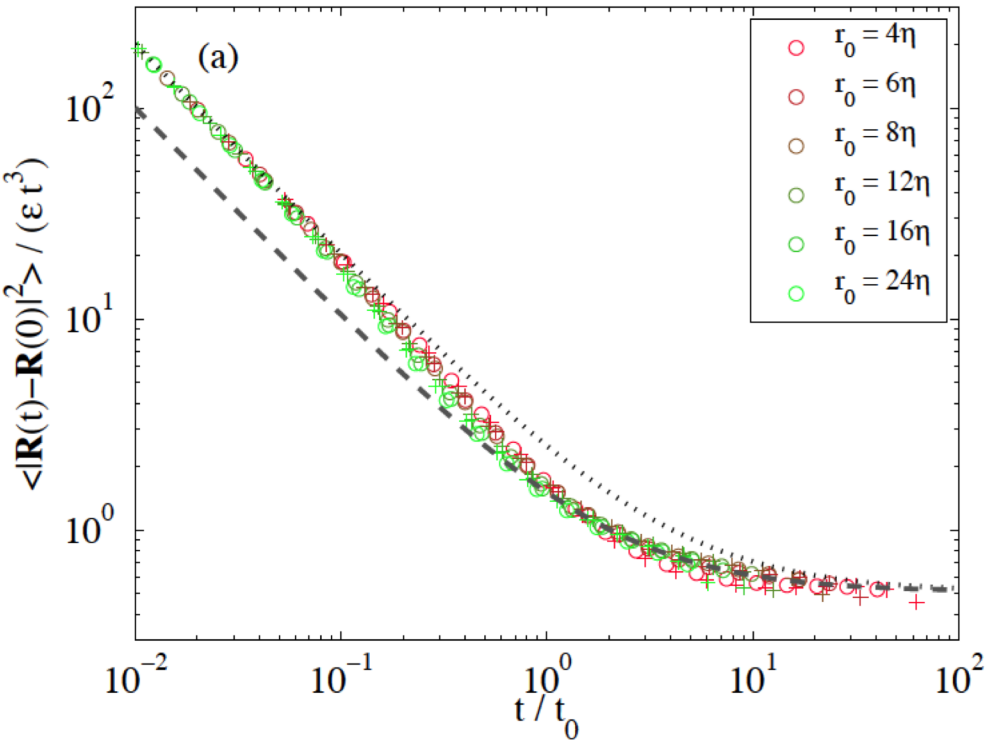

Figure 1.3: From Bitane et al. in 2012: Compensated mean-squared displacement $\langle|\mathbf{R}(t)-\mathbf{R}(0)|^2\rangle/(\epsilon t^3)$ as a function of t/t_0 with $t_0 = S_2(r_0)/(2\epsilon)$ for various initial separations and $R_\lambda = 730$ ($\circ$) and $R_\lambda = 460$ ($+$). The two curves show behaviors of the form $\langle|\mathbf{R}(t)-\mathbf{R}(0)|^2\rangle \simeq g\epsilon t^3 + At^2$, with with $A = S_2(r_0)$, given by Batchelors ballistic regime (black dotted line), and $A = 2.5/t_0^2$ (grey dashed line).

"faster" backward than forward. The Richardson constant has been evaluated in the literature to range between 0.52 and 0.64 depending on the Reynolds number for forward dispersion. In 2005 Sawford et al. [88] estimated the backward Richardson constant to be $g_B = 1.14$ and in 2011, Eyink estimated this constant to be $g_B = 1.35$ [40] (see figure 1.4).

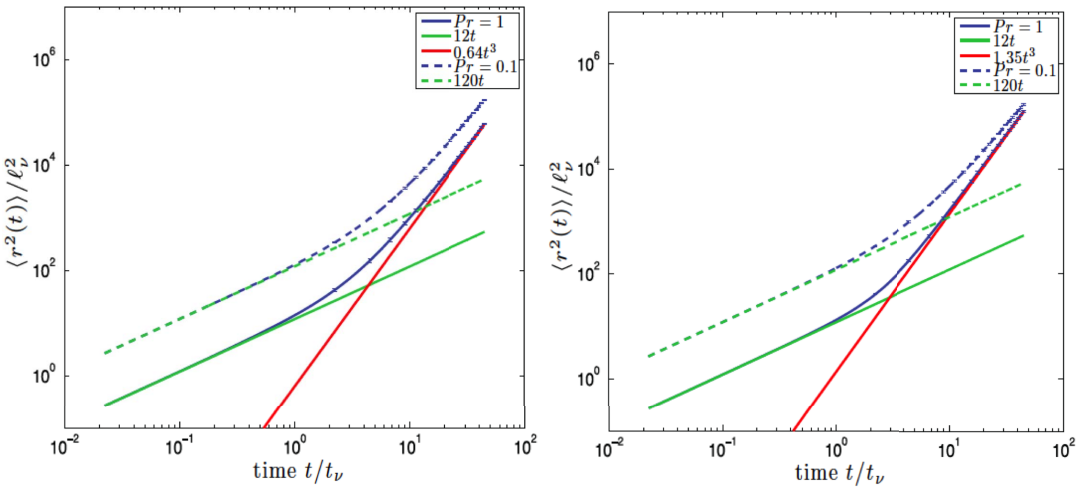

Figure 1.4: From Eyink 2011. Mean dispersion of particle pairs. On the left: forward dispersion. On the right: backward dispersion. The backward-in-time results are plotted against $t' = t_f - t$ and all quantities are nondimensionalized with viscous units.

1.2.3 Taylor diffusion outside the inertial range

Outside the inertial range the particles are separated by scales larger than the large-eddy turnover scale and their motions tend to be independent from each other. The dispersion become purely diffusive such that $\langle |\mathbf{r}(t) - \mathbf{r}_0|^2 \rangle \sim t$. This phenomenon has been understood by G.I. Taylor in 1921 [92] and is referred as the Taylor diffusion.

1.3 Diffusion models

1.3.1 Richardson diffusion model

In 1905, Albert Einstein described the molecular motion with a diffusion equation:

$$\frac{\partial \rho}{\partial t} = K \frac{\partial^2 \rho}{\partial x^2} \tag{1.10}$$

where K is the mass diffusivity and $\rho(x,t)$ is the density of Brownian particles at point x and at time t. He brought the solution of the problem to the attention of physicists, and presented it as a way to indirectly confirm the existence of atoms and molecules. In 1926, Lewis Fry Richardson inspired a whole new subfield of turbulence by attempting to describe the 2-particle dispersion in turbulence as a diffusion process with scale-dependent diffusivity. Richardson recollected numerous studies evaluating the measurement of the diffusivity (using $dx^2/dt = 2K$) for 2-particle dispersion in a turbulent flow at different scales (see figure 1.5). He modeled the diffusivity to be

$$K(r) \sim r^{4/3}. \tag{1.11}$$

Obukhov, a student of Kolmogorov, much later realized that the only dimensional form consistent with K41 for a scale only dependent diffusivity is

$$K(r) = k_0 \epsilon^{1/3} r^{4/3}. \tag{1.12}$$

Richardson then proposed the following diffusion equation for the relative dispersion

$$\frac{\partial P(r,t)}{\partial t} = \frac{1}{r^{d-1}} \frac{\partial}{\partial r} \left[r^{d-1} K(r) \frac{\partial}{\partial} P(r,t) \right] \tag{1.13}$$

where $P(r,t)$ is the probability distribution of separation between particle pairs and d is the space dimensionality. Equation (1.13) admits a self similar solution in 3 dimensions with (1.11) for $K(r)$

$$P(r,t) = \frac{429}{70} \sqrt{\frac{143}{2}} \left[\frac{1}{\pi \langle r^2(t) \rangle} \right] \exp \left[- \left(\frac{1287 r^2}{8 \langle r^2(t) \rangle} \right)^{1/3} \right] \tag{1.14}$$

with the mean square displacement

$$\langle r^2(t) \rangle = g \epsilon t^3 \tag{1.15}$$

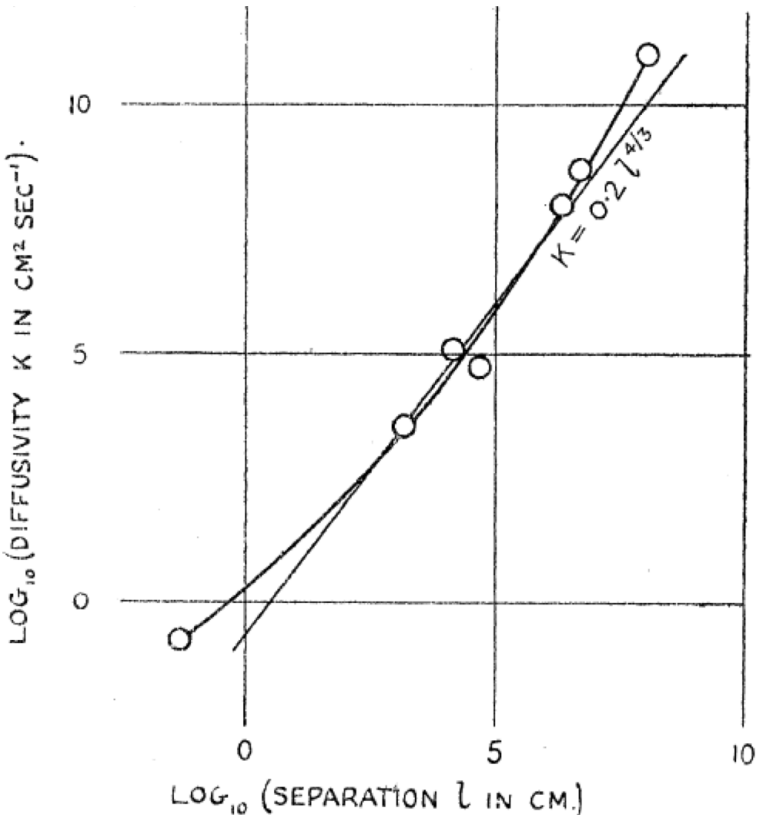

Figure 1.5: From Richardson 1926: Log-log plot of K versus particle separations lies on a line of slight curvature.

where $g = \frac{1144}{81} k_0^3$. It is interesting to note that, despite the crude heuristic derivation of the Richardson diffusivity, Richardson's predictions became a standard for the study of relative dispersion in turbulence. In Figure 1.6 we show the PDF measured by Bitane et al. [10] plotted in self-similarity units (units for which the Richardson PDF appears as a straight line). Most experimental and numerical studies (if not all) show strong agreement between the 2-particles separation PDF and the Richardson PDF for $0.4 \lesssim (r/\sqrt{\langle r(t)^2 \rangle})^{2/3} \lesssim 2$

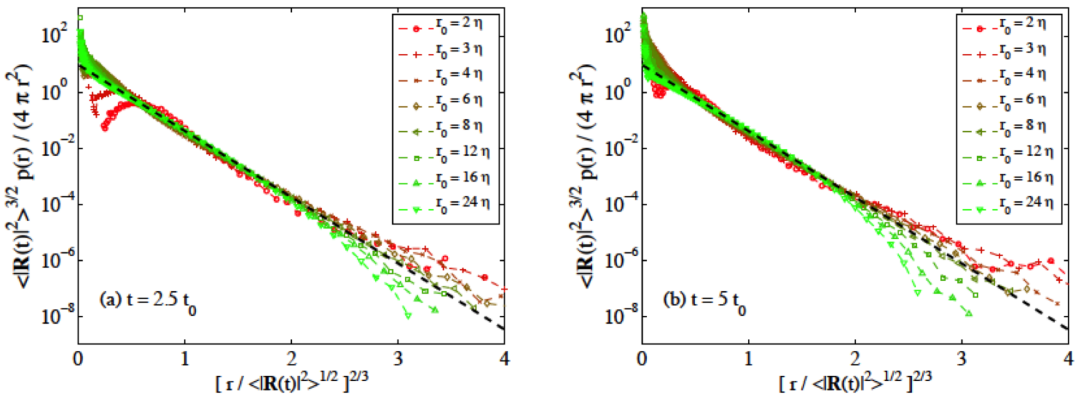

Figure 1.6: From Bitane et al. in 2012: Probability density function of the distance r at time $t = 2.5t_0$ (a) and $t = 5t_0$ (b) and for various values of the initial separation. The units are normalized such that Richardsons diffusive density distribution (1.14) appears as a straight line (represented here as a black dashed line).

1.3.2 The Batchelor model

In 1952, Batchelor [3] suggested that the diffusivity is time dependent rather than space dependent, i.e. $K(t) = k_0\epsilon t^2$, leading to similar dispersion behavior $\langle r^2(t)\rangle = g\epsilon t^3$ with $g = 2k_0$. The evolution of the probability distribution is however described by the Batchelor probability distribution

$$P(r,t) = \left[\frac{3}{2\pi\langle r^2(t)\rangle}\right]^{3/2} \exp\left[-\frac{3r^2}{2\langle r^2(t)\rangle}\right]. \tag{1.16}$$

In 1987, Klafter et al. [55] noted that K41 is consistent with a whole set of diffusivities $K(r,t) = k_0\epsilon^a t^b r^c$ yielding $\langle r^2(t)\rangle = g\epsilon t^3$ with the constraints $2b + 3c = 4$ and $a = 1 - c/2$. Figure 1.7 shows measurements by Ouelette et al. [74] of the probability distribution for different initial separations and the striking agreement with the Batchelor PDF for initial separations well into the inertial range and with the Richardson PDF for particles starting within the dissipation range.

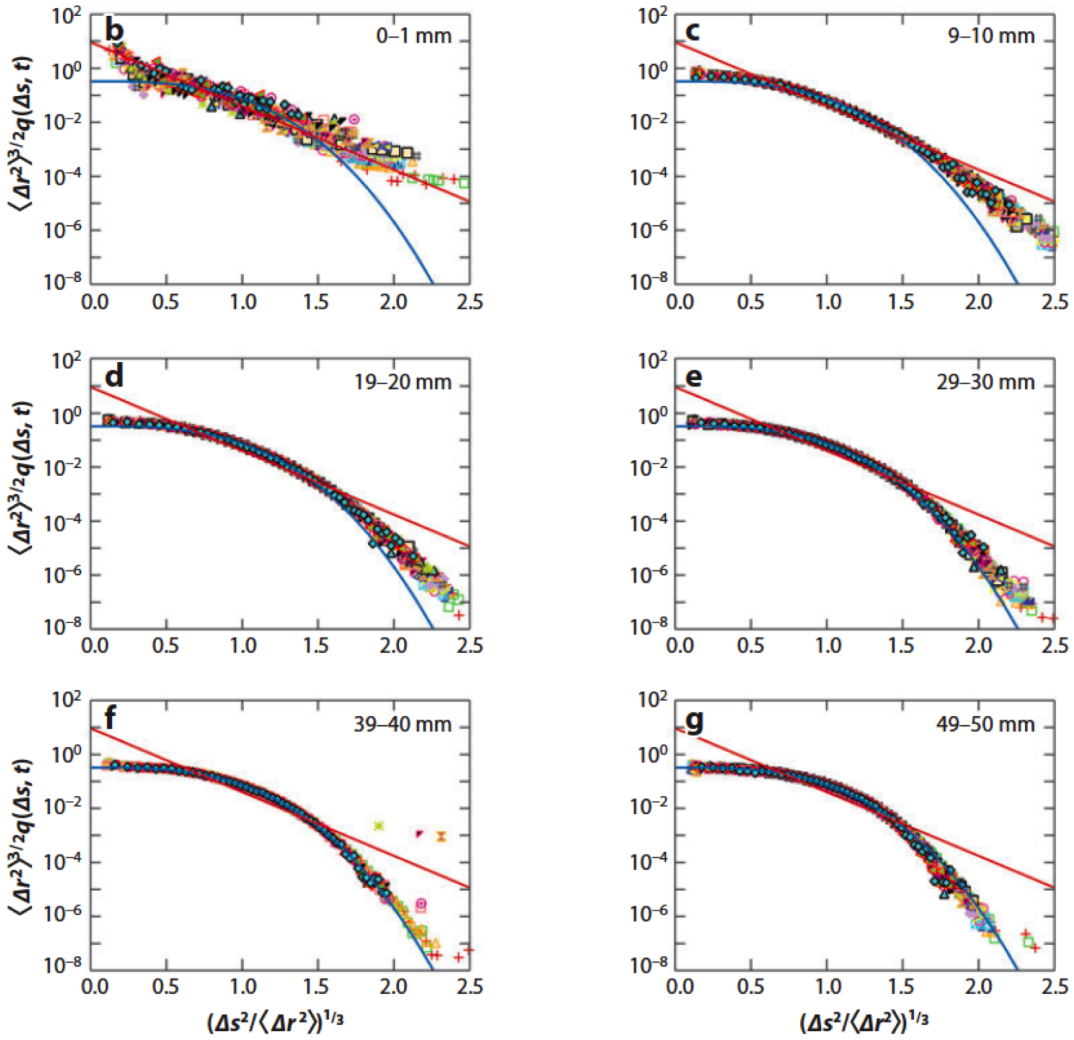

Figure 1.7: From Ouelette et al. 2006: Probability density functions (PDFs) of pair separations. The red straight line is the Richardson PDF, whereas the blue curved line is the Batchelor PDF. The symbols show the experimental measurements. Each plot shows a different initial separation; for each initial separation, PDFs from 20 times ranging from $0 - 20\tau_\eta$ are shown. $R_\lambda = 815$, $\Delta r(t) = |\mathbf{r}(t)\mathbf{r}_0|$, and $1mm \approx 43\eta$.

1.3.3 The Kraichnan diffusion model

In 1965 - 1966 Kraichnan [60, 61] developed a field theoretic approach to fluid dynamics similar to the ones used for quantum field problems namely the Lagragian Direct History Interaction Approximation (LHDIA). Applying the LHDIA theory for a convected scalar field [59], he was able to recover the Richardson's diffusion equation with the peculiar difference that the eddy diffusivity depends on the duration of the dispersion along with separation between the particles:

$$\frac{\partial P(\mathbf{r},t;\mathbf{r}_0,t_0)}{\partial t} = \frac{\partial}{\partial r_i}\left[K_{ij}(\mathbf{r},t,t_0)\frac{\partial P(\mathbf{r},t;\mathbf{r}_0,t_0)}{\partial r_j}\right] \tag{1.17}$$

with

$$K_{ij}(\mathbf{r},t,t_0) = \int_{t_0}^{t} < (u_i(\mathbf{x}+\mathbf{r},t) - u_i(\mathbf{x},t))((u_j(\mathbf{x}+\mathbf{r},t|s) - u_j(\mathbf{x},t|s)) > ds, \tag{1.18}$$

where $u_i(\mathbf{x},t|s)$ is the $i-$component of the velocity field at time s of the fluid particle which arrives at $\mathbf{x}$ at time t. This formula differs from the Batchelor's one since it involves tracking fluid particles backward in time being therefore additionally difficult to compute with standard numerical or experimental methods. The diffusivity for the PDF of particle separations obtained by Kraichnan has the form for isotropic statistic

$$K_L(r,t) = \epsilon^{1/3} r^{4/3} F(x) \tag{1.19}$$

with $x = \epsilon^{1/3} t/r^{2/3}$ and K_L and being the longitudinal component of the diffusivity. Ott & Mann [82] found a simple fitting formula for Kraichnan's LHDIA solution, of the form

$$F(x) = \frac{ax}{1+bx} \tag{1.20}$$

This formula reproduces the asymptotics of the LHDIA solution found by Kraichnan:

$$F(x) \sim ax, \qquad x \ll 1; a = 2.32$$

$$F(x) \sim a/b, \qquad x \gg 1; a = 2.00 \tag{1.21}$$

Note that a is just the spatial Kolmogorov constant in the 2/3rd-law and a/b is the coefficient of the asymptotic Richardson $r^{4/3}$ eddy-diffusivity. Thus, these constants can be easily obtained empirically as well as from LHDIA.

The self-similar solution of Kraichnan's PDF equation, with the important correction of Ott & Mann (2000), is

$$P(r,t) = \frac{1}{\epsilon^{3/2} t^{9/2} N} G(x) \tag{1.22}$$

with

$$G(x) = \exp\left[\frac{9}{4}\int_1^x \frac{ds}{s^2 F(s)}\right]. \tag{1.23}$$

The constant N is chosen to insure the normalization of the PDF $\int_0^\infty r^2 P(r,t)dr = 1$ from

$$N = \frac{3}{2}\int_0^\infty G(x) x^{-11/2} dx. \tag{1.24}$$

If one uses the fitting formula for $F(x)$ (1.20), one can obtain an analytical expression for the function $G(x)$:

$$G(x) = \exp\left[-\frac{9}{4}\left(\frac{1}{2ax^2} + \frac{b}{ax} - (\frac{1}{2a} + \frac{a}{b})\right)\right] \tag{1.25}$$

$$= C \exp\left[-\frac{9}{4}\left(\frac{1}{2ax^2} + \frac{b}{ax}\right)\right] \tag{1.26}$$

In figure 1.8 we present Ott & Mann measurement of the PDF particle separation and the how it compares to the Batchelor PDF, the Kraichnan PDF and the Richardson PDF [82].

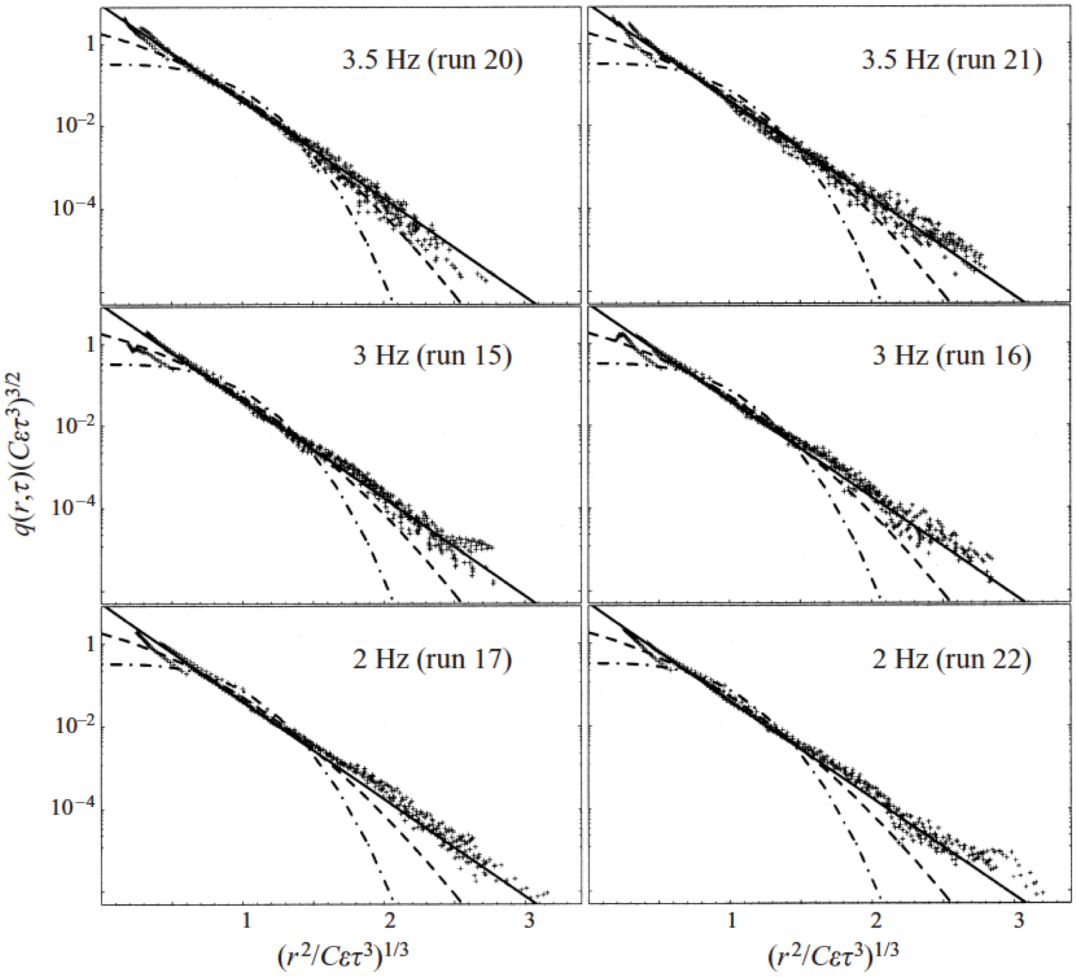

Figure 1.8: Probability distribution of particle pairs separation distance compared to the expressions of the Richardson PDF (solid), the Kraichnan PDF (dashed), and the Batchelor PDF (dot-dashed).

1.4 Synthetic turbulence models

The challenges related to the Navier-Stokes have led scientists to develop simplified models that could encapsulate some of the essential physics of turbulence. Elliot and Majda in 1996 developed one of the first synthetic models [34] with

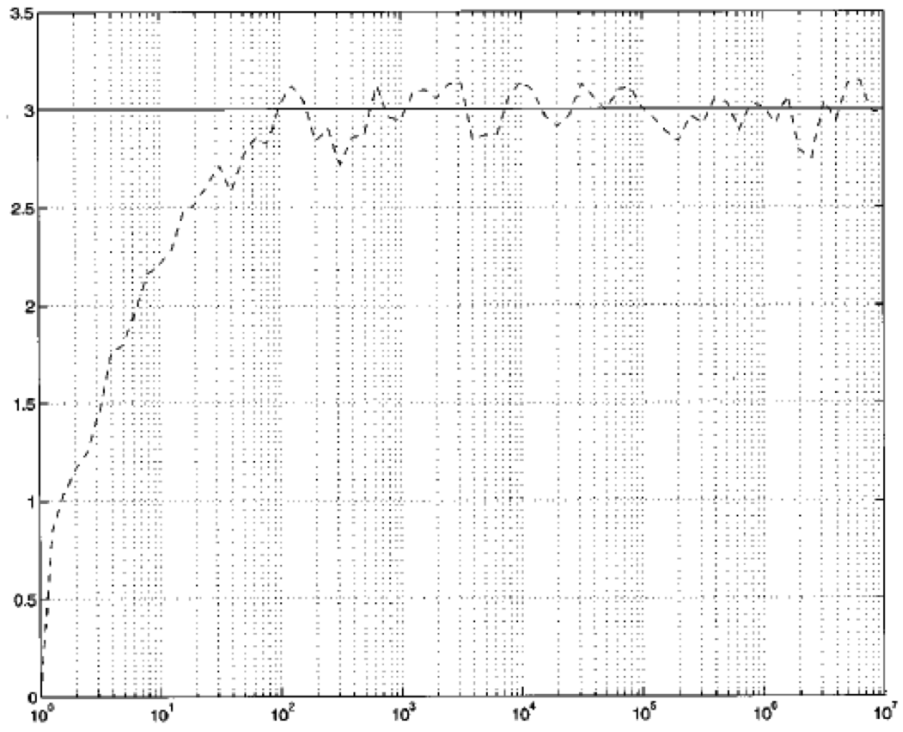

Figure 1.9: From Elliot and Madja in 1996: plot of the logarithmic derivative of mean squared dispersion versus time. The solid line indicates a t^3 scaling.

a Monte Carlo method for simulating an isotropic incompressible Gaussian random field satisfying the scaling relations

$$\langle |\delta \mathbf{u}(r)|^2 \rangle = C_h r^{2h} \tag{1.27}$$

for $0 < h < 1$. For $h = 1/3$, which corresponds to the familiar Kolmogorov spectrum, they found a t^3 law for the mean square particle dispersion for about eight decades (see figure 1.9). Such promising results inspired numerous subsequent works. However, despite the momentum of this field given by this seminal work by Elliot and Majda, D. J. Thomson and B. J. Devenish in 2005 [94] pointed out that the time-steps for the Monte Carlo simulation chosen might be too big to resolve the relevant dynamics of the model.

1.4.1 The Kinematic Simulation model

The kinematic simulation focus on generating an ensemble of random isotropic incompressible three-dimensional velocity fields. The model introduced by Fung and Vassilicos in 1998 [47] is somewhat different from the one developed by Elliot and Majda. The velocity at position $\mathbf{x}$ and time t is given by

$$\mathbf{u}(\mathbf{x},t) = \sum_{n=1}^{N} \mathbf{A}_n \cos(\mathbf{k}_n \cdot \mathbf{x} - \omega_n t) + \mathbf{B}_n \sin(\mathbf{k}_n \cdot \mathbf{x} - \omega_n t) \tag{1.28}$$

where N is the number of modes. The directions of $\mathbf{k}_n$, $\mathbf{A}_n$ and $\mathbf{B}_n$ are chosen at random with the constraints $\mathbf{k}_n \perp \mathbf{A}_n$ and $\mathbf{k}_n \perp \mathbf{B}_n$ and the magnitude are such that

$$A_n^2 = B_n^2 = 2E(k_n)\Delta k_n. \tag{1.29}$$

$E(k_n)$ is chosen to mimic the Kolmogorov spectrum

$$E(k_n) = \begin{cases} C_k \epsilon^{2/3} k^{-5/3} & \text{for } 2\pi/L \leq k_n \leq 2\pi/\eta \\ 0 & \text{otherwise.} \end{cases} \tag{1.30}$$

with C_k being the Fourier Kolmogorov constant, L the integral length scale and η the Kolmogorov scale. $k_1 = 2\pi/L$ and $k_N = 2\pi/\eta$. The K_n can be related to k_1 through a geometric relation ($k_n = k_1 a^{n-1}$) or an algebraic relation ($k_n = k_1 n^{\alpha}$) and k_N/k_1 can be thought as the Reynolds number.

1.4.2 The controversy

This model has showed similar t^3 scaling law as for real turbulence for small Reynolds number (see figure 1.10). In 2005 however, Thomson and Devenish opened the debate on the actual behavior of this model [94]. In real turbulence we expect typical time scale $\tau(r)$ of turn over time for eddies of size r to be proportional to $r^{2/3}/\epsilon^{1/3}$ (under K41 assumption), with $K(r) \sim \delta u^2(r)\tau(r)$

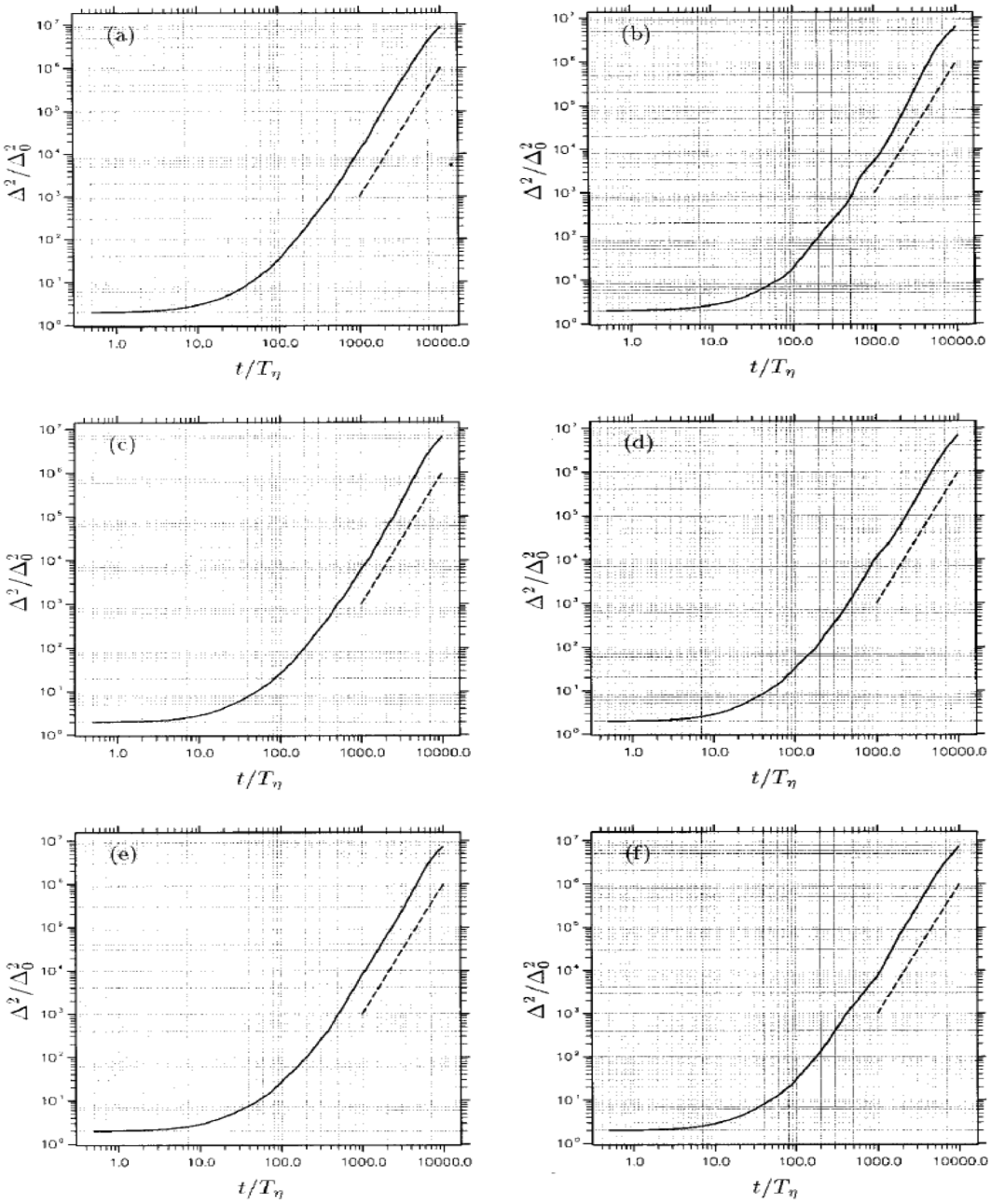

Figure 1.10: Fung and Vassilicos in 1998: Log-log plots of the dispersion in kinematic simulations for $k_N/k_1 = 1693$. The averages were calculated over 2000 particle pairs. The wave numbers k_n are distributed either algebraically (AD) or geometrically (GD). (a) GD and $N = 79$, (b) AD and $N = 20$, (c) AD and $N = 40$, (d) AD and $N = 79$, (e) AD and $N = 125$ and (f) AD and $N = 158$. The dashed line is a line with slope equals to 3.

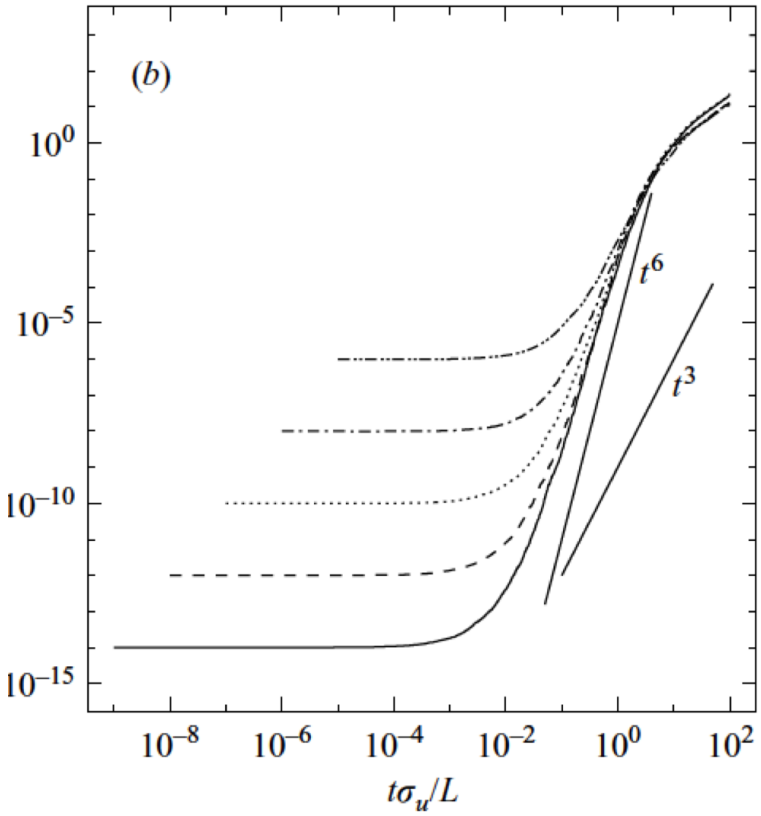

Figure 1.11: 2005 Thomson and Devenish: The evolution of $\langle r^2 \rangle$ for non zero mean velocity, 125 particle pairs per realization and 5 realizations of the flow $r_0/L = 10^{-7}$, 10^{-6}, 10^{-5}, 10^{-4} and 10^3 (bottom to top) with $L/\eta = 10^8$ and $N = 1600$. The straight lines are proportional to t^3 and t^6.

yielding the Richardson diffusivity $K(r) \sim \epsilon^{1/3} r^{4/3}$. For the kinematic simulations, unlike real turbulence, the smaller eddies are not swept be the larger eddies and the typical turn over time scale is simply $\tau(r) = r/u'$ where u' is the rms velocity of the flow (or the typical velocity scale). This leads to a diffusivity

$$K(r) \sim \delta u^2(r)\tau(r) \sim \frac{\epsilon^{2/3} r^{5/3}}{u'} \tag{1.31}$$

and a dispersion

$$\langle r^2(t) \rangle \sim \frac{\epsilon^4 t^6}{u'^6}. \tag{1.32}$$

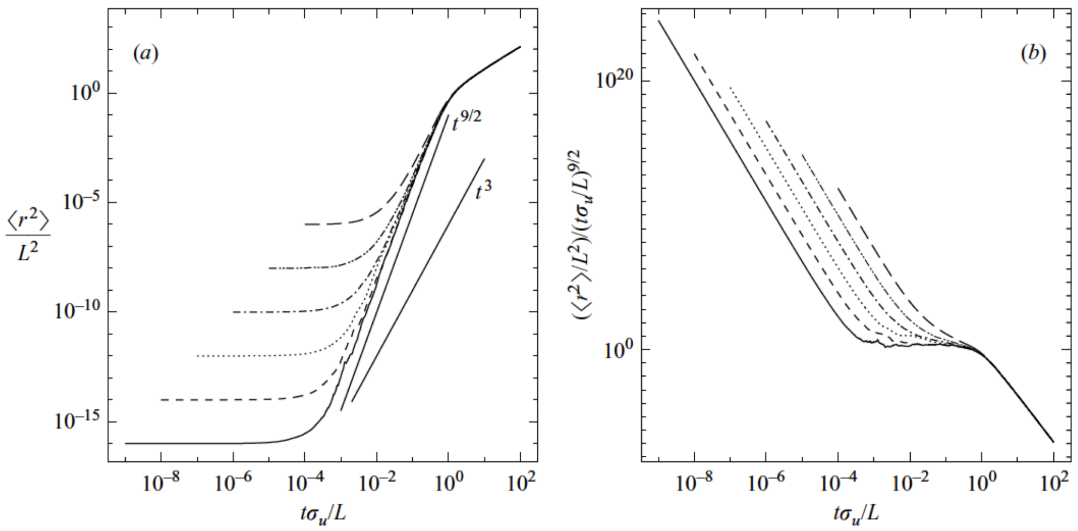

Figure 1.12: 2005 Thomson and Devenish: The evolution of $\langle r^2 \rangle$ for zero mean velocity, 125 particle pairs per realization and 5 realizations of the flow $r_0/L = 10^{-7}$, 10^{-6}, 10^{-5}, 10^{-4} and 10^3 (bottom to top) with $L/\eta = 10^8$. The straight lines are proportional to t^3 and $t^{9/2}$. (b) The evolution of $\langle r^2 \rangle / t^{9/2}$ for the same simulations.

Figure 1.11 from Thomson and Devenish 2005 presents strong evidence for the t^6 law in the case of non zero mean velocity. In the case of zero mean velocity, they argued that the particles undergo a mixture of t^3 and t^6 dispersion behavior and ultimately sustain an asymptotic $t^{9/2}$ behavior (see figure 1.12). u' being the local flow speed and $p(u')$ its PDF, this would results for the dispersion the following relation:

$$\langle r^2(t) \rangle \sim \int_0^{\sqrt{\epsilon t}} \epsilon t^3 p(u') du' + \int_{\sqrt{\epsilon t}}^{t\epsilon^{2/3}/r_0^{1/3}} \frac{\epsilon^4 t^6}{u'^6} p(u') du', \tag{1.33}$$

potentially making a $t^{9/2}$ contribution.

1.5 Conclusion

We introduced three different aspects of research related to particle pair dispersion. We demonstrated the challenges and motivations related to these particular fields. The following chapters will build on these foundations and present new perspectives on the matter.

Chapter 2

Understanding backward dispersion in turbulent flows

2.1 Introduction

The dispersion of fluid particles backwards-in-time is critical for understanding the mixing properties of turbulent flows [87]. Mixing is a process by which scalar or vector quantities such as dye concentration, temperature or magnetic fields, are transported due to the action of an underlying flow [91, 16]. These fields are stretched and contorted, often violently, and if they have intrinsic diffusive properties (as most naturally occurring systems do), they are dissipated. If the substance is non-diffusive, its value at a point is the initial value at the starting point of the backwards deterministic trajectory ending there. The separation of these trajectories ending at nearby points is the main subject of study for *backward deterministic particle dispersion*. For diffusive substances, initially separate bits of material can be brought together by the action of the turbulent flow and molecular effects. Here an averaging process over backwards stochastic trajectories recovers the value at the field at any point. The reversal of the process described above – coalescence of forward perturbed trajectories

– is known as *backwards stochastic particle dispersion*. Backwards particle dispersion is a key feature to understanding many physical problems ranging from hydrodynamic turbulence [35], passive scalar transport and dissipative anomalies [30, 93, 20], cloud formation [14], biological spread and enhanced growth [49, 48, 95, 31], air pollution [97] stellar evolution [53, 96], occurrence of solar flares [65] and galaxy formation [85].

It has been argued that in a turbulent flow, a pair of tracer particles separate proportionally to t^3 on average [83]. This prediction is now known as the Richardson-Obukhov scaling law [80] and it remains a subject of controversy and inquiry. Experimental and numerical studies of two-particle dispersion are challenging as they require achieving a wide range separation between the dissipation scale and the integral scale of the flow [87, 86]. Backward dispersion is particularly difficult because it involves integrating the Navier-Stokes equation forward in time and tracking the tracers backward in time. Most of the work on deterministic particle dispersion has therefore been in the forward-in-time setting. There the t^3 scaling has been numerically and experimentally thoroughly investigated though the physical mechanisms behind this growth are not completely well understood. Furthermore, it has been observed that backward and forward dispersion are quantitatively different [88, 36, 6]. For example, particles are observed to spread faster backwards-in-time than forwards. Since it is backward and not forward particle dispersion that matters for understanding mixing of passive fields, conclusive studies on scaling laws for backwards particle separations are of great importance.

2.2 Deterministic Tracers

Consider a passive tracer with position $\mathbf{x}(t)$ advected by the velocity field $\mathbf{u}$ and whose second derivative is the acceleration field $\mathbf{a}$. For a Navier-Stokes velocity $\mathbf{u}$, the $\mathbf{a}$ is given by: $\mathbf{a} \equiv \mathbf{f}_{\text{ext}} - \nabla p + \nu \triangle \mathbf{u}$. The tracer is labeled at the final time t_f and travels backward for times $t \leq t_f$. The dynamical relations are

$$\frac{\mathrm{d}}{\mathrm{d}t}\mathbf{x}(t) = \mathbf{u}(\mathbf{x}(t), t), \quad \mathbf{x}(t_f) = \mathbf{x}_f, \tag{2.1}$$

$$\frac{\mathrm{d}}{\mathrm{d}t}\mathbf{u}(\mathbf{x}(t), t) = \mathbf{a}(\mathbf{x}(t), t). \tag{2.2}$$

Defining $\tau(s) \equiv s - t$ and $\tau \equiv \tau(t_f)$, it follows from equations (2.1) and (2.2) that

$$\mathbf{x}(t) = \mathbf{x}_f - \tau \mathbf{u}(\mathbf{x}_f, t_f) + \int_t^{t_f} \tau(s)\mathbf{a}(\mathbf{x}(s), s)\mathrm{d}s. \tag{2.3}$$

The backward separation of particle pairs separated by $\mathbf{r}_f$ at the final time is $\mathbf{r}(\tau) \equiv \mathbf{x}(t; \mathbf{x}_f + \mathbf{r}_f) - \mathbf{x}(t; \mathbf{x}_f)$. The space-averaged squared separation satisfies:

$$\left\langle |\mathbf{r}(\tau) - \mathbf{r}_f|^2 \right\rangle_{\mathbf{x}_f} = \tau^2 S_2^{\mathbf{u}}(\mathbf{r}_f) + \left\langle \left| \int_t^{t_f} \tau(s) \delta \mathbf{a}_L(\mathbf{r}_f; s)\, \mathrm{d}s \right|^2 \right\rangle_{\mathbf{x}_f}$$

$$- 2\tau \int_t^{t_f} \tau(s) \left\langle \delta \mathbf{u}(\mathbf{r}_f; t_f) \cdot \delta \mathbf{a}_L(\mathbf{r}_f; s) \right\rangle_{\mathbf{x}_f} \mathrm{d}s, \tag{2.4}$$

where $S_2^{\mathbf{u}}(\mathbf{r}_f) = \left\langle |\delta \mathbf{u}(\mathbf{r}_f; t_f)|^2 \right\rangle_{\mathbf{x}_f}$ is the second order velocity structure function, $\delta \mathbf{u}(\mathbf{r}_f; t_f) \equiv \mathbf{u}(\mathbf{x}_f + \mathbf{r}_f, t_f) - \mathbf{u}(\mathbf{x}_f, t_f)$ is the Eulerian increment of the velocity field at the final time, $\delta \mathbf{a}_L(\mathbf{r}; s) \equiv \mathbf{a}(\mathbf{x}(s; \mathbf{x}_f + \mathbf{r}_f), s) - \mathbf{a}(\mathbf{x}(s; \mathbf{x}_f), s)$ is the Lagrangian acceleration increment and $\langle \cdot \rangle_{\mathbf{x}_f}$ denotes integration over the final particle positions $\mathbf{x}_f$. This formula is exact – no assumptions were needed to arrive at equation (2.4). The τ^2 term appearing in equation (2.4) is the so-called

Batchelor regime [4] where the particles undergo ballistic motion and is present for all time and is not the result of a short time expansion. Note that in the forward case, the last term would have an opposite sign and $\{\mathbf{u}_f, \mathbf{r}_f, t_f\}$ would be replaced by $\{\mathbf{u}_0, \mathbf{r}_0, t_0\}$. If we consider small τ, then a first order Taylor expansion of equation (2.4) yields:

$$\left\langle |\mathbf{r}(\tau) - \mathbf{r}_f|^2 \right\rangle_{\mathbf{x}_f} \approx S_2^{\mathbf{u}}(\mathbf{r}_f)\tau^2 + 2\langle\varepsilon\rangle_{\mathbf{x}}\tau^3 + \frac{1}{4}S_2^{\mathbf{a}}(\mathbf{r}_f)\tau^4 + \mathcal{O}(\tau^4) \tag{2.5}$$

where $S_2^{\mathbf{a}}(\mathbf{r}_f)$ is the second order acceleration structure function at the initial time. We here have neglected the τ^4 term coming out of the expansion of the last term in (2.4). Although we have no theoretical argument to do so, it agrees with the numerical results presented later. We have also assumed that the initial separation $\mathbf{r}_f$ is in the inertial range so as to use the Ott-Mann relation – an (instantaneous) Lagrangian analogue of the 4/5th law – expressing $\langle \delta\mathbf{u}(\mathbf{r}_f; t_f) \cdot \delta\mathbf{a}(\mathbf{r}_f; t_f) \rangle_{\mathbf{x}_f} \approx -2\langle\varepsilon\rangle_{\mathbf{x}}$ where ε is the viscous energy dissipation [42, 82]. The τ^3 term appearing in (2.5) has been derived in [10] for the forward case with an opposite sign and explored in DNS studies in [13]. The equivalent term to our τ^4 term has also been observed for the case of the velocity difference statistics [13]. There it is described as the initial abrupt variation of the velocity difference and here we can further understand it as a Bachelor-type-range (in a sense of first order expansion in time) for the velocity separation.

2.3 Stochastic Tracers

Consider now the following backward stochastic equation governing the flow of passive tracer particles:

$$\mathrm{d}\widetilde{\mathbf{x}}(t) = \mathbf{u}(\widetilde{\mathbf{x}}(t), t)\mathrm{d}t + \sqrt{2\kappa}\ \hat{\mathrm{d}}\mathbf{W}_t, \quad \widetilde{\mathbf{x}}(t_f) = \mathbf{x}_f. \tag{2.6}$$

Here κ is the molecular diffusivity, $\mathbf{W}_t$ is the standard Brownian motion and $\hat{\mathrm{d}}$ is the backwards Itô differential [63]. Note that if the viscosity of the fluid is fixed and $\kappa \to 0$, we recover the deterministic equation (2.1). Along a path defined by equation (2.6), the backward Itô lemma [63, 27] can be used to show that the Navier-Stokes velocity satisfies

$$\begin{aligned}
\mathrm{d}\mathbf{u}(\widetilde{\mathbf{x}}(t),t) &= (\partial_s \mathbf{u} + \mathbf{u}\cdot\nabla\mathbf{u} - \kappa\Delta\mathbf{u}) \mid_{(\widetilde{\mathbf{x}}(t),t)} \mathrm{d}t + \sqrt{2\kappa}\nabla\mathbf{u} \mid_{(\widetilde{\mathbf{x}}(t),t)} \cdot\hat{\mathrm{d}}\mathbf{W}_t \\
&= ((\nu-\kappa)\Delta\mathbf{u} - \nabla p) \mid_{(\widetilde{\mathbf{x}}(t),t)} \mathrm{d}t + \sqrt{2\kappa}\nabla\mathbf{u} \mid_{(\widetilde{\mathbf{x}}(t),t)} \cdot\hat{\mathrm{d}}\mathbf{W}_t \\
&= \mathbf{a}^{\kappa}(\widetilde{\mathbf{x}}(t),t)\mathrm{d}t + \sqrt{2\kappa}\nabla\mathbf{u} \mid_{(\widetilde{\mathbf{x}}(t),t)} \cdot\hat{\mathrm{d}}\mathbf{W}_t, \qquad (2.7)
\end{aligned}$$

This is a stochastic generalization of equation (2.2). The quadratic variation term $-\kappa\Delta\mathbf{u}$ appearing in the backward Itô Lemma has the opposite sign than the forward case which would yield a similar expression but with $\mathbf{a}^{\kappa}_{\text{forw}} \equiv \mathbf{f}_{\text{ext}} - \boldsymbol{\nabla} p + (\nu+\kappa)\Delta\mathbf{u}$. By integrating, we obtain

$$\begin{aligned}
\widetilde{\mathbf{x}}(t) &= \mathbf{x}_f - \tau\mathbf{u}(\mathbf{x}_f,t_f) + \int_t^{t_f} \tau(s)\mathbf{a}^{\kappa}(\widetilde{\mathbf{x}}(s),s)ds \\
&+ \sqrt{2\kappa}\int_t^{t_f} \tau(s)\boldsymbol{\nabla}\mathbf{u}(\widetilde{\mathbf{x}}(s),s)\cdot\hat{\mathrm{d}}\mathbf{W}_s - \sqrt{2\kappa}\mathbf{W}_t. \qquad (2.8)
\end{aligned}$$

This equation is the analogue of equation (2.3) but for paths with intrinsic additive white noise. Note that setting $\kappa = \nu$ leads to a dramatic simplification where the laplacian term in the acceleration vanishes: $\mathbf{a}^{\nu} = \mathbf{f}_{\text{ext}} - \nabla p$. Further, Eyink in [36] has shown strong evidence that the backward dispersion is independent of κ at long times. Motivated by its simplicity and the result of [36], for the remainder of this thesis – in both the theoretical and numerical results – we make the choice of $\kappa = \nu$, i.e. we study unity Schmidt/Prandtl numbers.

Consider two trajectories $\widetilde{\mathbf{x}}^1(t)$ and $\widetilde{\mathbf{x}}^2(t)$ ending at the same point $\mathbf{x}_f$ and satisfying equation (2.6) with independent Brownian motions $\mathbf{W}^1$ and $\mathbf{W}^2$ respectively. The natural object of study in this setting is the spaced averaged mean (in the sense of averaging over the Brownian motions) squared distance $\tilde{\mathbf{r}}(\tau) \equiv \widetilde{\mathbf{x}}^1(t_f - \tau) - \widetilde{\mathbf{x}}^2(t_f - \tau)$ between the trajectories advected by independent Brownian motions. In the deterministic case, in order to study the squared separation of two particles it was necessary to consider particles which (at the final time) were separated by a positive distance $|\mathbf{r}_f|$. In the stochastic setting this is no longer necessary and starting particles at the same point effectively removes the dependence on the final separation and final velocity difference. We have:

$$\begin{aligned} |\widetilde{\mathbf{r}}(\tau) + \sqrt{2\nu}\delta\mathbf{W}_t|^2 = &\left| \delta \int_t^t \tau(s)\mathbf{a}^\nu(\widetilde{\mathbf{x}}(s), s)\mathrm{d}\tau \right|^2 \\ &+ 2\sqrt{2\nu} \int_t^{t_f} \int_t^{t_f} \tau(s)\tau(s')\delta\mathbf{a}^\nu(\widetilde{\mathbf{x}}(s), s) \cdot \delta \left[\nabla\mathbf{u}(\widetilde{\mathbf{x}}(s'), s') \cdot \hat{\mathrm{d}}\mathbf{W}_{s'} \right] \mathrm{d}s \\ &+ 2\nu \left| \delta \int_t^{t_f} \tau(s) \boldsymbol{\nabla}\mathbf{u}(\widetilde{\mathbf{x}}(s), s) \cdot \hat{\mathrm{d}}\mathbf{W}_s \right|^2 \end{aligned} \tag{2.9}$$

Lets consider the last term on the right hand side and take the expectation over the two independent Brownian motions. We get by Itô isometry

$$\mathbb{E}_{1,2}\left[\left| \int_t^{t_f} \tau(s)\delta\boldsymbol{\nabla}\mathbf{u}(\widetilde{\mathbf{x}}(s), s) \cdot \hat{\mathrm{d}}\mathbf{W}_s \right|^2 \right] = \mathbb{E}_{1,2}\left[\int_t^{t_f} \tau(s)^2 |\delta\boldsymbol{\nabla}\mathbf{u}(\widetilde{\mathbf{x}}(s), s)|^2 \mathrm{d}s \right]. \tag{2.10}$$

$\mathbb{E}_{1,2}[\cdot]$ being the ensemble average over the two independent Brownian motions. Letting $\langle\cdot\rangle_{\mathbf{x}_f}$ denote the space average, we find using the properties of the Brownian motion and homogeneous and isotropic turbulence

$$\mathbb{E}_{1,2}\left[\langle |\delta\boldsymbol{\nabla}\mathbf{u}(\widetilde{\mathbf{x}}(s), s)|^2 \rangle_{\mathbf{x}_f} \right] = 2\mathbb{E}_{1,2}\left[\langle |\boldsymbol{\nabla}\mathbf{u}(\widetilde{\mathbf{x}}(s), s)|^2 \rangle_{\mathbf{x}_f} \right]. \tag{2.11}$$

The two Brownian motions being independent, the ensemble average over the cross term is identically 0 in equation (2.11). Using the fact that $\langle\varepsilon\rangle_{\mathbf{x}} = \nu\langle|\nabla\mathbf{u}|^2\rangle_{\mathbf{x}}$ we finally obtain

$$\mathbb{E}_{1,2}\left\langle|\widetilde{\mathbf{r}}(\tau)+\sqrt{2\nu}\delta\mathbf{W}_t|^2\right\rangle_{\mathbf{x}_f} = \frac{4}{3}\langle\varepsilon\rangle_{\mathbf{x}}\tau^3 + \mathcal{E}(\tau) \tag{2.12}$$

where

$$\mathcal{E}(\tau) = \mathbb{E}_{1,2}\langle|\delta\mathbf{A}(\tau)|^2\rangle_{\mathbf{x}_f} + \mathbb{E}_{1,2}\left\langle\delta\mathbf{A}(\tau)\delta\mathbf{U}(\tau)\right\rangle_{\mathbf{x}_f}. \tag{2.13}$$

with

$$\mathbf{A}(\tau) = \int_t^t \tau(s)\mathbf{a}^\nu(\widetilde{\mathbf{x}}(s),s)\mathrm{d}\tau \tag{2.14}$$

and

$$\mathbf{U}(\tau) = \int_t^{t_f} \tau(s)\boldsymbol{\nabla}\mathbf{u}(\widetilde{\mathbf{x}}(s),s)\cdot\hat{\mathrm{d}}\mathbf{W}_s. \tag{2.15}$$

If the turbulence is homogeneous, time stationary and space ergodic, then the space averaged energy dissipation $\langle\varepsilon\rangle_{\mathbf{x}}$ is constant in time. If we instead decided to study forward stochastic tracers, then equation (2.12) still holds but with minor differences in the error term including that integral $\mathbf{A}(\tau)$ involve $\mathbf{a}^\nu_{\text{forw}}$ (defined earlier) instead of $\mathbf{a}^\nu$. It is also important to remind the reader that the simplicity of (2.12) is a consequence of the choice of $\kappa = \nu$. The strong evidences shown in [36] that the long time behavior in independent of the choice of κ lead to believe that, despite a more complex analytical form for $\mathbb{E}_{1,2}\left\langle|\widetilde{\mathbf{r}}(\tau)+\sqrt{2\nu}\delta\mathbf{W}_t|^2\right\rangle_{\mathbf{x}_f}$ with $\kappa\neq\nu$, it would yield the same behavior.

2.4 Numerical Results

In order to understand the behavior of the different terms in equation (2.12), we evaluate them using turbulence data from direct numerical simulations. We

use the Johns Hopkins Turbulence Databases (JHTDB) [67, 26], which provides online DNS data over an entire large-eddy turnover time for isotropic and homogeneous turbulence at Taylor-scale Reynolds number $Re_\lambda = 433$. The integration of particle trajectories is performed inside the database using the getPosition functionality [99] and a backward second-order Runge-Kutta integration scheme.

Figure 2.1 shows our results for the different terms in (2.12) compensated by $4/3\langle\varepsilon\rangle_{\mathbf{x}}\tau^3$. Error bars are calculated by the maximum difference between two subensembles of $N/2$ samples and $N = 5 \times 10^8$. The terms $\mathbb{E}_{1,2}\langle|\delta\mathbf{A}(\tau)|^2\rangle_{\mathbf{x}_f}$ and $-\mathbb{E}_{1,2}\left\langle\delta\mathbf{A}(\tau)\delta\mathbf{U}(\tau)\right\rangle_{\mathbf{x}_f}$ behave in a very similar fashion. They grow as τ^5 for short time and seem to reach an asymptotic τ^3 for $\tau \gg \tau_\nu$, τ_ν being the Kolmogorov time-scale. The difference $\mathcal{E}(\tau)$ between these two terms however never exceeds 16% of $4/3\langle\varepsilon\rangle_{\mathbf{x}}\tau^3$ (29% including the error bars) at all points in time. See inset of Figure 2.1. As a consequence of $\mathcal{E}(t)$ being small relative to $4/3\langle\varepsilon\rangle_{\mathbf{x}}\tau^3$, we observe the dispersion is

$$\mathbb{E}_{1,2}\left\langle|\widetilde{\mathbf{r}}(\tau) + \sqrt{2\nu}\delta\mathbf{W}_t|^2\right\rangle_{\mathbf{x}_f} \approx \frac{4}{3}\langle\varepsilon\rangle_{\mathbf{x}}\tau^3 \tag{2.16}$$

for almost three decades.

We now take a moment to speculate on the behavior of particle trajectories for very high Reynolds number turbulence. Note that, by the zeroth law of turbulence $\langle\varepsilon\rangle_{\mathbf{x}}$ tends to a non-zero constant in the inviscid limit. Therefore the $\frac{4}{3}\langle\varepsilon\rangle_{\mathbf{x}}\tau^3$ term will remain for arbitrarily small viscosity. Figure 2.1 shows that, in the inertial range, the terms $\mathcal{E}(t)$ is small compared to $\frac{4}{3}\langle\varepsilon\rangle_{\mathbf{x}}\tau^3$. In the inviscid limit, the inertial range expands to all scales and if $\mathcal{E}(t)$ is generically small in this range then there is good evidence for spontaneous separation of

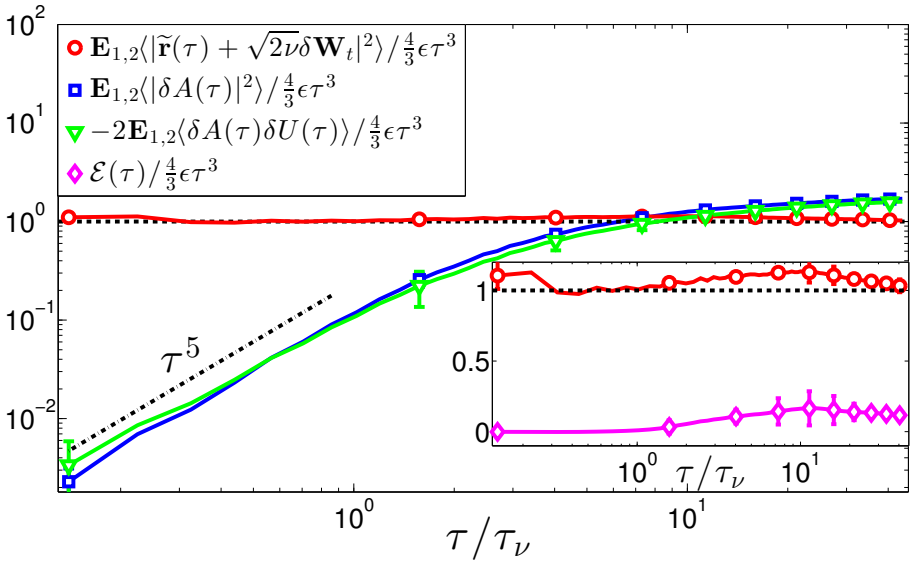

Figure 2.1: Plots of the different terms of equations (2.12) and (2.13). The dash-dotted line goes like τ^5 and the dashed lines represent $\frac{4}{3}\langle\varepsilon\rangle_{\mathbf{x}}\tau^3$. The inset is a closed-up view in semi logarithmic scale to compare the dispersion to $\mathcal{E}(\tau)$.

particle trajectories emanating from a single point in the zero viscosity limit. This is the hallmark of the phenomenon of spontaneous stochasticity [8, 50, 23, 64, 32, 33, 23, 36].

We now compare the stochastic particle dispersion of section 2.3 to the deterministic dispersion of section 2.2 measured for finite final separations. We study the statistics of $\boldsymbol{\rho}(\tau;\mathbf{r}_f) \equiv \mathbf{r}(\tau) - \mathbf{r}_f + \tau\delta\mathbf{u}(\mathbf{r}_f;t_f)$. By doing so, we effectively "remove" the effect of the Bachelor regime and expose a longer range of τ^3 scaling. It is equivalent to consider only the integral term over $\delta\mathbf{a}(\mathbf{r}_f;s)$ in (2.4). It was numerically verified that the quantity $\langle|\boldsymbol{\rho}(\tau;\mathbf{r}_f)|^2\rangle_{\mathbf{x}_f}$ has the asymptotic behavior

$$\left\langle|\boldsymbol{\rho}(\tau;\mathbf{r}_f)|^2\right\rangle_{\mathbf{x}_f} \approx \begin{cases} \langle|\mathbf{r}(\tau)|^2\rangle_{\mathbf{x}_f} & \tau \gg \tau_\nu \\ \frac{\tau^4}{4}S_2^{\mathbf{a}}(\mathbf{r}_f) & \tau \lesssim \tau_\nu \end{cases}. \tag{2.17}$$

In Figure 2.2 we highlight the limiting cases given by (2.17). The inset shows

the $\frac{\tau^4}{4} S_2^{\mathbf{a}}(\mathbf{r}_f)$ scaling law up to $\tau \approx \tau_\nu$ as predicted analytically. In the main plot, results rescaled by $\frac{4}{3}\langle\varepsilon\rangle_{\mathbf{x}}\tau^3$ are shown for eight different final separations $r_f \in [\eta, 20\eta]$ where η is the Kolmogorov length scale and T_L is the large scale turn-over time. The dispersion of the particles advected by the Brownian motion is in good agreement with the deterministic separations and all the curves tend to converge toward the stochastic dispersion. Defining $g_{\mathbf{r}_f} = \langle|\boldsymbol{\rho}(T_L;\mathbf{r}_f)|^2\rangle_{\mathbf{x}_f} / \langle\varepsilon\rangle_{\mathbf{x}} T_L^3$, we record these measured "Richardson constant" values in Table 2.1. The longest τ^3 scaling (one decade) observed for deterministic dispersion is for $|\mathbf{r}_f| = 6\eta$ and $g_{6\eta} = 4/3$ within numerical error. Note that in backwards setting, our measured Richardson constant is larger than forward results ($g \approx 0.5, 0.52$) [86, 10, 13] and is in good agreement with the measurements in [88, 6, 36].

We have also numerically calculated the probability distribution functions (PDF) $P(\rho,\tau)$, $P(\widetilde{\rho},\tau)$ for the deterministic ρ and stochastic $\widetilde{\rho}$ where $\rho \equiv \sqrt{\langle|\boldsymbol{\rho}(\tau;\mathbf{r}_f)|^2\rangle_{\mathbf{x}_f}}$ and $\widetilde{\rho} = \sqrt{\mathbb{E}_{1,2}\left\langle|\widetilde{\mathbf{r}}(\tau) + \sqrt{2\nu}\delta\mathbf{W}_t|^2\right\rangle_{\mathbf{x}_f}}$. Figure 2.3 plots for $\tau = T_L$ the probability distributions with similarity scaling. The straight dashed line is the Richardson PDF:

$$P(\rho,t) = \frac{B}{\langle\rho(\tau)^2\rangle} \exp\left[-A\left(\frac{\rho}{\langle\rho(\tau)^2\rangle^{1/2}}\right)^{2/3}\right]. \tag{2.18}$$

All the curves are in good agreement with each others and Richardson for $0.4 \lesssim$

Table 2.1: Values of $g_{\mathbf{r}_f}$

$\lvert\mathbf{r}_f\rvert/\eta$	4	6	8	
$g_{\mathbf{r}_f}/(4/3)$	0.86 ± 0.10	0.99 ± 0.08	1.17 ± 0.02	
$\lvert\mathbf{r}_f\rvert/\eta$	1	3	10	20
$g_{\mathbf{r}_f}/(4/3)$	0.50 ± 0.07	0.76 ± 0.01	1.24 ± 0.07	1.71 ± 0.05

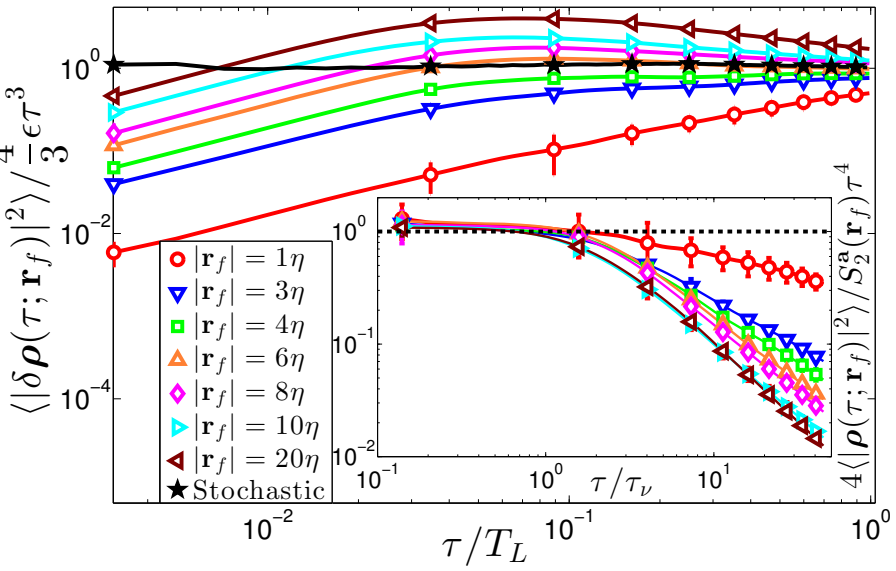

Figure 2.2: Particle dispersion $\langle|\boldsymbol{\rho}(\tau;\mathbf{r}_f)|^2\rangle_{\mathbf{x}_f}$ for eight different initial separations in pure DNS data compared to the dispersion for the stochastic advection model. The curves are compensated by $\frac{4}{3}\langle\varepsilon\rangle_{\mathbf{x}}\tau^3$. The inset shows the same pure DNS curves (without the stochastic case) rescaled by $\frac{\tau^4}{4}S_2^{\mathbf{a}}(\mathbf{r}_f)$. The dashed line represents $\frac{\tau^4}{4}S_2^{\mathbf{a}}(\mathbf{r}_f)$.

$(\rho/\sqrt{\langle\rho(\tau)^2\rangle})^{2/3} \lesssim 2$. Note that L, the integral scale, we have

$$\left(L/\sqrt{\frac{4}{3}\langle\varepsilon\rangle_{\mathbf{x}}T_L^3}\right)^{2/3} \simeq 1.24 \tag{2.19}$$

in our case. Particle separations beyond that limit are outside the inertial range. Notice that the PDFs tends to spike above the Richardson PDF at small ρ indicating strong intermittency at small scales.

Figure 2.4 plots the PDF for the stochastic advection model at seven different times $\tau \in [0.023\tau_\nu, 44.1\tau_\nu]$. The probability distribution exhibits a clear self-similarity behavior for $0 \lesssim (\rho/\sqrt{\langle\rho(\tau)^2\rangle})^{2/3} \lesssim 2$ at all times. Note that even though we effectively removed the dependency of the dispersion on the final separation, the PDF is still not well described by Richardson (2.18) at large

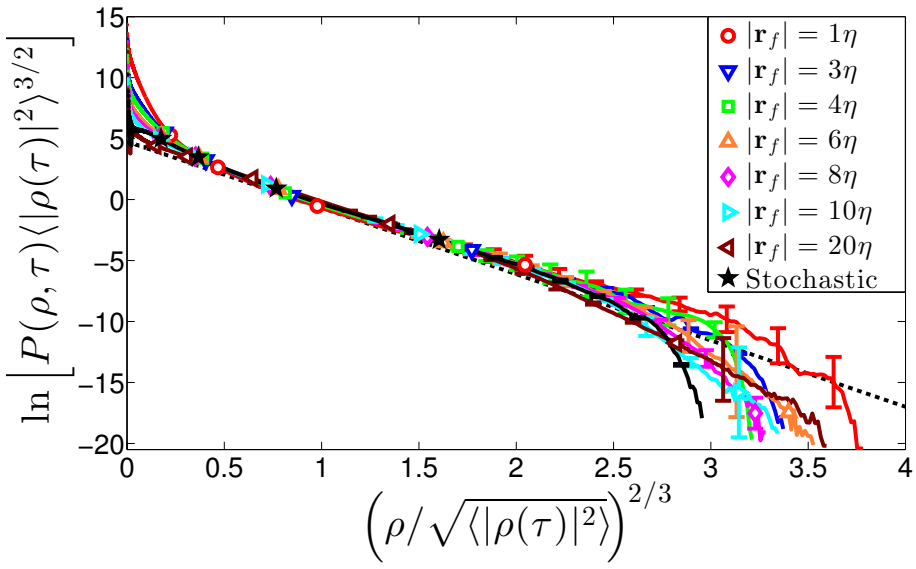

Figure 2.3: Pair separation PDF for eight different initial separations in pure DNS data compared to the dispersion for the stochastic advection model with similarity scaling. Infinite Reynolds self-similar PDFs are shown for Richardson (straight dashed line).

scales (greater than 2 in similarity units) as the pairs are outside the inertial range (see (2.19)).

2.5 Conclusion

We have investigated properties of backward dispersion for both deterministic and stochastic particle passive tracers in a turbulent flow. This is the highest Reynolds number investigation so far of backward 2-particle dispersion in turbulence. We analytically predicted small time rms behavior for deterministic backwards dispersion and investigated the τ^4-scaling law numerically. We also looked at the convergence towards a long-time τ^3 scaling law of the backwards

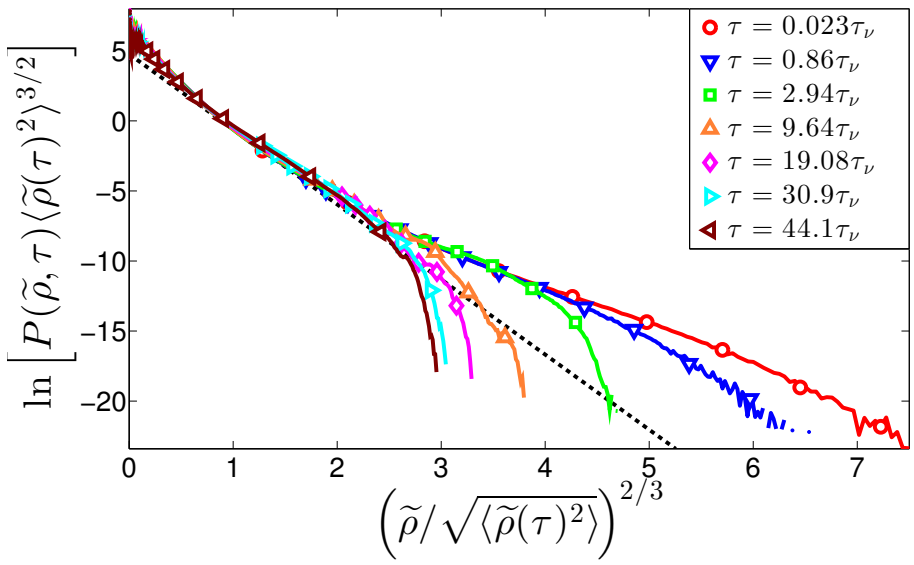

Figure 2.4: Pair separation PDF for seven different times for the stochastic advection case with similarity scaling. The straight dashed line is the Infinite Reynolds self-similar PDF.

dispersion for different final separations. In addition, we developed a mathematical formalism for studying backwards stochastic particle trajectories with additive white noise. Using this formalism we derived a formula for the mean dispersion and showed that the main contribution to this dispersion is an exact $4/3\langle\varepsilon\rangle_{\mathbf{x}}\tau^3$ term which was calculated analytically (Figure 2.1). We showed a striking agreement between the deterministic and stochastic cases for long times as all the dispersions seem to converge toward $4/3\langle\varepsilon\rangle_{\mathbf{x}}\tau^3$ (Figure 2.2). There has been previous attempts to derive an analytical value for the Richardson constant [15] and it is the first time an exact t^3 contribution is derived with a simple numerical value for the Richardson constant in the backward case. Finally, we numerically computed the PDFs of particle separations in both the deterministic and stochastic settings. In agreement with previous results for the

forward case, the PDFs seem to be well described by Richardson probability distribution for the same similarity units range. As in the case of dispersion, the stochastic and deterministic case are in good agreement in this range. Not only does the $4/3\langle\varepsilon\rangle_{\mathbf{x}}\tau^3$ persist for all times, the PDF of the stochastic dispersion is self-similar for all times up to 2 (in similarity units).

There are a number of ways that the ideas in this work could be further pursued. First, we find it theoretically appealing that energy dissipation – under mild assumptions – can be related in a simple manner to the particle dispersion. It would be interesting to probe the implications to the "zeroth law of turbulence" from our framework. Next, in the present work, we make a particular choice of the noise strength which seems to be privileged for the case of backwards particle dispersion. It would therefore be interesting to do a systematic study of the effect of changing the noise strength on the squared separation and probability distributions of the particles. It would also be of great interest to use this formalism to – for example – predict features of multipoint statistical observables [44]. In principle one could study these quantities by using stochastic Lagrangian tracers and directly applying Itô calculus methods coupled with numerics.

Chapter 3

The Diffusion Approximation in Turbulent Two-Particle Dispersion

3.1 Introduction

L. F. Richardson, in a classic paper [83], initiated the study of dispersion of particle pairs in turbulent flows, introducing a diffusion model with a scale-dependent eddy-diffusivity. There has since been much discussion about the accuracy of this description. In the case of advection by a Gaussian random velocity field which is white-noise in time, the Kraichnan rapid-change model [62], the diffusion approximation is known to be exact [41]. This fact has led to a common idea that Richardson's diffusion theory requires for its validity a quasi-Gaussian velocity field that is nearly delta-correlated in time [41, 89, 12, 11]. Nevertheless, several numerical studies, including those in the previous chapters, have shown that the key predictions of Richardson's diffusion equation for the pair-separation probability density, such as its self-similarity in time and the precise stretched-exponential form, hold quite accurately in Navier-Stokes turbulence over a range of separations $0.5-2$ rms [9, 36, 11]. If Richardson's theory

required delta-correlated Gaussian velocities, then this would be quite puzzling, because the statistics and time-correlations of the true turbulent velocities are quite different. It is the purpose of this chapter to justify carefully the (limited) applicability of Richardson's diffusion theory to turbulent 2-particle dispersion. Our approach also helps to explain deviations from Richardson's theory and to develop improved approximations, both topics of current interest [89, 12, 11].

3.2 An exact diffusion equation for turbulence

Let $\mathbf{u}(\mathbf{x}, t)$ be the random turbulent velocity field and let $\mathbf{x}_\mathbf{u}(t; \mathbf{x}_0, t_0)$ be the fluid particle position that satisfies

$$\frac{d}{dt}\mathbf{x}(t) = \mathbf{u}(\mathbf{x}, t) \tag{3.1}$$

and $\mathbf{x}(t_0) = \mathbf{x}_0$. Define also the Lagrangian fluid velocity

$$\mathbf{u}(t|\mathbf{x}_0, t_0) = \mathbf{u}(\mathbf{x}_\mathbf{u}(t|\mathbf{x}_0, t_0), t).$$

Here $\mathbf{u}(t|\mathbf{x}_0, t_0)$ is the velocity at time t of the fluid particle at $\mathbf{x}_0$ at time t_0. Define the "fine-grained PDF" of particle separations

$$P_\mathbf{u}(\mathbf{r}, t|\mathbf{x}_0, \mathbf{r}_0, t_0) = \delta^3(\mathbf{r} - \mathbf{R}_\mathbf{u}(t|\mathbf{x}_0, \mathbf{r}_0, t_0)) \tag{3.2}$$

with

$$\mathbf{R}_\mathbf{u}(t|\mathbf{x}_0, \mathbf{r}_0, t_0) = \mathbf{x}_\mathbf{u}(t|\mathbf{x}_0 + \mathbf{r}_0, t_0) - \mathbf{x}_\mathbf{u}(t|\mathbf{x}_0, t_0)$$

the vector separation at time t of the two particles starting at $\mathbf{x}_0$ and $\mathbf{x}_0 + \mathbf{r}_0$ at time t_0. The transition probability for 2-particle separations is given by

$$P(\mathbf{r}, t|\mathbf{r}_0, t_0) = \langle P_\mathbf{u}(\mathbf{r}, t|\mathbf{x}_0, \mathbf{r}_0, t_0)\rangle \tag{3.3}$$

where the average is over the random velocity field $\mathbf{u}$.

Taking the time-derivative of (3.2) and using (3.1) it is a calculus exercise to show that

$$\partial_t P_{\mathbf{u}}(\mathbf{r}, t|\mathbf{x}_0, \mathbf{r}_0, t_0) = \\ -\boldsymbol{\nabla}_{\mathbf{r}} \cdot \Big[\Big(\mathbf{u}(t|\mathbf{x}_0 + \mathbf{r}_0, t_0) - \mathbf{u}(t|\mathbf{x}_0, t_0) \Big) P_{\mathbf{u}}(\mathbf{r}, t|\mathbf{x}_0, \mathbf{r}_0, t_0) \Big]. \tag{3.4}$$

This equation may be rewritten in integral form as

$$P_{\mathbf{u}}(\mathbf{r}, t|\mathbf{x}_0, \mathbf{r}_0, t_0) = \delta^3(\mathbf{r} - \mathbf{r}_0) \\ -\boldsymbol{\nabla}_{\mathbf{r}} \cdot \int_{t_0}^{t} ds \ \Big[\Big(\mathbf{u}(s|\mathbf{x}_0 + \mathbf{r}_0, t_0) - \mathbf{u}(s|\mathbf{x}_0, t_0) \Big) \\ \times P_{\mathbf{u}}(\mathbf{r}, s|\mathbf{x}_0, \mathbf{r}_0, t_0) \Big]. \tag{3.5}$$

Substituting (3.5) back into (3.4) gives

$$\partial_t P_{\mathbf{u}}(\mathbf{r}, t|\mathbf{x}_0, \mathbf{r}_0, t_0) \\ = -\boldsymbol{\nabla}_{\mathbf{r}} \cdot \left[\left(\mathbf{u}(t|\mathbf{x}_0 + \mathbf{r}_0, t_0) - \mathbf{u}(t|\mathbf{x}_0, t_0) \right) \delta^3(\mathbf{r} - \mathbf{r}_0) \right] \\ +\partial_{r_i} \partial_{r_j} \int_{t_0}^{t} ds \ \left(u_i(t|\mathbf{x}_0 + \mathbf{r}_0, s) - u_i(t|\mathbf{x}_0, t_0) \right) \\ \times \left(u_j(s|\mathbf{x}_0 + \mathbf{r}_0, t_0) - u_j(s|\mathbf{x}_0, t_0) \right) \\ \times P_{\mathbf{u}}(\mathbf{r}, s|\mathbf{x}_0, \mathbf{r}_0, t_0). \tag{3.6}$$

This is an exact equation for $P_{\mathbf{u}}(\mathbf{r}, t|\mathbf{x}_0, \mathbf{r}_0, t_0)$.

It remains to average over the random velocity field $\mathbf{u}$. Assuming statistical space-homogeneity,

$$\langle \mathbf{u}(t|\mathbf{x}_0 + \mathbf{r}_0, t_0) \rangle = \langle \mathbf{u}(t|\mathbf{x}_0, t_0) \rangle.$$

Thus, averaging the first term in (3.6) over $\mathbf{u}$ with $\mathbf{r}_0$ fixed gives a vanishing result. Finally, using the definition of the conditional expectation

$$\Big\langle A \Big| \mathbf{R}(s|\mathbf{x}_0, \mathbf{r}_0, t_0) = \mathbf{r} \Big\rangle = \frac{\Big\langle A P_{\mathbf{u}}(\mathbf{r}, t|\mathbf{x}_0, \mathbf{r}_0, t_0) \Big\rangle}{P(\mathbf{r}, t|\mathbf{r}_0, t_0)},$$

and the fact that

$$\begin{aligned}
&(u_i(t|\mathbf{x}_0+\mathbf{r}_0,s)-u_i(t|\mathbf{x}_0,t_0))\\
&\quad\times(u_j(s|\mathbf{x}_0+\mathbf{r}_0,t_0)-u_j(s|\mathbf{x}_0,t_0))\,P_{\mathbf{u}}(\mathbf{r},s|\mathbf{x}_0,\mathbf{r}_0,t_0)\\
&=(u_i(t|\mathbf{x}(s)+\mathbf{r},s)-u_i(t|\mathbf{x}(s),s))\\
&\quad\times(u_j(\mathbf{x}(s)+\mathbf{r},s)-u_j(\mathbf{x}(s),s))\,P_{\mathbf{u}}(\mathbf{r},s|\mathbf{x}_0,\mathbf{r}_0,t_0) \qquad (3.7)
\end{aligned}$$

we see that averaging the second term in (3.6) gives

$$\partial_t P(\mathbf{r},t|\mathbf{r}_0,t_0)=\partial_{r_i}\partial_{r_j}\int_{t_0}^{t}ds\,S_{ij}(t;\mathbf{r},s|\mathbf{r}_0,t_0)P(\mathbf{r},s|\mathbf{r}_0,t_0), \qquad (3.8)$$

where $S_{ij}(t;\mathbf{r},s|\mathbf{r}_0,t_0)$ is the following 2-time Lagrangian, conditionally-averaged 2nd-order structure function:

$$\begin{aligned}
S_{ij}(t;\mathbf{r},s|\mathbf{r}_0,t_0)=\Big\langle\Big(u_i(t|\mathbf{x}(s)+\mathbf{r},s)-u_i(t|\mathbf{x}(s),s)\Big)\times\\
\Big(u_j(\mathbf{x}(s)+\mathbf{r},s)-u_j(\mathbf{x}(s),s)\Big)\Big|\mathbf{R}(s|\mathbf{x}_0,\mathbf{r}_0,t_0)=\mathbf{r}\Big\rangle \qquad (3.9)
\end{aligned}$$

An equivalent expression can be derived for the conditional Lagrangian structure function in (3.9) by inserting $\int d^3x\,\delta^3(\mathbf{x}-\mathbf{x}(s))=1$ inside the average and then changing the order of space-integral and expectation to obtain

$$\begin{aligned}
S_{ij}(t;\mathbf{r},s|\mathbf{r}_0,t_0)=\int d^3x\;P(\mathbf{x},s|\mathbf{x}_0,\mathbf{r}_0,t_0;\mathbf{r},s)\Big\langle[u_i(t|\mathbf{x}+\mathbf{r},s)-u_i(t|\mathbf{x},s)]\\
\times[u_j(\mathbf{x}+\mathbf{r},s)-u_j(\mathbf{x},s)]\Big|\mathbf{x}+\mathbf{r},\mathbf{x},s;\mathbf{x}_0+\mathbf{r}_0,\mathbf{x}_0,t_0\Big\rangle, \qquad (3.10)
\end{aligned}$$

where $P(\mathbf{x},s|\mathbf{x}_0,\mathbf{r}_0,t_0;\mathbf{r},s)$ is the transition probability for a single particle starting at $\mathbf{x}_0$ at time t_0 to arrive at $\mathbf{x}$ at time s, conditioned on a second particle starting at $\mathbf{x}_0+\mathbf{r}_0$ at time t_0 and arriving at $\mathbf{x}+\mathbf{r}$ at time s.

The exact equation (3.8) (or (3.10)) can be rewritten as

$$\partial_t P(\mathbf{r},t|\mathbf{r}_0,t_0)=\partial_{r_i}\partial_{r_j}\left[K^*_{ij}(\mathbf{r},t|\mathbf{r}_0,t_0)P(\mathbf{r},t|\mathbf{r}_0,t_0)\right], \qquad (3.11)$$

with

$$K^*_{ij}(\mathbf{r},t|\mathbf{r}_0,t_0) = \int_{t_0}^{t} ds\, S_{ij}(t;\mathbf{r},s|\mathbf{r}_0,t_0)\frac{P(\mathbf{r},s|\mathbf{r}_0,t_0)}{P(\mathbf{r},t|\mathbf{r}_0,t_0)}. \tag{3.12}$$

The equation (3.11) is not, of course, a diffusion equation (or even Markovian) because the "diffusion tensor" (3.12) depends on the entire past history of the separation PDF itself. However, the results (4.36),(3.12) imply that, for any choice of initial $\mathbf{r}_0, t_0$, there is a true Markov diffusion process which yields the same evolution of the separation PDF $P(\mathbf{r},t|\mathbf{r}_0,t_0)$ *for that particular* $\mathbf{r}_0, t_0$. In this precise sense we have solved an "inverse problem" for 2-particle dispersion: for any time sequence $P(\mathbf{r},t|\mathbf{r}_0,t_0),\ t > t_0$ of separation PDF's we have found a corresponding time-dependent diffusion tensor $K^*_{ij}(\mathbf{r},t|\mathbf{r}_0,t_0),\ t > t_0$ which exactly reproduces the PDF's as the solution of a diffusion equation. If the initial data are taken to be random with PDF $P(\mathbf{r}_0,t_0)$, then one can obtain an analogous result by using

$$P(\mathbf{r},t) = \int d^d r_0\ P(\mathbf{r},t|\mathbf{r}_0,t_0)P(\mathbf{r}_0,t_0)$$

to obtain from (3.8)

$$\partial_t P(\mathbf{r},t) = \partial_{r_i}\partial_{r_j}\left[K^*_{ij}(\mathbf{r},t)P(\mathbf{r},t)\right], \tag{3.13}$$

with

$$K^*_{ij}(\mathbf{r},t) = \int_{t_0}^{t} ds \int d^d r_0\, S_{ij}(t;\mathbf{r},s|\mathbf{r}_0,t_0)P(\mathbf{r},s|\mathbf{r}_0,t_0)\frac{P(\mathbf{r}_0,t_0)}{P(\mathbf{r},t)}. \tag{3.14}$$

In each case, we obtain an appropriate diffusion equation to reproduce the PDF's. Note that in case of isotropic turbulence the diffusion equation can be simplified to a 1-D equation with the longitudinal component K^*_L with

$$K^*_{ij}(\mathbf{r},t) = K^*_N(r,t)\delta_{ij} + [K^*_L(r,t) - K^*_N(r,t)]\frac{r_i r_j}{r^2}, \tag{3.15}$$

where K_N^* is the normal component.

It is very important to emphasize that no assumption of short correlation times was necessary to derive the diffusion equations (4.36) and (3.13), which hold with very great generality. *Our main thesis is that the (partial) validity of Richardson's diffusion approximation has its explanation in these results and is not due to any short-time correlation property of turbulent velocity fields.* Indeed, as has been noted before (e.g. [41]), the natural correlation time of Lagrangian velocity increments (the eddy-turnover time $\varepsilon^{-1/3}r^{2/3}$) is of the same order as the overall evolution time $t - t_0$ in a Richardson t^3-range. Thus, an assumption of short time-correlations in turbulence is marginal, at best. Previous theoretical attempts by Kraichnan [59] and Lundgren [69] to derive the diffusion equation from first principles (Navier-Stokes) have instead employed a short-time correlation/Markovian assumption which, we will show, is directly responsible for the overestimation of the Richardson's constant by these theories.

3.3 Reasonable Approximations

We exploit the exact equation (3.8) for the transition probability $P(\mathbf{r}, t|\mathbf{r}_0, t_0)$. In Navier-Stokes turbulence the eddies are advected together with the particles and the relative velocity of the pair should decorrelate on the slower scale of the turnover-time of the smallest eddy that contains them. Since this set of eddies remains the same for any velocity $\overline{\mathbf{u}}$ of the pair, there should be no dependence of the conditional average in (3.10) upon $\mathbf{x} - \mathbf{x}_0$. In that case, we can integrate

over $\mathbf{x}$ to obtain

$$S_{ij}(t;\mathbf{r},s|\mathbf{r}_0,t_0) = \langle \delta u_i(t|\mathbf{r},s)\delta u_j(\mathbf{r},s)|\mathbf{r},s;\mathbf{r}_0,t_0\rangle. \tag{3.16}$$

Here $\delta\mathbf{u}(t|\mathbf{r},s;\mathbf{x}) = \mathbf{u}(t|\mathbf{x}+\mathbf{r},s) - \mathbf{u}(t|\mathbf{x},s)$ is the Lagrangian velocity increment in label space. The considerable reduction in complexity of (3.16) compared with (3.10) depends upon the nontrivial sweeping properties of Navier-Stokes turbulence.

A straightforward simplification occurs for $t - t_0 \ll \tau_{r_0}$, where $\tau_r = r/\delta u(r)$ is the eddy-turnover time at separation r. Taylor expansion about $t = t_0$ in (3.35) gives

$$\partial_t P(t) = (t-t_0)\partial_{r^i}\partial_{r^j}\left[S_{ij}(\mathbf{r}_0)\delta^3(\mathbf{r}-\mathbf{r}_0)\right] + O((t-t_0)^2) \tag{3.17}$$

with $S_{ij}(\mathbf{r})$ the usual velocity structure-function tensor. This is an exact result to leading order for $t - t_0 \ll \tau_{r_0}$, corresponding to the Batchelor regime of ballistic separation of particles [4].

Deeper simplifications occur in the long-time limit $t - t_0 \gg \tau_{r_0}$. Note that the correlation function (3.16) is expected to decay in a time $t - s$ of order $\tau_r = r/\delta u(r)$, while the solution $P(\mathbf{r},s)$ is expected to change at a slower rate. For example, self-similar solutions of the type derived by Richardson have the form $P(\mathbf{r},t) = L^{-3}(t)F(\mathbf{r}/L(t))$ with $L(t) \sim (t-t_0)^p$ for some power p, and no dependence on $\mathbf{r}_0, t_0$ at sufficiently long times. Since $L(t)/\dot{L}(t) = t - t_0 \simeq t$, the time-scale for an order one change in $P(\mathbf{r},t)$ is the current time t for any $\mathbf{r}$. Thus, one should be able to substitute $P(\mathbf{r},s)/P(\mathbf{r},t) \simeq 1$ in $K^*_{ij}(t,t_0)$ for those $\mathbf{r}$ with $\tau_r \lesssim t$. This *short-memory approximation* yields a P-independent

"diffusion tensor"

$$K_{ij}(\mathbf{r},t;\mathbf{r}_0,t_0) = \int_{t_0}^{t} ds\ S_{ij}(t;\mathbf{r},s|\mathbf{r}_0,t_0), \quad \tau_r \lesssim t \tag{3.18}$$

Note that this approximation is reasonable for separations r with a sufficiently rapid decay of velocity correlations, but it does *not* assume delta-correlation in time. Similarly, one can argue that the s-dependence through the conditioning event in (3.16) is slow, and approximate

$$S_{ij}(t,s) \simeq \langle \delta u_i(t|\mathbf{r},s)\delta u_j(\mathbf{r},s)|\mathbf{r},t;\mathbf{r}_0,t_0\rangle. \tag{3.19}$$

inside the time-integral (3.18) defining $K(t,t_0)$. Kraichnan and Lundgren [59, 69] went further in their earlier derivations and assumed (implicitly) that the s-dependence in Lagrangian particle labels also is slow. Taking $\mathbf{u}(\mathbf{x},s) = \mathbf{u}(s|\mathbf{x},s) \simeq \mathbf{u}(s|\mathbf{x},t)$, $\mathbf{u}(t|\mathbf{x},s) \simeq \mathbf{u}(t|\mathbf{x},t) = \mathbf{u}(\mathbf{x},t)$ yields

$$S^{KL}_{ij}(t,s) \simeq \langle \delta u_i(\mathbf{r},t)\delta u_j(s|\mathbf{r},t)|\mathbf{r},t;\mathbf{r}_0,t_0\rangle. \tag{3.20}$$

The "diffusion equation" (3.11) with diffusivity $K_{ij}(t,t_0)$ given by (3.18) is valid in the short-time limit $t - t_0 \ll \tau_{r_0}$ also, where it reproduces the exact result (3.17). It is not Markovian in that limit, however, because the "diffusion constant" (3.18) is dependent on $\mathbf{r}_0$, the separation at the initial time t_0. There is strong dependence upon $\mathbf{r}_0$ because $(\mathbf{r}-\mathbf{r}_0)/(t-t_0)$ determines the relative velocity $\mathbf{v}$ of the pair, which is nearly unchanging for short times. However, for $t - t_0 \gtrsim \tau_{r_0}$ one can expect that the diffusivity becomes independent of $\mathbf{r}_0, t_0$. More specifically, one can argue that the conditioning on the event $\{\mathbf{r},t;\mathbf{r}_0,t_0\}$ in the average (3.19) becomes irrelevant if $\mathbf{r}$ is a "typical" separation at time t, with $|\mathbf{r}| \simeq \langle r^2(t)\rangle^{1/2}$. That is, for such typical separations the restricted ensemble is

representative of the entire ensemble and the average may be evaluated without the condition:

$$S_{ij}(t,s) \simeq \langle \delta u_i(t|\mathbf{r},s)\delta u_j(\mathbf{r},s)\rangle, \quad |\mathbf{r}| \simeq \langle r^2(t)\rangle^{1/2} \tag{3.21}$$

We shall refer to this as the *mean-field approximation*, because it ignores fluctuations effects in separation $\mathbf{r}$ (within the stated limits). Notice when the Richardson law $\langle r^2(t)\rangle \sim \varepsilon t^3$ holds, then the condition $r \lesssim \langle r^2(t)\rangle^{1/2}$ coincides with the condition $\tau_r \lesssim t$ in (3.18) for $\tau_r = \varepsilon^{-1/3} r^{2/3}$. However, in addition to avoiding unusually large separations $r \gg \langle r^2(t)\rangle^{1/2}$ one must also in (3.21) avoid unusually small separations $r \ll \langle r^2(t)\rangle^{1/2}$. Both of these conditions can be expected to alter the statistics of velocity increments substantially. Notice that a similar mean-field approximation may be made in (3.20), yielding the Kraichnan-Lundgren (KS) formula for the eddy-diffusivity [59, 69]. In either case, a Markovian diffusion equation is obtained for evolution of the probability distribution of pair-separations in the range $r \simeq \langle r^2(t)\rangle^{1/2}$.

3.4 Comparison with Kraichnan and Lundgren theories

Since our derivation is very closely related to that of Lundgren [69], it is worthwhile to point out the significant differences. The first steps of the derivation are, in fact, identical. Like us, Lundgren employs a "fine-grained PDF" [his eq.(2.7)] and his equation (2.6) is essentially the same as our equation (3.18). However, from this point the derivations crucially deviate. In particular, Lundgren never obtained the analogue of our equation (3.19) which, when substituted

back into (3.18) and averaged over velocity statistics yields our exact diffusion equations. Instead, Lundgren's argument—translated into our notations—was to solve the equation

$$\frac{d}{dt}\mathbf{R}_{\mathbf{u}}(t|\mathbf{x}_0, \mathbf{r}_0, t_0) = \mathbf{u}(t|\mathbf{x}_0 + \mathbf{r}_0, t_0) - \mathbf{u}(t|\mathbf{x}_0, t_0)$$

by a formal integration

$$\mathbf{R}_{\mathbf{u}}(t|\mathbf{x}_0, \mathbf{r}_0, t_0) = \mathbf{r}_0 + \int_{t_0}^{t} ds\,[\mathbf{u}(s|\mathbf{x}_0 + \mathbf{r}_0, t_0) - \mathbf{u}(s|\mathbf{x}_0, t_0)],$$

and then substitute the latter into the analogue of our eqs.(3.2) and (3.4). The results are Lundgren's equations (2.6) and (2.10), which are exact but *not* of the form of a diffusion equation. Lundgren only obtained a diffusion equation [his equation (2.12)] by several subsequent approximations, including Taylor-expansion of (coarse-grained) PDF's which are assumed to be smooth and—especially— a hypothesis of short-time correlations. Quoting directly from Lundgren's 1981 paper (p.31):

> "It is now assumed that Δt is larger than the correlation time of the velocity field so that $f(t - \Delta t)$ will be statistically independent of the current time velocity, $\mathbf{u}(\mathbf{x}_j, t)$. ... If the velocity field had vanishingly small correlation time, as for a Markoff process, they would be statistically independent. It will be assumed that they are approximately independent..."

It is one of the central points of this chapter that this hypothesis of short time-correlations is both unnecessary to derive a diffusion equation and is also physically incorrect for turbulent flow. As we show by our numerical work, this

erroneous hypothesis leads to the over-prediction of Richardson's constant by the Kraichnan-Lundgren theory.

As a final note, our derivation makes fewer unnecessary assumptions than that of Kraichnan and Lundgren, e.g. incompressibility is nowhere employed.

3.5 Numerical results

In order to test validity of the physical approximations and to obtain concrete, quantitative results, we may evaluate the theoretical formulas for eddy-diffusivities derived above, both exact and approximate, using turbulence data from numerical simulations. We here evaluate the Kraichnan-Lundgren [59, 69] formula for the case of turbulence which is statistically stationary:

$$K_{ij}^{KL}(\mathbf{r},t) \;=\; \int_{-t}^{0} ds\; \langle \delta u_i(\mathbf{r},0)\delta u_j(s|\mathbf{r},0)\rangle. \tag{3.22}$$

This formula involves pairs of particle trajectories integrated backward in time s from positions displaced by $\mathbf{r}$ at the current time 0. It thus requires space-time data for turbulent velocity fields. We exploit here the JHU Turbulence Database Cluster [67, 54], which provides online data over an entire large-eddy turnover time for isotropic and homogenous turbulence at Taylor-scale Reynolds number $Re_\lambda = 433$. The integration of particle trajectories is performed inside the database using the *getPosition* functionality [99]. Because of isotropy and incompressibility, the diffusivity is fully defined by its longitudinal part $K_L(r,t)$ as a function of $r = |\mathbf{r}|$. The formula (3.22) is used directly for $4\ell_\nu < r < L$, with L the integral scale and l_ν the Kolmogorov scale, by averaging over $N \sim 6\times 10^9$ particle pairs distributed throughout the flow domain and integrating in s by the composite trapezoidal rule. For smaller r, spatial intermittency makes the

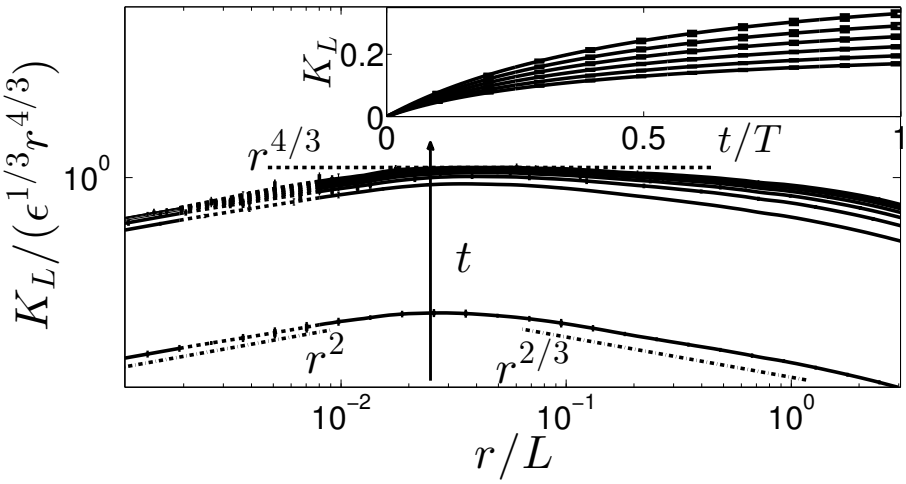

Figure 3.1: $K_L(r,t)$ vs. r for 8 different times $t = \{0.02, 6.74, 13.46, 20.17, 26.89, 33.61, 40.33, 44.79\}t_\nu$. The arrow indicates increasing time. Inset: $K_L(r,t)$ vs. t for 6 values of r around $r \sim 5 \times 10^{-2}L$.

ensemble average converge slowly in N and we instead expand the velocity increments in (3.22) to leading order in $\mathbf{r}$ to obtain $K_L(r,t) = \lambda_L(t)r^2$ with

$$\lambda_T(t) \;=\; \frac{1}{3}\int_{-t}^{0} ds \langle \frac{\partial u_i}{\partial x_j}(\mathbf{r},0)\frac{\partial u_i}{\partial x_j}(s|\mathbf{r},0)\rangle \tag{3.23}$$

and $\lambda_L(t) = \lambda_T(t)/5$ by incompressibility. Cf. [18]. Eq.(3.23) can be evaluated accurately by averaging over only $N = 2 \times 10^4$ single-particle trajectories and the diffusivity for $r > 4l_\nu$ from (3.22) is then spline interpolated to the $r \to 0$ result from (3.23).

Fig. 3.1 plots our results for $K_L(r,t)$ versus r, compensated by $\epsilon^{1/3}r^{4/3}$, for 8 different times $t \in [t_\nu, T_L]$, with t_ν the Kolmogorov time and T_L the large-eddy turnover time. The dashed portion of the curves show the interpolated range. Error bars are calculated by the maximum difference between two subensembles of $N/2$ samples. Both dissipation range scaling $K_L(r,t) \propto r^2$ and short-time Batchelor ballistic range scaling $K_L(r,t) \simeq S_L(r)t$, which follow analytically

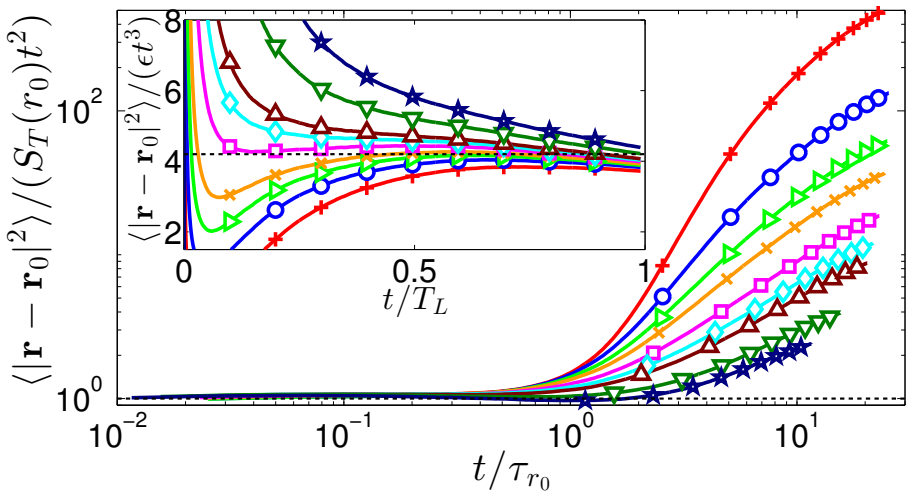

Figure 3.2: (Colors online) Particle dispersion $\langle|\mathbf{r}(t)-\mathbf{r}_0|^2\rangle$ for KL diffusion model compensated by the Batchelor t^2-law, with initial separations $r_0 = l_\nu$ ($+$), $r_0 = 2l_\nu$ ($\circ$), $r_0 = 3l_\nu$ ($\triangleright$), $r_0 = 4l_\nu$ ($\times$), $r_0 = 6l_\nu$ ($\square$), $r_0 = 8l_\nu$ ($\diamond$), $r_0 = 10l_\nu$ ($\triangle$), $r_0 = 20l_\nu$ ($\triangledown$), $r_0 = 35l_\nu$ ($\star$). Inset: curves compensated by t^3.

from (3.22), are observed. For large times the diffusivity converges to a $r^{4/3}$ scaling law for r at the low end of the inertial range ($r \sim 5\times10^{-2}L$). Because τ_r is greater for larger r, one expects slower convergence at the upper end. The inset of Fig. 3.1 shows the diffusivity as a function of time for 6 different r-values in the range $[3, 6.3]\times10^{-2}L$. At late times, K_L increases very slowly and in the inertial range appears to approach at long times a Richardson diffusivity $K_L(r,\infty) = k_0\varepsilon^{1/3}r^{4/3}$ with $k_0 = 1.47$, comparable to Kraichnan's LHDIA prediction $k_0 = 2.00$ [59].

The diffusion model with $K_L(r,t)$ in Fig. 3.1 predicts results for pair dispersion $\langle r^2(t)\rangle$ and PDF $P(r,t)$ which may be compared with results from direct numerical simulation (DNS) for the same turbulence database [36]. To solve the diffusion equation we employ a standard Monte Carlo method [94], using

$N = 10^5$ samples. We first consider pairs separated by various distances r_0 at initial time $t_0 = 0$. Fig. 3.2 for the dispersion $\langle |\mathbf{r}(t) - \mathbf{r}_0|^2 \rangle$ exhibits a clear Batchelor ballistic regime at times $t \ll \tau_{r_0}$. The inset shows convergence toward a t^3 regime for times close to T_L, with a Richardson constant $g \simeq 4$. The best t^3 range occurs for $r_0 = 4\ell_\nu$ (cf. [11]) but there is considerable scatter in the values of g for different r_0. It was found in the previous chapter and in [36] that the Richardson t^3-law is more well-defined for stochastic Lagrangian trajectories solving $d\mathbf{x} = \mathbf{u}(\mathbf{x}, t)dt + \sqrt{2\nu}d\mathbf{W}(t)$ with an added white-noise, all started at the same initial point. For such stochastic trajectories our diffusion model must be modified (to leading order) by adding 2ν to the diagonal elements of $K_{ij}(\mathbf{r}, t)$. Fig. 3.3 plots Monte Carlo results for the dispersion $\langle r^2(t) \rangle$ in this modified diffusion model with $r_0 = 0$, together with DNS results of [36]. The early-time $\sim 12\nu t$-law is reproduced very well by the diffusion model, followed by a reasonable t^3 range. However, the t^3 power-law starts too soon and the Richardson constant is $g \simeq 4.4 \pm 0.2$ (see inset), much larger than the value $g \simeq 0.64$ from DNS [36]. It is well-known that the KL formula when evaluated by closures [59, 69] leads to a value of g which is an order of magnitude too large [82]. Our results show that this defect is intrinsic to the KL theory, even when their diffusivity formula (3.22) is evaluated by Navier-Stokes solutions, not by uncontrolled closures.

To understand why, consider the two main assumptions which led to (3.22). The mean-field approximation has no obvious systematic effect on the rate of dispersion, but the short-memory approximation must increase the diffusivity. Note indeed that the ratio $P(r, s)/P(r, t)$ for $s < t$ in the effective diffusivity $K^*_{ij}(r, t)$ is < 1 at the peak of $r^4 P(r, t)$ where most of the contribution to $\langle r^2(t) \rangle$

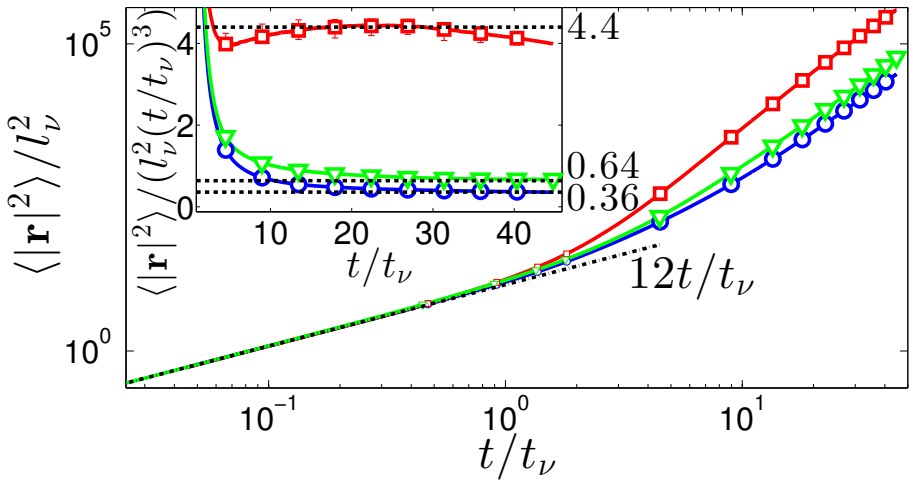

Figure 3.3: Particle dispersion $\langle|\mathbf{r}(t)|^2\rangle$ for the diffusive model with $K_{ij}^{KL}(\mathbf{r},t)$ (□), $K_{ij}^{KL^*}(\mathbf{r},t)$ (○) and the DNS results [36](▽). The straight dash-dotted line is the fit to the diffusive regime. Inset: curves compensated by t^3 (viscous units).

arises, under the normalization $\int r^2 P(r,t)\,dr = 1$. This can be checked for the DNS results of [36] and it is a simple calculus exercise to prove for Richardson's self-similar PDF $P(r,t) = (B/\langle r^2(t)\rangle^{3/2}) \exp\left[-A(r/\langle r^2(t)\rangle^{1/2})^{2/3}\right]$, which agrees well with the DNS. Thus, setting the ratio = 1 increases the diffusivity near the peak. To check whether this effect can account quantitatively for the excess diffusivity in KL theory, we reintroduce the ratio of PDF's into the KL formula, using P-values from [36]:

$$K_{ij}^{KL^*}(\mathbf{r},t) \;=\; \int_{-t}^{0} ds\; \langle \delta u_i(\mathbf{r},0)\delta u_j(s|\mathbf{r},0)\rangle \frac{P(\mathbf{r},s)}{P(\mathbf{r},0)}. \tag{3.24}$$

Monte Carlo results with $N = 10^5$ for this modified KL diffusivity are also plotted in Fig. 3.3, showing a t^3 regime with a reduced Richardson constant $g^* \simeq 0.36 \pm 0.02$. We conclude that the overestimated dispersion in the KL theory is mainly due to the neglect of memory effects.

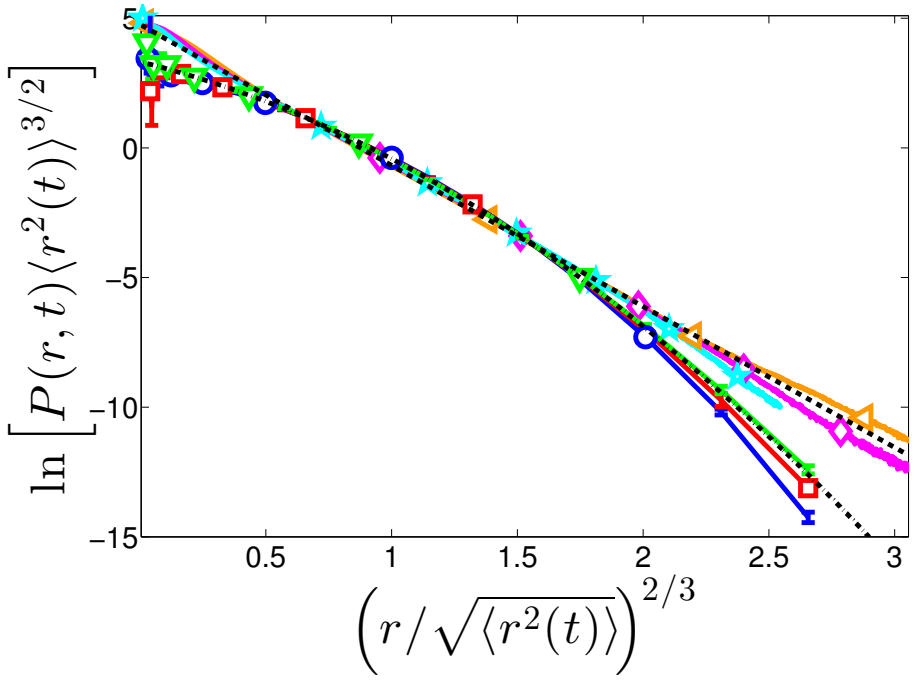

Figure 3.4: The pair separation PDF for our KL diffusion model (DM) and DNS [36] for 3 different times (with viscous units) in the t^3 regime $t = 22.37$ (DM: $\triangledown$, DNS: $\triangleleft$), $t = 33.57$ (DM: $\square$, DNS: $\diamond$)) and $t = 44.79$ (DM: $\circ$, DNS: $\star$). Infinite Reynolds self-similar PDF's are shown for Richardson (straight dashed line) and for KL theory (dot-dashed curve).

Although the short-memory approximation introduces some quantitative errors, it and the other approximations we have made are expected to be qualitatively correct in the limited range of dispersions $r \simeq \langle r^2(t)\rangle^{1/2}$. To test this, Fig. 3.27 plots $P(r,t)$ with similarity scaling at three different times in the t^3 regime for the diffusive model with $K_{ij}^{KL}(\mathbf{r},t)$ (using $N = 10^6$), the DNS results [36], Richardson's self-similar PDF, and the self-similar PDF of KL theory [59, 82]. All the results (different models and different times) collapse well in the range $[0.5, 1.6]$ of the similarity variable $\rho = (r/\langle r^2(t)\rangle^{1/2})^{2/3}$, as expected. It is also true that the DNS results agree better with Richardson's solution over

a longer range, while our KL diffusion model results agree best with the infinite Reynolds-number KL similarity solution. Nothing should be concluded about differences at $\rho > 3.0$, 2.1, 1.6 for the three times, resp., since these lie outside the inertial range. However, differences inside those ranges must be due to the additional approximation (3.20) in KL theory. We expect that a diffusion model based instead on (3.21) should yield a more accurate result.

3.6 Exact Equation for PDF of Pair-Separation & Relative Velocity

The approach developed for the particle separations, combining exact relations, physically motivated approximations and numerical evaluation, can be exploited also in frameworks that extend Richardson's. An old idea [79, 68] is to consider the joint transition probability $P(t) = P(\mathbf{r}, \mathbf{v}, t|\mathbf{r}_0, \mathbf{v}_0, t_0)$ of both the relative position $\mathbf{r}$ and the relative velocity $\mathbf{v}$ of two Lagrangian particles, an approach which has recently received renewed attention [12, 11]. In this case also it is possible to derive exact evolution equations, which can be simplified by the rational approximations presented in section 3.3 to obtain a simplified equation $\partial_t P + \mathbf{v}\cdot\boldsymbol{\nabla}_r P = \partial_{v^i}\partial_{v^j}\left[Q_{ij}(t, t_0)P(t)\right]$ with

$$Q_{ij}(t, s) = \int_{t_0}^{t} ds\ \langle \delta a_i(t|\mathbf{r}, s)\delta a_j(\mathbf{r}, s)|\mathbf{r}, \mathbf{v}, t; \mathbf{r}_0, \mathbf{v}_0, t_0\rangle, \tag{3.25}$$

$\mathbf{a}(\mathbf{x}, t) = -\boldsymbol{\nabla}p + \nu\triangle\mathbf{u} + \mathbf{f}$ is the Eulerian acceleration field for incompressible Navier-Stokes and $\mathbf{a}(t|\mathbf{x}, s)$ is the corresponding Lagrangian field. In deriving these results, a short-memory approximation has been made analogous to that in (3.18) and (3.19) . As has been long understood [79, 68] this approximation is justified for a much greater range of positions (and velocities) than in (3.18)

because the acceleration field is temporally correlated on the scale of the Kolmogorov viscous time $\tau_\nu = (\nu/\varepsilon)^{1/2}$. For times $t - t_0 \lesssim \tau_\nu$, (3.25) implies a velocity ballistic range in which $\langle |\mathbf{v}(t) - \mathbf{v}_0|^2 \rangle \propto t^2$. At longer times, it can be expected that there is no dependence of the diffusivity Q upon $\mathbf{r}_0, \mathbf{v}_0, t_0$, but evidence has been presented in [12] that acceleration increments have strong statistical dependence upon the instantaneous values $\mathbf{r}, \mathbf{v}$ of relative positions and velocities. This implies that the mean-field approximation is more limited in this setting. The formula (3.25) provides a systematic framework within which to explore these dependences and to exploit numerical simulation data to develop a well-founded model.

Formally, the argument is quite similar to that presented in the previous section for the PDF of pair-separation alone. Physically, however, the situation is quite different. As we shall see below, the derivation of the diffusion equation and diffusivity in the form (3.25) uses much more essentially a short time-correlation assumption for the Lagrangian acceleration increments. Furthermore, as has long been realized [73, 68] this type of Markovian assumption is far better justified for accelerations than it is for velocities.

We thus consider the Lagrangian acceleration

$$\mathbf{a}_\mathbf{u}(t|\mathbf{x}_0, t_0) = \frac{d^2}{dt^2}\mathbf{x}_\mathbf{u}(t|\mathbf{x}_0, t_0) = \mathbf{a}(\mathbf{x}_\mathbf{u}(t|\boldsymbol{\xi}, t_0), t), \tag{3.26}$$

where $\mathbf{a}(\mathbf{x}, t) = (\partial_t + \mathbf{u}(\mathbf{x}, t) \cdot \nabla_x)\mathbf{u}(\mathbf{x}, t)$ is the Eulerian acceleration field, and define the fine-grained PDF

$$P_\mathbf{u}(\mathbf{r}, \mathbf{v}, t; \mathbf{v_0}, t_0|\mathbf{x}_0, \mathbf{r}_0, t_0) = \delta^3(\mathbf{r} - \mathbf{x}_\mathbf{u}(t|\mathbf{x}_0 + \mathbf{r}_0, t_0) + \mathbf{x}_\mathbf{u}(t|\mathbf{x}_0, t_0)) \tag{3.27}$$

$$\times \delta^3(\mathbf{v} - \mathbf{u}(t|\mathbf{x}_0 + \mathbf{r}_0, t_0) + \mathbf{u}(t|\mathbf{x}_0, t_0))\, \delta^3(\mathbf{v}_0 - \mathbf{u}(\mathbf{x}_0 + \mathbf{r}_0, t_0) + \mathbf{u}(\mathbf{x}_0, t_0))$$

We take the time derivative of (3.27) and we get

$$\partial_t P_{\mathbf{u}}(t) = -\nabla_{\mathbf{r}} \cdot [\mathbf{v} P_{\mathbf{u}}(t)] - \nabla_{\mathbf{v}} \cdot [(\mathbf{a}(t|\mathbf{x}_0 + \mathbf{r}_0, t_0) - \mathbf{a}(t|\mathbf{x}_0, t_0)) P_{\mathbf{u}}(t)] \quad (3.28)$$

where we employ the simplified notation $P_{\mathbf{u}}(t) = P_{\mathbf{u}}(\mathbf{r}, \mathbf{v}, t; \mathbf{v_0}, t_0|\mathbf{x}_0, \mathbf{r}_0, t_0)$. Let us also introduce the shorthand notation

$$P_{\mathbf{u}}(\mathbf{r} - \mathbf{v}(t-s), s) \equiv P_{\mathbf{u}}(\mathbf{r} - \mathbf{v}(t-s), \mathbf{v}, s; \mathbf{v_0}, t_0|\mathbf{x}_0, \mathbf{r}_0, t_0) \quad (3.29)$$

which allows us to integrate (3.28) formally as

$$P_{\mathbf{u}}(t) = P_{\mathbf{u}}(\mathbf{r} - \mathbf{v}(t-t_0), t_0) \quad (3.30)$$

$$-\nabla_{\mathbf{v}} \cdot \Big[\int_{t_0}^{t} ds \, (\mathbf{a}(s|\mathbf{x}_0 + \mathbf{r}_0, t_0) - \mathbf{a}(s|\mathbf{x}_0, t_0)) \, P_{\mathbf{u}}(\mathbf{r} - \mathbf{v}(t-s), s) \Big].$$

The quantity $P_{\mathbf{u}}(\mathbf{r} - \mathbf{v}(t-s), s)$ has an interesting interpretation. Note that

$$P_{\mathbf{u}}(\mathbf{r} - \mathbf{v}(t-s), s) = \delta^3(\mathbf{r} - \tilde{\mathbf{x}}_{\mathbf{u},s}(t|\mathbf{x}_0 + \mathbf{r}_0, t_0) + \tilde{\mathbf{x}}_{\mathbf{u},s}(t|\mathbf{x}_0, t_0))$$

$$\times \;\; \delta^3(\mathbf{v} - \mathbf{u}(s|\mathbf{x}_0 + \mathbf{r}_0, t_0) + \mathbf{u}(s|\mathbf{x}_0, t_0)) \, \delta^3(\mathbf{v}_0 - \mathbf{u}(\mathbf{x}_0 + \mathbf{r}_0, t_0) + \mathbf{u}(\mathbf{x}_0, t_0))$$

where

$$\tilde{\mathbf{x}}_{\mathbf{u},s}(t|\mathbf{x}_0, t_0) = \mathbf{x}_{\mathbf{u}}(s|\mathbf{x}_0, t_0) + \mathbf{u}(s|\mathbf{x}_0, t_0) \cdot (t - s)$$

is particle position at time t linearly extrapolated from its position and velocity at time s. Note as a special case for $s = t_0$ that

$$P_{\mathbf{u}}(\mathbf{r} - \mathbf{v}(t-t_0), t_0)$$

$$= \delta^3(\mathbf{r} - \mathbf{r}_0 - \mathbf{v}_0(t-t_0))\delta^3(\mathbf{v} - \mathbf{v}_0)) \, \delta^3(\mathbf{v}_0 - \mathbf{u}(\mathbf{x}_0 + \mathbf{r}_0, t_0) + \mathbf{u}(\mathbf{x}_0, t_0))$$

We can now substitute (3.30) into (3.28) to obtain

$$\partial_t P_{\mathbf{u}}(t) + \nabla_{\mathbf{r}} \cdot [\mathbf{v} P_{\mathbf{u}}(t)] \tag{3.31}$$

$$+\nabla_{\mathbf{v}} \cdot [(\mathbf{a}(t|\mathbf{x}_0 + \mathbf{r}_0, t_0) - \mathbf{a}(t|\mathbf{x}_0, t_0)) P_{\mathbf{u}}(\mathbf{r} - \mathbf{v}(t - t_0), t_0)]$$

$$= \partial_{v_i} \partial_{v_j} \Big[\int_{t_0}^{t} ds (a_i(t|\mathbf{x}_0 + \mathbf{r}_0, t_0) - a_i(t|\mathbf{x}_0, t_0))(a_j(s|\mathbf{x}_0 + \mathbf{r}_0, t_0)$$

$$-a_j(s|\mathbf{x}_0, t_0)) P_{\mathbf{u}}(\mathbf{r} - \mathbf{v}(t - s), s) \Big].$$

We average (3.31) over the ensemble of random velocity fields $\mathbf{u}$ to obtain an equation for $P(t) = \langle P_{\mathbf{u}}(t) \rangle$. The average of the first term on the right hand side of (3.31) is

$$\langle (\mathbf{a}(t|\mathbf{x}_0 + \mathbf{r}_0, t_0) - \mathbf{a}(t|\mathbf{x}_0, t_0)) P_{\mathbf{u}}(\mathbf{r} - \mathbf{v}(t - t_0), t_0) \rangle \tag{3.32}$$

$$= \delta^3(\mathbf{r} - \mathbf{r}_0 - \mathbf{v}_0(t - t_0)) \delta^3(\mathbf{v} - \mathbf{v}_0)) \langle \mathbf{a}(t|\mathbf{x}_0 + \mathbf{r}_0, t_0) - \mathbf{a}(t|\mathbf{x}_0, t_0) | \mathbf{v}_0, t_0 \rangle P(\mathbf{v}_0, \mathbf{r}_0, t_0)$$

Note by integrating in time t that

$$\langle (\mathbf{a}(t|\mathbf{x}_0 + \mathbf{r}_0, t_0) - \mathbf{a}(t|\mathbf{x}_0, t_0)) | \mathbf{v}_0, t_0 \rangle = 0, \quad t \geq t_0 \tag{3.33}$$

$$\iff \langle \mathbf{v}(t) | \mathbf{v}_0, t_0 \rangle = \mathbf{v}_0, \quad t \geq t_0$$

Thus, a *martingale property* of the process $\mathbf{v}(t) = \mathbf{u}(t|\mathbf{x}_0 + \mathbf{r}_0, t_0) - \mathbf{u}(t|\mathbf{x}_0, t_0)$ implies the vanishing of the first term. The process $\mathbf{v}(t)$ has long been compared [73, 68] with a vector Brownian motion, e.g. its mean is zero and its covariance is $\langle v_i(t) v_j(t) \rangle = C \langle \varepsilon \rangle \delta_{ij} t$ in K41 theory. This fact and the short time-correlation of the Lagrangian acceleration make the martingale property plausible. Without this assumption there would be an extra drift term in the final diffusion equation.

Next note that

$$(a_i(t|\mathbf{x}_0+\mathbf{r}_0,t_0)-a_i(t|\mathbf{x}_0,t_0))(a_j(s|\mathbf{x}_0+\mathbf{r}_0,t_0)-a_j(s|\mathbf{x}_0,t_0)P_{\mathbf{u}}(\mathbf{r}-\mathbf{v}(t-s),s) \tag{3.34}$$

$$=(a_i(t|\mathbf{x}(s)+\mathbf{r}-\mathbf{v}(t-s),s)-a_i(t|\mathbf{x}(s),s))(a_j(\mathbf{x}(s)+\mathbf{r}-\mathbf{v}(t-s),s)-a_j(\mathbf{x}(s),s)$$

$$\times P_{\mathbf{u}}(\mathbf{r}-\mathbf{v}(t-s),s)$$

with $\mathbf{x}(s)=\mathbf{x}_{\mathbf{u}}(s|\mathbf{x}_0,t_0)$. Using this identity in the second term of (3.31), we finally obtain after averaging

$$\partial_t P(t)+\mathbf{v}\cdot\nabla_{\mathbf{r}}P(t)=\partial_{v_i}\partial_{v_j}\Big[\int_{t_0}^{t}ds\,R_{ij}(t;\mathbf{r},\mathbf{v},s|\mathbf{r}_0,\mathbf{v}_0,t_0)P(\mathbf{r}-\mathbf{v}(t-s),s)\Big] \tag{3.35}$$

with

$$R_{ij}(t;\mathbf{r},\mathbf{v},s|\mathbf{r}_0,\mathbf{v}_0,t_0)=\Big\langle\Big(a_i(t|\mathbf{x}(s)+\mathbf{r}-\mathbf{v}(t-s),s)-a_i(t|\mathbf{x}(s),s)\Big) \tag{3.36}$$

$$\times\Big(a_j(\mathbf{x}(s)+\mathbf{r}-\mathbf{v}(t-s),s)-a_j(\mathbf{x}(s),s)\Big)\Big|\mathbf{r}-\mathbf{v}(t-s),\mathbf{v},s;\mathbf{x}_0,\mathbf{r}_0,\mathbf{v}_0,t_0\Big\rangle.$$

Introducing the term $\int d^3x\,\delta^3(\mathbf{x}-\mathbf{x}(s))=1$, this can be rewritten as

$$R_{ij}(t;\mathbf{r},\mathbf{v},s|\mathbf{r}_0,\mathbf{v}_0,t_0)= \tag{3.37}$$

$$\int d^3x\;P(\mathbf{x},s|\mathbf{x}_0,\mathbf{r}_0,\mathbf{v}_0,t_0;\mathbf{r}-\mathbf{v}(t-s),\mathbf{v},s)\Big\langle\Big(a_i(t|\mathbf{x}+\mathbf{r}-\mathbf{v}(t-s),s)-a_i(t|\mathbf{x},s)\Big)$$

$$\times\Big(a_j(\mathbf{x}+\mathbf{r}-\mathbf{v}(t-s),s)-a_j(\mathbf{x},s)\Big)\Big|\mathbf{x},\mathbf{r}-\mathbf{v}(t-s),\mathbf{v},s;\mathbf{x}_0,\mathbf{r}_0,\mathbf{v}_0,t_0\Big\rangle$$

The standard definition of conditional probability

$$P(\mathbf{r},\mathbf{v},t|\mathbf{r}_0,\mathbf{v}_0,t_0)=P(\mathbf{r},\mathbf{v},t;\mathbf{v_0},t_0|\mathbf{r}_0,t_0)/P(\mathbf{v}_0,\mathbf{r}_0,t_0)$$

shows that the transition probability also satisfies (3.35). To obtain the formula for the diffusivity tensor in (3.25) we must finally use the short-time correlation assumption for the acceleration to drop all terms of the form $\mathbf{v}(t-s)$.

This result is for now only an analytical formula but it could be computed using the similar techniques that in the previous subsection.

3.7 Conclusion

In this chapter we derived for the first time an exact diffusion equation for the turbulence problem. In fact this formalism is not limited to applications to turbulence physics but can be applied to any dynamical system in principle. We then applied successive approximations to re-derive the diffusion equations by Kraichnan and Lungdren making it clear which approximations are necessary to arrive to their results. We showed that the assumption of short time-correlations is unnecessary to derive a diffusion equation and is also physically incorrect for turbulent flow. We numerically computed the diffusivity and realized this short time-correlations hypothesis leads to the over-prediction of Richardson's constant by the Kraichnan-Lundgren theory. We derived a similar diffusion equation for the join probability distribution for both the separations and velocity difference that might be better suited as a more accurate model for turbulence.

Our computations used the properties of isotropic turbulence that simplified the problem to a one-dimensional diffusion problem. Although a diffusion equation for the joint probability distribution seems a better model, it is however a much more complex problem because the simplifications related to isotropic turbulence cannot be used here as we need to keep track of the angles between $\mathbf{r}$, $\mathbf{v}$, $\mathbf{r}_0$ and $\mathbf{v}_0$. It would be a very challenging and interesting problem to try to solve.

Chapter 4

How sweeping effects in synthetic turbulence suppresses particle dispersion

4.1 Introduction

How particle pairs separate in a turbulent flow has been a central subject of turbulence research since the classical work of Richardson [83]. Unfortunately, the phenomenon has proved quite difficult to investigate by numerical solution of the fluid equations and by controlled laboratory experiments, especially because of the very large Reynolds numbers required. Many studies have therefore employed "synthetic turbulence" or ensembles of random velocity fields with some of the scaling properties of real turbulent velocities but which can be efficiently sampled even for very long scaling ranges. For example, papers [34, 47, 70, 28, 76] have followed this approach and have reported substantial agreement of their numerical simulations with the predictions of Richardson, including the famous "t^3-law" for the growth in time of mean square pair separation distances.

The validity of these results has been called into question, however. A paper

of Chaves et al. [22] pointed out that the use of synthetic turbulence to model Eulerian velocity statistics implies sweeping effects of large-scale eddies on particle motions that diverge with the Reynolds number. Those authors suggested to employ synthetic ensembles such as Gaussian random fields to model instead the turbulent statistics of Lagrangian velocities. In a simple one-dimensional Gaussian model of Eulerian velocities they found analytically that large-scale sweeping effects "localized" particle pairs and prevented them from separating. Subsequently, in a very interesting paper [94], Thomson & Devenish have proposed an intuitive picture how sweeping affects particle dispersion in synthetic models of Eulerian turbulence. The key point is that large-scale eddies in real turbulence advect both particles and smaller scale eddies, while large-scale eddies in synthetic turbulence advect only particle pairs and not smaller eddies. This fact implies that particle pairs at separations r in synthetic turbulence should experience rapidly changing relative velocities, as they are swept into new, statistically independent eddies. This occurs on a "sweeping" time-scale $\tau_{sw}(r) \sim r/v_0$, where v_0 is the rms velocity set by the largest eddies in the synthetic ensemble. Thomson & Devenish assume a diffusion process of pair separations with an eddy-diffusivity $K(r) \sim \delta u^2(r)\tau_{sw}(r)$ and $\delta u^2(r)$ the mean-square relative velocity at separation r. In an ensemble with Kolmogorov scaling $\delta u^2(r) \sim (\varepsilon r)^{2/3}$, this yields $dr^2/dt \sim K(r) \sim \varepsilon^{2/3} r^{5/3}/v_0$ and the solution

$$\langle r^2(t) \rangle \sim \frac{\varepsilon^4 t^6}{v_0^6}. \tag{4.1}$$

Note that this implies considerably slower growth than Richardson's t^3-law [1].

[1] The two laws can be written as $<r^2(t)>_{\rm Rich} \sim L^2(t/t_L)^3$ and $<r^2(t)>_{\rm TD} \sim L^2(t/t_L)^6$ in terms of the velocity integral scale L and the large-eddy turnover time $t_L \sim L/v_0$, by using $\varepsilon \sim v_0^3/L$. In their regime of validity $t < t_L$, one has $<r^2(t)>_{\rm TD} \ll <r^2(t)>_{\rm Rich}$.

Thomson & Devenish argued for the above prediction in the case of a large mean sweeping, with v_0 replaced by the mean speed $\overline{u}$. In the case of a zero-mean velocity ensemble, they argued instead for a $t^{9/2}$-growth law, intermediate between t^3 and t^6 (see our section 4.3 below). These predictions were supported in [94] by the numerical technique of "Kinematic Simulations" (KS) [34, 47, 70, 28, 76]. The previous contrary numerical results were explained on various grounds, e.g. the use of an adaptive time-stepping scheme in [34] which did not resolve the small sweeping time $\tau_{sw}(r)$ and its effect on particle dispersion.

The issues raised by the paper of Thomson & Devenish have still not been fully resolved. The numerical simulations in [94] used another form of adaptive time-stepping, which was suggested in [81] to be responsible for the observation of a $t^{9/2}$ growth. Thomson & Devenish then repeated their simulations with a fixed small time-step and reported the same $t^{9/2}$ law [29]. The most recent simulations of Nicolleau & Nowakowski [78] for their longest scaling ranges show some evidence of the Thomson-Devenish sweeping effects, but the reported scaling laws are intermediate between those of Richardson and of Thomson-Devenish and agree with neither theory. Thus, there is still considerable uncertainty in the literature regarding the validity of the Thomson-Devenish theory. The question is important, because synthetic turbulence is a useful testing ground for numerical and theoretical methods, and because comparison of particle dispersion in synthetic and real turbulence illuminates the physical mechanisms of the latter.

Because of the disagreement of the numerical simulations of different groups, it is useful to have analytic results. The Thomson-Devenish arguments apply to a wide array of synthetic turbulence models, but Gaussian velocity ensembles

are the most mathematically tractable. We therefore consider here the use of Gaussian random fields as models of turbulent Eulerian velocities. More precisely, we take the advecting velocity field $\mathbf{u}(\mathbf{x},t)$ to be a Gaussian random field with mean $\overline{\mathbf{u}}(\mathbf{x},t)$ and covariance $C_{ij}(\mathbf{x},t;\mathbf{y},s) = \langle u_i'(\mathbf{x},t)u_j'(\mathbf{y},s)\rangle$ for the fluctuations $\mathbf{u}' = \mathbf{u} - \overline{\mathbf{u}}$. Specific models of interest are similar to those studied in [22], with $\overline{\mathbf{u}}(\mathbf{x},t) = \overline{\mathbf{u}}$ independent of space and time and with covariance defined for $0 < \alpha < 2, 0 < \beta < 2$ by

$$C_{ij}(\mathbf{x},t;\mathbf{y},s) = D_2 \int d^d k \; e^{-D_3 k_L^\beta |t-s|} \frac{e^{i\mathbf{k}\cdot(\mathbf{x}-\mathbf{y})}}{k_L^{d+\alpha}} P_{ij}(\mathbf{k}). \tag{4.2}$$

Here $k_L^2 = k^2 + 1/L^2$ and $P_{ij}(\mathbf{k}) = \delta_{ij} - k_i k_j/k^2$ is the projection onto the subspace of $\mathbb{R}^d$ orthogonal to $\mathbf{k}$. The normalization constant D_2 is of dimension $length^{2-\alpha}/time^2$ and D_3 of dimension $length^\beta/time$. The Gaussian random field $\mathbf{u}(\mathbf{x},t)$ so defined is statistically homogeneous in space, stationary in time, and solenoidal. The length L is proportional to the integral length-scale. The scaling properties of the model at scales smaller than L are similar to those of real turbulence. For example, the single-time covariance for $r \ll L$ is calculated to be

$$C_{ij}(\mathbf{x},t;\mathbf{y},t) \sim D_0 L^\alpha - D_1 r^\alpha [(d+\alpha-1)\delta_{ij} - \alpha \hat{r}_i \hat{r}_j] + O(r^2/L^2) \tag{4.3}$$

with $\mathbf{r} = \mathbf{x} - \mathbf{y}$. See [39], p.686. Kolmogorov 1941 dimensional scaling corresponds to the exponents $\alpha = \beta = 2/3$. We shall consider also Gaussian velocity models whose energy spectra coincide with KS models which have been studied numerically [94, 81, 29, 78]. The incompressibility of these models will be used in an essential way, although much of our analysis applies to more general models, e.g. with any degree of compressibility.

The principal results are as follows. For a general Gaussian model of Eulerian turbulence we carefully derive the diffusion approximation for pair dispersion assumed in the argument of Thomson-Devenish [94], under the assumption of short memory times for particle locations. We furthermore obtain a closed formula, eq.(4.54), for the 2-particle eddy-diffusivity in a general Gaussian model. For the specific models with covariance (4.2) we obtained more explicit results, which, under the conditions $\alpha < 1$ and either $\beta < 1$ or frozen turbulence with $D_3 = 0$, verify the Thomson-Devenish argument about sweeping decorrelation effects. In particular, we obtain under these conditions a 2-particle eddy-diffusivity tensor of the form $K_{ij}(\mathbf{r}, t) = S_{ij}(\mathbf{r})\tau(r, t)$, where $S_{ij}(\mathbf{r})$ is the structure-function tensor and $\tau(r, t)$ is an effective correlation time of velocity increments. Crucially, $\tau(r, t)$ is the minimum of the intrinsic turnover time $\tau_{eddy}(r)$ at separation r, the overall evolution time t, and the sweeping time r/v_0. Although this result confirms the sweeping decorrelation effect, it leads to a pair-dispersion law for zero mean-velocity ensembles at high Reynolds numbers different from the $t^{9/2}$ suggested by Thomson & Devenish [94]. We show that it gives rise to distinct ranges of power-laws t^2, t^1, t^6 and then t^1 again at successively longer times, exactly as Thomson & Devenish argued for ensembles with large mean velocities. We carry out careful numerical Monte Carlo simulations with our diffusion model which verify these behaviors in the model at very high Reynolds numbers. We also present Monte Carlo results for our diffusion model at the moderate Reynolds numbers employed in current KS work, and reproduce then both the "t^3-law" and "$t^{9/2}$-law" that have been reported in KS at comparable Reynolds numbers. One possibility is that the current KS results in the literature are not yet probing asymptotic regimes and the true scaling in

KS at very high Reynolds numbers will be the same as in our diffusion model. A more likely conclusion however, according to our current understanding, is that the t^6 law is an artifact of the Markovian approximation we employ and the true scaling asymptotically for long inertial ranges is the $t^{9/2}$-law proposed by Thomson and Devenish (2005).

The detailed analytical derivation of diffusion models is presented in section 4.2 of the paper, and predictions for their dispersion laws discussed in section 4.3. Our numerical methods are described and validated in section 4.4 , and then used to obtain results for mean-square particle separations and other statistics. A concluding section 4.5 briefly discusses the results.

4.2 Derivation of the Diffusion Model

In this section we present the derivations of our main analytical results. A reader who is only interested in physical conclusions and not the detailed justifications may skip to our final formula (4.54) for the pair-diffusivity and the following discussion.

4.2.1 Gaussian Integration-by-Parts Identity

We show first that the transition probability of particle pairs in Gaussian velocity ensembles obeys an exact evolution equation, as a consequence of the well-known integration-by-parts identity or Donsker-Furutsu-Novikov relation (see [43], section 4.1). Let $\mathbf{u}(\mathbf{x}, t)$ be the random turbulent velocity field and let the fluid particle position that satisfies

$$\frac{d}{dt}\mathbf{x}(t) = \mathbf{u}(\mathbf{x}, t), \quad \mathbf{x}(t_0) = \mathbf{a} \tag{4.4}$$

be denoted as $\mathbf{x}_{\mathbf{u}}(\mathbf{a}, t_0|t)$, or $\mathbf{x}(\mathbf{a}, t)$ for short. Define the "fine-grained PDF" of 2-particle positions as

$$P_{2,\mathbf{u}}(\mathbf{x}_2, \mathbf{x}_1, t|\mathbf{a}_2, \mathbf{a}_1, t_0) = \prod_{n=1}^{2} \delta^d(\mathbf{x}_n - \mathbf{x}_{\mathbf{u}}(\mathbf{a}_n, t_0|t)). \tag{4.5}$$

Then the PDF of 2-particle positions is given by

$$P_2(\mathbf{x}_2, \mathbf{x}_1, t|\mathbf{a}_2, \mathbf{a}_1, t_0) = \langle P_{2,\mathbf{u}}(\mathbf{x}_2, \mathbf{x}_1, t|\mathbf{a}_2, \mathbf{a}_1, t_0)\rangle, \tag{4.6}$$

where the average is over the random velocity field $\mathbf{u}$.

Taking the time-derivative of (4.5) and using (4.4) it is a calculus exercise to show that

$$\partial_t P_{2,\mathbf{u}}(t) = -\sum_{n=1}^{2} \boldsymbol{\nabla}_{\mathbf{x}_n} \cdot \left[(\overline{\mathbf{u}}(\mathbf{x}_n, t) + \mathbf{u}'(\mathbf{x}_n, t))P_{2,\mathbf{u}}(t)\right], \tag{4.7}$$

where the velocity has been decomposed into its mean and fluctuating part $\mathbf{u}(\mathbf{x}, t) = \overline{\mathbf{u}}(\mathbf{x}, t) + \mathbf{u}'(\mathbf{x}, t)$. The average of the second term on the right-hand side can be obtained using Gaussian integration-by-parts [43]

$$\langle u_i'(\mathbf{x}, t))P_{2,\mathbf{u}}(t)\rangle \;=\; \int d^d y \int ds\; C_{ik}(\mathbf{x}, t; \mathbf{y}, s) \times \left\langle \frac{\delta}{\delta u_k(\mathbf{y}, s)} P_{2,\mathbf{u}}(t) \right\rangle \tag{4.8}$$

where $C_{ij}(\mathbf{x}, t; \mathbf{y}, s) = \langle u_i'(\mathbf{x}, t)u_j'(\mathbf{y}, s)\rangle$. To represent the functional derivative we introduce the Lagrangian response function

$$G_{ij}(\mathbf{a}, t; \mathbf{y}, s) \equiv \frac{\delta x_i(\mathbf{a}, t)}{\delta u_j(\mathbf{y}, s)}, \tag{4.9}$$

so that

$$\frac{\delta}{\delta u_k(\mathbf{y}, s)} P_{2,\mathbf{u}}(t) = \sum_{m=1}^{2} -\partial_{x_m^j} P_{2,\mathbf{u}}(t) \cdot G_{jk}(\mathbf{a}_m, t; \mathbf{y}, s). \tag{4.10}$$

The result of averaging (4.7) is the drift-diffusion equation

$$\partial_t P_2(t) = -\sum_{n=1}^{2} \boldsymbol{\nabla}_{\mathbf{x}_n} \cdot [\overline{\mathbf{u}}^*(\mathbf{x}_n, t)P_2(t)]$$

$$+ \sum_{n,m=1}^{2} \partial_{x_n^i} \partial_{x_m^j} \left[D_{ij}(\mathbf{x}_n, \mathbf{x}_m, t, t_0) P_2(t) \right]. \tag{4.11}$$

with

$$\overline{\mathbf{u}}^*(\mathbf{x}, t) = \overline{\mathbf{u}}(\mathbf{x}, t) + \partial_{x^j} D_{ij}(\mathbf{x}, \mathbf{x}', t, t_0)|_{\mathbf{x}'=\mathbf{x}} \tag{4.12}$$

the mean velocity plus a fluctuation-induced drift, and with the diffusivity tensor

$$\begin{aligned} D_{ij}(\mathbf{x}_n, \mathbf{x}_m, t, t_0) \equiv \int_{t_0}^{t} ds \int d^d y \; C_{ik}(\mathbf{x}_n, t; \mathbf{y}, s) \\ \times \langle G_{jk}(\mathbf{a}_m, t; \mathbf{y}, s) | \mathbf{x}_2, \mathbf{x}_1, t; \mathbf{a}_2, \mathbf{a}_1, t_0 \rangle \end{aligned} \tag{4.13}$$

where

$$\langle G_{jk}(\mathbf{a}_m, t; \mathbf{y}, s) | \mathbf{x}_2, \mathbf{x}_1, t; \mathbf{a}_2, \mathbf{a}_1, t_0 \rangle = \frac{\langle G_{jk}(\mathbf{a}_m, t; \mathbf{y}, s) P_{2,\mathbf{u}}(t) \rangle}{P_2(t)} \tag{4.14}$$

is the conditional average of the response function given that the two particles start in locations $\mathbf{a}_2, \mathbf{a}_1$ at time t_0 and end up at locations $\mathbf{x}_2, \mathbf{x}_1$ at time t.

We now develop a more useful expression for the response function (4.9). It is straightforward to show by functional differentiation of the equation of motion (4.4) that

$$\partial_t G_{ij} = \frac{\partial u_i}{\partial x_k}(\mathbf{x}(\mathbf{a}, t_0|t), t) G_{kj} + \delta_{ij} \delta^d(\mathbf{y} - \mathbf{x}(\mathbf{a}, t_0|t)) \delta(t - s). \tag{4.15}$$

This equation may be solved as

$$G_{ij}(\mathbf{a}, t; \mathbf{y}, s) = \begin{cases} g_{ij}(\mathbf{y}, s|t) \delta^d(\mathbf{y} - \mathbf{x}(\mathbf{a}, t_0|s)) & t > s > t_0 \\ 0 & \text{o.w.} \end{cases} \tag{4.16}$$

with $\mathbf{g}(\mathbf{y}, s|t) = \mathrm{Texp}\left(\int_s^t dr \, \frac{\partial \mathbf{u}}{\partial \mathbf{x}}(\mathbf{x}(\mathbf{a}, t_0|r), r) \right)$ the time-ordered exponential matrix for the trajectory which satisfies $\mathbf{x}(\mathbf{a}, t_0|s) = \mathbf{y}$. This notation is made natural by an alternative derivation of (4.16) based on the flow composition identity

$$\mathbf{x}(\mathbf{a}, t_0|t) = \mathbf{x}(\mathbf{x}(\mathbf{a}, t_0|s), s|t). \tag{4.17}$$

Taking the functional derivative $\delta/\delta u_j(\mathbf{y},s)$ of (4.17) and using the chain rule gives

$$\frac{\delta x_i(\mathbf{a},t)}{\delta u_j(\mathbf{y},s)} = \frac{\partial x_i}{\partial y_k}(\mathbf{y},s|t)\bigg|_{\mathbf{y}=\mathbf{x}(\mathbf{a},s)} \frac{\delta x_k(\mathbf{a},s)}{\delta u_j(\mathbf{y},s)}. \tag{4.18}$$

On the other hand, it is readily seen that the functional derivative of the integral form of the particle equation of motion (4.4), gives

$$\frac{\delta x_k(\mathbf{a},s)}{\delta u_j(\mathbf{y},s)} = \delta_{jk}\delta^d(\mathbf{y}-\mathbf{x}(\mathbf{a},t_0|s))\theta(s-t_0). \tag{4.19}$$

Thus, eq.(4.16) is rederived with $g_{ij}(\mathbf{y},s|t) = \frac{\partial x_i}{\partial y_j}(\mathbf{y},s|t)$. If (4.16) is substituted into the formula (4.13) it yields

$$\begin{aligned} D_{ij}(\mathbf{x}_n,\mathbf{x}_m,t,t_0) \equiv \int_{t_0}^{t} ds \int d^d y_m \; & C_{ik}(\mathbf{x}_n,t;\mathbf{y}_m,s) \\ & \times \langle g_{jk}(\mathbf{y}_m,s|t)|\mathbf{x}_2,\mathbf{x}_1,t;\mathbf{y}_m,s;\mathbf{a}_2,\mathbf{a}_1,t_0\rangle \\ & \times P(\mathbf{y}_m,s|\mathbf{x}_2,\mathbf{x}_1,t;\mathbf{a}_2,\mathbf{a}_1,t_0) \end{aligned} \tag{4.20}$$

where $P(\mathbf{y}_m,s|\mathbf{x}_2,\mathbf{x}_1,t;\mathbf{a}_2,\mathbf{a}_1,t_0)$ is the conditional probability density of the position of particle m at time s given the positions of both particles at times t and t_0. This formula for the diffusivity when substituted into (4.11),(4.12) gives the final form of our exact evolution equation for the 2-particle transition probability.

4.2.2 Markovian Approximation

Despite appearances, the evolution in the exact equation (4.11) is non-Markovian in general. It is clear from formula (4.20) that the 2-particle diffusion matrix is a function not only of the particle positions $\mathbf{x}_1,\mathbf{x}_2$ at time t, but also of the positions $\mathbf{a}_1,\mathbf{a}_2$ at time t_0. This dependence was suppressed in our notations, but the evolution, in principle, retains a long-time memory of the initial conditions. Only in special cases can the evolution be shown to be Markovian. The

famous example is the Gaussian velocity field that is delta-correlated in time, the so-called *Kraichnan model* [62, 41], for which

$$C_{ik}(\mathbf{x}, t; \mathbf{y}, s) = C_{ik}(\mathbf{x}, \mathbf{y}; t)\delta(t - s). \tag{4.21}$$

Substituting into (4.20) and using

$$g_{jk}(\mathbf{y}_m, t|t) = \delta_{jk} \tag{4.22}$$

and

$$P(\mathbf{y}_m, t|\mathbf{x}_2, \mathbf{x}_1, t; \mathbf{a}_2, \mathbf{a}_1, t_0) = \delta^d(\mathbf{y}_m - \mathbf{x}_m) \tag{4.23}$$

gives (with the "$\frac{1}{2}$ delta-function rule" for the upper limit of integration)

$$D_{ij}(\mathbf{x}_n, \mathbf{x}_m, t, t_0) = \frac{1}{2}C_{ij}(\mathbf{x}_n, \mathbf{x}_m, t).$$

Thus, in this case rigorously there is no dependence of the diffusion matrix $\mathbf{D}$ on $\mathbf{a}_1, \mathbf{a}_2$ and the well-known diffusion model is obtained [62, 41]. Another example with Markovian particle evolution is the velocity field obtained as the superposition of Gaussian random wave trains with very high frequencies, so that the group velocity of the waves greatly exceeds the root-mean-square velocity [2]. This example has direct relevance to KS simulations with "eddy-turnover frequency" $\omega_n = \lambda\sqrt{k_n^3 E(k_n)}$ in the limit $\lambda \gg 1$ of large "unsteadiness" parameter.

The description as a diffusion should generally hold reasonably well if the correlation time of the Gaussian velocity field is short enough, since the integrand in (4.20) then becomes negligible at values of $s < t$ for which there is sizable dependence on $\mathbf{a}_1, \mathbf{a}_2$. With this motivation, we make the *Markovian approximation*

$$D_{ij}(\mathbf{x}_n, \mathbf{x}_m, t, t_0) \equiv \int_{t_0}^{t} ds \int d^d y_m \; C_{ik}(\mathbf{x}_n, t; \mathbf{y}_m, s)$$

$$\times \langle g_{jk}(\mathbf{y}_m, s|t)|\mathbf{x}_2, \mathbf{x}_1, t; \mathbf{y}_m, s\rangle P(\mathbf{y}_m, s|\mathbf{x}_2, \mathbf{x}_1, t). \tag{4.24}$$

The physical assumption is that for times ordered as $t_0 \ll s < t$ the position of the particle at time s is determined mainly by its position at time t and is negligibly dependent on the position at the initial time t_0. The worst case for this approximation is clearly the "frozen velocity" model with infinite correlation time, when times $s \gtrsim t_0$ in the integral are not suppressed by decay of correlations. Such s values give an undamped contribution also in general for times $t - t_0$ much smaller than the velocity correlation time. However, it is easy to check that the exact result (4.13) [or (4.20)] and the Markovianized result (4.24) both give

$$\frac{d}{dt} D_{ij}(\mathbf{x}_n, \mathbf{x}_m, t, t_0) = C_{ij}(\mathbf{x}_n, t; \mathbf{x}_m, t) + O(t - t_0) \tag{4.25}$$

so that, for $t - t_0$ much smaller than the correlation time,

$$D_{ij}(\mathbf{x}_n, \mathbf{x}_m, t, t_0) = C_{ij}(\mathbf{x}_n, t_0; \mathbf{x}_m, t_0)(t - t_0) + O((t - t_0)^2). \tag{4.26}$$

Thus the Markovian approximation becomes exact in this limit. We note in passing that the Kraichnan-Lundgren theory of 2-particle dispersion [59, 69] when applied to the Gaussian velocity ensemble gives a result almost identical to the formula (4.24). As we discuss later, however, the Markovian approximation is seriously deficient, except when the advecting random velocity field has time correlations which are much shorter than the advecting sweeping time scale.

The formula (4.24) from the Markovian approximation can be further simplified. It is intuitively clear that conditioning on the location of both particles is superfluous in an average of a random variable that involves only one of these particles. In fact, it can be easily established from the definitions (4.5),(4.6)

that

$$\begin{aligned} P(\mathbf{y}, s|\mathbf{x}', \mathbf{x}, t) &= \int d^d y' \, P(\mathbf{y}', \mathbf{y}, s|\mathbf{x}', \mathbf{x}, t) \\ &= \int d^d y' \, \langle \delta^d(\mathbf{y}' - \mathbf{x}(\mathbf{x}', t|s)) \delta^d(\mathbf{y} - \mathbf{x}(\mathbf{x}, t|s)) \rangle \\ &= \langle \delta^d(\mathbf{y} - \mathbf{x}(\mathbf{x}, t|s)) \rangle = P(\mathbf{y}, s|\mathbf{x}, t). \end{aligned} \tag{4.27}$$

A similar argument gives

$$\langle g_{jk}(\mathbf{y}, s|t)|\mathbf{x}', \mathbf{x}, t; \mathbf{y}, s\rangle = \langle g_{jk}(\mathbf{y}, s|t)|\mathbf{x}, t; \mathbf{y}, s\rangle. \tag{4.28}$$

More generally, we may define the PDF

$$\begin{aligned} &P(\mathbf{g}, t; \mathbf{y}', \mathbf{y}, s|\mathbf{x}', \mathbf{x}, t) = \\ &\langle \delta^{d\times d}(\mathbf{g} - \mathbf{g}(\mathbf{y}, s|t)) \delta^d(\mathbf{y}' - \mathbf{x}(\mathbf{x}', t|s)) \delta^d(\mathbf{y} - \mathbf{x}(\mathbf{x}, t|s)) \rangle \end{aligned} \tag{4.29}$$

and mimic the previous argument to show that

$$P(\mathbf{g}, t; \mathbf{y}, s|\mathbf{x}', \mathbf{x}, t) = P(\mathbf{g}, t; \mathbf{y}, s|\mathbf{x}, t). \tag{4.30}$$

Then

$$\begin{aligned} P(\mathbf{g}, t|\mathbf{y}, s; \mathbf{x}', \mathbf{x}, t) &= \frac{P(\mathbf{g}, t; \mathbf{y}, s|\mathbf{x}', \mathbf{x}, t)}{P(\mathbf{y}, s|\mathbf{x}', \mathbf{x}, t)} \\ &= \frac{P(\mathbf{g}, t; \mathbf{y}, s|\mathbf{x}, t)}{P(\mathbf{y}, s|\mathbf{x}, t)} \\ &= P(\mathbf{g}, t|\mathbf{y}, s; \mathbf{x}, t). \end{aligned} \tag{4.31}$$

It follows from these facts that

$$\begin{aligned} D_{ij}(\mathbf{x}_n, \mathbf{x}_m, t, t_0) \equiv \int_{t_0}^{t} ds \int d^d y_m \; C_{ik}(\mathbf{x}_n, t; \mathbf{y}_m, s) \\ \times \langle g_{jk}(\mathbf{y}_m, s|t)|\mathbf{x}_m, t; \mathbf{y}_m, s\rangle P(\mathbf{y}_m, s|\mathbf{x}_m, t), \end{aligned} \tag{4.32}$$

which is the final form of the Markovian approximation for the diffusion tensor.

We now consider the special case when the velocity field is statistically homogeneous in space. In that case, the drift velocity in (4.12) is independent of $\mathbf{x}$ and simplifies to $\overline{\mathbf{u}}^*(t) = \overline{\mathbf{u}}(t)$, due to homogeneity and incompressibility [2]. Furthermore, a simplified equation can be derived for the transition probability of the 2-particle separation vector $\mathbf{r} = \mathbf{x}_2 - \mathbf{x}_1$, defined by

$$\begin{aligned} P_2(\mathbf{r}, t|\mathbf{r}_0, t_0) &= \int d^d a \; P_2(\mathbf{x}+\mathbf{r}, \mathbf{x}, t|\mathbf{a}+\mathbf{r}_0, \mathbf{a}, t_0) \\ &= \int d^d a \; P_2(\mathbf{x}, \mathbf{x}-\mathbf{r}, t|\mathbf{a}+\mathbf{r}_0, \mathbf{a}, t_0), \end{aligned} \tag{4.33}$$

which is also independent of $\mathbf{x}$. Since the diffusion tensor $D_{ij}(\mathbf{x}_n, \mathbf{x}_m, t)$ depends only on the difference $\mathbf{x}_n - \mathbf{x}_m$ in the homogeneous case, the equation (4.11) with the substitutions $\mathbf{r} = \mathbf{x}_2 - \mathbf{x}_1$ and

$$\boldsymbol{\nabla}_{\mathbf{x}_2} \longrightarrow \boldsymbol{\nabla}_{\mathbf{r}}, \quad \boldsymbol{\nabla}_{\mathbf{x}_1} \longrightarrow -\boldsymbol{\nabla}_{\mathbf{r}}, \tag{4.34}$$

yields the diffusion equation

$$\partial_t P_2(\mathbf{r}, t|\mathbf{r}_0, t_0) = \partial_{r^i}\partial_{r^j}\left[K_{ij}(\mathbf{r}, t, t_0) P_2(\mathbf{r}, t|\mathbf{r}_0, t_0)\right], \tag{4.35}$$

with the eddy-diffusivity tensor

$$\begin{aligned} &K_{ij}(\mathbf{r}, t, t_0) \\ &= 2D_{ij}(\mathbf{0}, \mathbf{0}, t, t_0) - D_{ij}(\mathbf{r}, \mathbf{0}, t, t_0) - D_{ij}(\mathbf{0}, \mathbf{r}, t, t_0) \\ &= \int_{t_0}^{t} ds \int d^d y \, S_{ik}(\mathbf{r}; \mathbf{y}, t, s) \times \langle g_{jk}(\mathbf{y}, s|t)|\mathbf{0}, t; \mathbf{y}, s\rangle P(\mathbf{y}, s|\mathbf{0}, t) \end{aligned} \tag{4.36}$$

[2] This is the first point where we have invoked incompressibility.

and we define the 2nd-order structure function of velocity increments at two points $\mathbf{0}, \mathbf{y}$ and two times t, s :

$$S_{ik}(\mathbf{r}; \mathbf{y}, t, s) = \langle [u_i'(\mathbf{r}, t) - u_i'(\mathbf{0}, t)][u_k'(\mathbf{y} + \mathbf{r}, s) - u_k'(\mathbf{y}, s)] \rangle. \tag{4.37}$$

If furthermore the velocity field is assumed to be statistically stationary in time, then we can take $t - t_0 \longrightarrow t$ and $t_0 \longrightarrow 0$, to obtain

$$\partial_t P_2(\mathbf{r}, t|\mathbf{r}_0, 0) = \partial_{r^i} \partial_{r^j} \left[K_{ij}(\mathbf{r}, t) P_2(\mathbf{r}, t|\mathbf{r}_0, 0) \right], \tag{4.38}$$

with

$$\begin{aligned} K_{ij}(\mathbf{r}, t) = \int_{-t}^{0} d\tau \int d^d y \, S_{ik}(\mathbf{r}; \mathbf{y}, 0, \tau) \\ \times \langle g_{jk}(\mathbf{y}, \tau|0)|\mathbf{0}, 0; \mathbf{y}, \tau \rangle P(\mathbf{y}, \tau|\mathbf{0}, 0) \end{aligned} \tag{4.39}$$

by the change of variables $\tau = s - t$.

4.2.3 Structure Function and One-Particle Distribution Function

The integral over $\mathbf{y}$ in the above formula (4.39) converges at large y because of decay in the two-point structure function and in the 1-particle transition probability. Physically, rapid decay is due to the facts that increments separated by great distances are uncorrelated and particles have low probability to be swept to large distances. Both of these effects can be easily quantified.

To evaluate the two-point structure function, we use a standard identity that expresses it in terms of the single-point 2nd-order structure function ([73], p.102):

$$S_{ik}(\mathbf{r}; \mathbf{y}, 0, \tau) = \frac{1}{2} \left[S_{ik}(\mathbf{y} + \mathbf{r}, 0, \tau) + S_{ik}(\mathbf{y} - \mathbf{r}, 0, \tau) - 2 S_{ik}(\mathbf{y}, 0, \tau) \right]. \tag{4.40}$$

We first consider the single-time case with $\tau = 0$. For the spatial power-law covariance (4.3) with $0 < \alpha < 2$, the single-point structure function becomes

$$\begin{aligned} S_{ij}(\mathbf{r}) &= 2\left[C_{ij}(\mathbf{0},\tau) - C_{ij}(\mathbf{r},\tau)\right]\big|_{\tau=0} \\ &\sim 2D_1 r^\alpha \left[(d+\alpha-1)\delta_{ij} - \alpha \hat{r}_i \hat{r}_j\right] + O(r^2/L^2) \end{aligned} \tag{4.41}$$

for $r \ll L$. The formula (4.40) implies in general that $S_{ik}(\mathbf{r};\mathbf{y},0,\tau=0) \sim S_{ik}(\mathbf{r})$ for $y \ll r$, whereas in the particular case (4.41) it gives

$$S_{ik}(\mathbf{r};\mathbf{y},0,\tau=0) = O(r^2/y^{2-\alpha}) \tag{4.42}$$

for $r \ll y \ll L$. When $y \gg L$, there is generally exponential or fast power-law decay, depending on the precise assumptions about the fall-off of the spectrum at low k. The 2-time structure function $S_{ij}(\mathbf{r};0,\tau)$ shows a similar behavior as the single-time structure function, except that there is a new length $L_\beta(\tau) = (D_3|\tau|)^{1/\beta}$ with eddies smaller than this scale decorrelated by time $|\tau|$. As seen from (4.2), the decorrelation is associated to an exponential decay of the cospectrum, with $L_\beta(t)$ acting as an effective "dissipation scale." Thus, $S_{ij}(\mathbf{r};0,\tau)$ scales $\propto r^2$ for $r \ll L_\beta(\tau)$, while formula (4.41) holds for $L_\beta(\tau) \ll r \ll L$. Thus, the decay law (4.42) is found when $\tau \neq 0$ only for the range of values $\max\{r, L_\beta(\tau)\} \ll y \ll L$ and is limited to times $|\tau| < L^\beta/D_3$. For $y \ll \max\{r, L_\beta(\tau)\}$ instead $S_{ik}(\mathbf{r};\mathbf{y},0,\tau)$ is independent of $\mathbf{y}$ and for $y \gg L$ the decay is again like that for $\tau = 0$.

The 1-particle transition probability should be dominated by large-scale sweeping and thus have the form

$$P(\mathbf{y},\tau|\mathbf{0},0) = \frac{1}{(2\pi)^{d/2} v_0^d |\tau|^d} \exp(-|\mathbf{y} - \overline{\mathbf{u}}\tau|^2/2v_0^2\tau^2) \tag{4.43}$$

to a good approximation, with v_0 the root mean square velocity. We hereafter consider mainly the case $\overline{\mathbf{u}} = \mathbf{0}$. For the Gaussian random field with mean zero and covariance (4.2), $v_0 \propto D_2 L^\alpha$. In that case, it has been verified by a formal scaling analysis in [22], section 7, that the leading-order motion of particles for large L is indeed ballistic with a constant, random velocity $\mathbf{v} = \mathbf{y}/\tau$ chosen from a Gaussian ensemble with rms value v_0. Subleading corrections were also obtained in [22] to account for the effects of the change of the velocity in space and time. Note that (4.43) decays rapidly for $y \gg v_0|\tau|$.

4.2.4 Stability Matrix

The most difficult term to evaluate in (4.39) is the conditional average of the stability matrix $\mathbf{g}(\mathbf{y}, \tau|0)$. Existence of this matrix requires a short-distance cutoff η on the "inertial-range" scaling behavior in the model covariance (4.2) and (4.3), which otherwise corresponds to velocity fields only Hölder continuous and non-differentiable in space. Even with the cutoff, the matrix $\mathbf{g}(\mathbf{y}, \tau|0)$ will grow exponentially in $|\tau|$ almost surely, with rate determined by the leading Lyapunov exponent $\lambda \propto (D_1/\eta^{2-\alpha})^{1/2}$. It is thus far from clear *a priori* that the conditional average even remains finite in the limit $\eta \to 0$.

We begin by evaluating this term for the "frozen" velocity field with infinite correlation time (or $D_3 = 0$ in eq.(4.2)). A key observation here is that the Gaussian transition probability (4.43) implies that particles are swept from point $\mathbf{y}$ to $\mathbf{0}$ in time $|\tau|$ along straight lines with a constant speed $v = y/\tau$ generally of order v_0. The velocity-gradient field $\boldsymbol{\nabla}\mathbf{u}(\mathbf{x}, t)$ has a spatial correlation of order η, so that the particle trajectories contributing in (4.39) will see a constant in space but rapidly changing velocity-gradient with a correlation time $\sim \eta/v_0$. Thus, one

can expect that the Lagrangian velocity-gradient will be well approximated by the model of a Gaussian field that is delta-correlated in time, for which the statistics of the stability matrix has been much studied.

To make this argument more formally, consider the spatial covariance of the velocity-gradient in the frozen case $C_{ij,mn}(\mathbf{r}) = \langle u'_{i,m}(\mathbf{r}) u'_{j,n}(\mathbf{0}) \rangle$, where $u'_{i,m} = \partial u'_i / \partial x_m$. By twice differentiating (4.3) and then averaging over the direction of the unit vector $\hat{\mathbf{r}}$, it is calculated to be

$$\overline{C}_{ij,mn}(r) = D'_1 r^{\alpha-2} \left[(d+1)\delta_{ij}\delta_{mn} - (\delta_{im}\delta_{jn} + \delta_{in}\delta_{jm}) \right] \tag{4.44}$$

with $D'_1 = \frac{D_1 \alpha(\alpha-2)}{d} \left[\frac{\alpha-4}{d+2} + 2 + \frac{d}{\alpha-2} \right] > 0$ for $d \geq 2$ and $0 < \alpha < 2$. This covariance holds for $r > \eta$, whereas the covariance for $r < \eta$ is essentially constant and can be taken to be given by (4.44) with $r = \eta$. A particle swept with velocity v will see a random velocity-gradient with temporal correlation obtained by substituting $r = vt$ in (4.44). Thus, the (Eulerian) velocity-gradients in a Lagrangian frame can be taken as Gaussian with covariance

$$\langle u'_{i,m}(t) u'_{j,n}(0) \rangle = D''_1 \frac{\eta^{\alpha-1}}{v} \delta_\eta(t) \left[(d+1)\delta_{ij}\delta_{mn} - (\delta_{im}\delta_{jn} + \delta_{in}\delta_{jm}) \right] \tag{4.45}$$

with $D''_1 = 2 \left(\frac{2-\alpha}{1-\alpha} \right) D'_1$ and $\delta_\eta(t) = \frac{1}{t_\eta} \Delta(\frac{1}{t_\eta})$, for $t_\eta = \eta / v$ and

$$\Delta(t) = \frac{1-\alpha}{2(2-\alpha)} \times \begin{cases} 1 & \text{for } |t| < 1 \\ t^{\alpha-2} & \text{for } |t| > 1 \end{cases} . \tag{4.46}$$

Since $\Delta(t)$ is integrable for $\alpha < 1$ with $\int_{-\infty}^{+\infty} dt \ \Delta(t) = 1$, one then has $\lim_{\eta \to 0} \delta_\eta(t) = \delta(t)$. It follows from these arguments that the velocity-gradient experienced by the particle should be approximated by a Gaussian matrix-valued process, constant in space and delta-correlated in time, if $\alpha < 1$. This approximation could break down for fixed $\eta \ll L$ if there happens to be a small advection speed $v \ll v_0$.

Now consider the non-frozen velocity field, with covariance given by (4.2) and (4.3) for $D_3 \neq 0$. In this case the single-point, 2-time covariance of the velocity-gradient averaged over directions has the form

$$\overline{C}_{ij,mn}(r=0,\tau) = D_1' \eta^{\alpha-2} e^{-D_3|\tau|/\eta^\beta} \left[(d+1)\delta_{ij}\delta_{mn} - (\delta_{im}\delta_{jn} + \delta_{in}\delta_{jm})\right] \quad (4.47)$$

There is now a short correlation time $t_\eta = \eta^\beta / D_3$, which allows us to write

$$\langle u_{i,m}'(t) u_{j,n}'(0)\rangle = \frac{2D_1'}{D_3} \eta^{\alpha+\beta-2} \delta_\eta(t) \left[(d+1)\delta_{ij}\delta_{mn} - (\delta_{im}\delta_{jn} + \delta_{in}\delta_{jm})\right] \quad (4.48)$$

with $\delta_\eta(t) = \frac{1}{t_\eta}\Delta(\frac{1}{t_\eta})$ for $\Delta(t) = 2\exp(-|t|)$. Thus, the single-point statistics of the velocity-gradient becomes temporally delta-correlated for vanishing η. In addition, there is the same decorrelation effect of rapid sweeping through space that occurs in the frozen-field case. The latter will dominate when $\eta/v \ll \eta^\beta/D_3$ at small η and when the spatial decay of correlations is fast enough, that is, when both $\beta < 1$ and $\alpha < 1$. In any case, we obtain again a model for Lagrangian velocity-gradients that are Gaussian, constant in space and delta-correlated in time. There is here no problem with small speeds $v \ll v_0$, since the correlation time will never be larger than η^β/D_3.

The stability matrix has been well-studied for Gaussian velocity-gradient fields, constant in space and white-noise in time. In particular, it has been shown in [7] that the matrix random process $\mathbf{g}(\mathbf{y}, \tau|0)$ is a diffusion on the group $SL(d)$ of $d \times d$ matrices with determinant 1. We shall use specifically the formula for the transition probability density $p_\tau(\mathbf{g})$ of this process starting at the identity, Eq.(7.14) in [7] for $n = 2$:

$$\int_{SL(d)} p_\tau(\mathbf{g}) f(\mathbf{g}\mathbf{r}_0) d\mu(\mathbf{g}) = \int P_2(\mathbf{r}, \tau|\mathbf{r}_0, 0) f(\mathbf{r})\, d^d r \quad (4.49)$$

where μ is Haar measure on $SL(d)$ and

$$\partial_\tau P_2(\mathbf{r},\tau|\mathbf{r}_0,0) = \mathcal{M}_2 P_2(\mathbf{r},\tau|\mathbf{r}_0,0) \tag{4.50}$$

for

$$\begin{aligned}\mathcal{M}_2 f(\mathbf{r}) &= D[(d+1)\delta_{ij}r^2 - 2r_i r_j]\partial_{r_i}\partial_{r_j} f(\mathbf{r}) \\ &= D\partial_{r_i}\partial_{r_j}\big\{[(d+1)\delta_{ij}r^2 - 2r_i r_j]f(\mathbf{r})\big\},\end{aligned} \tag{4.51}$$

where the second line follows by incompressibility. This implies also that the operator is self-adjoint. Since $\mathcal{M}_2 f \equiv 0$ for a general linear function $f(\mathbf{r}) = \mathbf{a}\cdot\mathbf{r}$, and considering in (4.49) arbitrary choices of $\mathbf{a}, \mathbf{r}_0$, it follows that

$$\int_{SL(d)} \mathbf{g}\, p_\tau(\mathbf{g})\, d\mu(\mathbf{g}) = \mathbf{I}, \tag{4.52}$$

the identity matrix. This result is due essentially to the fact that a diffusion leaves invariant a linear profile. Finally, we can conclude that

$$\langle g_{jk}(\mathbf{y},\tau|0)|\mathbf{0},0;\mathbf{y},\tau\rangle = \delta_{jk}. \tag{4.53}$$

The exponential growth of the individual realizations is offset by their rapid rotation in space which leads to large cancellations in the ensemble average. Incompressibility was necessary to the argument.

The result (4.53) is only strictly known to be valid when the velocity covariance converges to an η-independent result as $\eta \to 0$, whereas (4.45) diverges as $\sim \eta^{\alpha-1}$ for $\alpha < 1$ and (4.48) diverges as $\sim \eta^{\alpha+\beta-2}$ for $\alpha + \beta < 2$. However, the final result (4.53) is independent of the amplitude of the covariance (i.e. the value of D_1) and thus we conjecture that it extends even to the present cases with diverging covariance. The result yields a simplified formula for the

2-particle eddy-diffusivity:

$$K_{ij}(\mathbf{r},t) = \int_{-t}^{0} d\tau \int d^d y \, S_{ij}(\mathbf{r};\mathbf{y},0,\tau) P(\mathbf{y},\tau|\mathbf{0},0), \tag{4.54}$$

together with (4.40),(4.43). We shall now use this formula to obtain concrete results for the eddy-diffusivity in the Gaussian ensembles whose covariances are given by (4.2).

4.2.5 The Frozen-in-Time Velocity Field

The simplest case to analyze is the "frozen" field so that

$$S_{ij}(\mathbf{r};\mathbf{y},0,\tau) = S_{ij}(\mathbf{r};\mathbf{y}). \tag{4.55}$$

Making the change of variables $u = y^2/2v_0^2\tau^2$,

$$\int_{-t}^{0} d\tau \, P(\mathbf{y},\tau|\mathbf{0},0) = \frac{1}{\sqrt{8}\pi^{d/2}} \frac{1}{v_0 y^{d-1}} \Gamma\left(\frac{d-1}{2}, \frac{y^2}{2v_0^2 t^2}\right) \tag{4.56}$$

with the (upper) incomplete gamma function defined by $\Gamma(s,z) = \int_z^\infty du \, u^{s-1} e^{-u}$. Since $d^d y = y^{d-1} dy \, d\Omega_y$, with $d\Omega_y$ the element of d-dimensional solid angle, we get from (4.54) that

$$K_{ij}(\mathbf{r},t) = \frac{1}{\sqrt{2}\Gamma\left(\frac{d}{2}\right)} \int_0^\infty \frac{dy}{v_0} \overline{S}_{ij}(\mathbf{r};y) \Gamma\left(\frac{d-1}{2}, \frac{y^2}{2v_0^2 t^2}\right) \tag{4.57}$$

where the angle-averaged structure function is defined by

$$\overline{S}_{ij}(\mathbf{r};y) = \frac{1}{S_d} \int d\Omega_y S_{ij}(\mathbf{r};\mathbf{y}) \tag{4.58}$$

for $S_d = 2\pi^{d/2}/\Gamma\left(\frac{d}{2}\right)$ the $(d-1)$-dimensional area of the unit hypersphere in d-dimensional space.

When the velocity statistics are isotropic, as for the model with zero mean and covariance (4.2), the eddy-diffusivity tensor can be reduced to two scalar functions K_L, K_N defined by

$$K_{ij}(\mathbf{r},t) = K_L(r,t)\hat{r}_i\hat{r}_j + K_N(r,t)(\delta_{ij} - \hat{r}_i\hat{r}_j). \tag{4.59}$$

These two functions are related by incompressibility as $K_N = K_L + rK_L'/(d-1)$ and it is convenient to base further analysis on K_L. As is well known, if the separation statistics are also isotropic, then the diffusion equation (4.35) can be expressed entirely in terms of K_L, as

$$\partial_t P(r,t) = \frac{1}{r^{d-1}}\frac{\partial}{\partial r}\left(r^{d-1}K_L(r,t)\frac{\partial P}{\partial r}(r,t)\right). \tag{4.60}$$

Here the separation PDF satisfies

$$\int_0^\infty P(r,t)\, r^{d-1} dr = 1. \tag{4.61}$$

as normalization condition.

The displacement vector $\mathbf{y}$ in (4.55) breaks rotation invariance, but the average over solid angle restores isotropy. We can thus decompose also

$$\overline{S}_{ij}(\mathbf{r};y) = \overline{S}_L(r;y)\hat{r}_i\hat{r}_j + \overline{S}_N(r;y)(\delta_{ij} - \hat{r}_i\hat{r}_j) \tag{4.62}$$

into longitudinal and transverse contributions with respect to the separation vector $\mathbf{r}$. By dimensional analysis one can write

$$\overline{S}_L(r;y) = S_L(r)F\left(\frac{y}{r},\frac{L}{r}\right) = S_L(r)F\left(\frac{y}{r}\right), \tag{4.63}$$

the latter for $L \gg r$. The function $F(y/r)$ can be interpreted as the correlation coefficient of (longitudinal) velocity increments $\delta v_L(r)$ at points a distance y

apart. For the velocity covariance (4.2) with $D_3 = 0$ it is possible to derive a complicated, closed-form expression for the function $F(w)$ as suitable combinations of Gaussian hypergeometric functions of the argument w^2. However, we shall not pursue this here. The most important property of F, which follows from (4.42), is

$$F(w) \sim \begin{cases} 1 & w \ll 1 \\ (const.)w^{-(2-\alpha)} & w \gg 1 \end{cases} . \tag{4.64}$$

Thus, we can write $K_L(r,t) = S_L(r)\tau(r,t)$ where

$$\tau(r,t) = \frac{1}{\sqrt{2}\Gamma\left(\frac{d}{2}\right)} \int_0^\infty \frac{dy}{v_0} F\left(\frac{y}{r}\right) \Gamma\left(\frac{d-1}{2}, \frac{y^2}{2v_0^2 t^2}\right) \tag{4.65}$$

is a 2-particle Lagrangian correlation time. With the substitution $y = rw$, this becomes

$$\tau(r,t) = \frac{r}{v_0} J(x), \quad x = \frac{v_0 t}{r} \tag{4.66}$$

for

$$J(x) = \frac{1}{\sqrt{2}\Gamma\left(\frac{d}{2}\right)} \int_0^\infty dw\, F(w) \Gamma\left(\frac{d-1}{2}, \frac{w^2}{2x^2}\right) \tag{4.67}$$

For $d = 3$, $\Gamma(1,z) = e^{-z}$ and (4.67) is a Laplace transform in the variable w^2. The most directly useful consequence of (4.67) is the asymptotic behaviors

$$J(x) \sim \begin{cases} x & x \ll 1 \\ J_\infty & x \gg 1 \end{cases} , \tag{4.68}$$

where we have used $\int_0^\infty dv\, \Gamma\left(\frac{d-1}{2}, \frac{v^2}{2}\right) = \sqrt{2}\Gamma\left(\frac{d}{2}\right)$ and we have defined

$$J_\infty = \frac{\Gamma\left(\frac{d-1}{2}\right)}{\sqrt{2}\Gamma\left(\frac{d}{2}\right)} \int_0^\infty dw\, F(w). \tag{4.69}$$

The latter integral converges for $\alpha < 1$. We conclude that

$$\tau(r,t) \sim \begin{cases} t & t \ll r/v_0 \\ J_\infty \frac{r}{v_0} & t \gg r/v_0 \end{cases} . \tag{4.70}$$

Our result is quite similar to that obtained by [94] for the case of large mean velocity $\overline{\mathbf{u}}$; see their equation (8). Some differences are that our eddy-diffusivity is isotropic and has the short-time behavior proportional to t. However, most importantly we see the same sweeping decorrelation effect, with the 2-particle correlation time at long times proportional to the sweeping time r/v_0. With no such effect one would instead expect the correlation time to be always proportional to t in the frozen-field case. It should be emphasized that we obtain this result in the zero mean-velocity ensemble, where [94] have predicted different behavior. We shall compare our results with theirs in more detail in section 4.3, where we shall also derive the quantitative predictions of our formula for the growth of mean-square particle separations.

4.2.6 Finite Time-Correlated Velocity Field

We now study the Gaussian model with covariance (4.2) for $D_3 \neq 0$. More generally, consider any velocity field statistically homogeneous in space and stationary in time. Then (4.32) together with (4.43) & (4.53) give

$$D_{ij}(\mathbf{x}'-\mathbf{x},t) = \int_0^t ds \int d^d y\, C_{ij}(\mathbf{x}'-\mathbf{y},t-s) \times \frac{1}{[2\pi v_0^2(t-s)^2]^{d/2}} \exp\left[-\frac{|\mathbf{y}-\mathbf{x}-\overline{\mathbf{u}}(t-s)|^2}{2v_0^2|t-s|^2}\right] \tag{4.71}$$

Since the $\mathbf{y}$-integration has the form of a convolution, it is easily evaluated by a Fourier transform:

$$\hat{D}_{ij}(\mathbf{k},t) = \int_0^t ds\, \hat{C}_{ij}(\mathbf{k},t-s) \times \exp\left[i\mathbf{k}\cdot\overline{\mathbf{u}}(t-s) - \frac{1}{2}v_0^2k^2(t-s)^2\right] \tag{4.72}$$

For the model in (4.2) note $\hat{C}_{ij}(\mathbf{k},t) = \hat{C}_{ij}(\mathbf{k})\exp(-\gamma_k|t|)$ with $\hat{C}_{ij}(\mathbf{k}) = D_2P_{ij}(\mathbf{k})/k_L^{d+\alpha}$ and $\gamma_k = D_3k_L^\beta$. For large $\overline{\mathbf{u}}$, see [94]. Hereafter we take $\overline{\mathbf{u}} = \mathbf{0}$. Then making

the change of variables $\sigma = v_0 k(t-s)$, one obtains

$$\hat{D}_{ij}(\mathbf{k},t) = \frac{1}{v_0 k}\int_0^{v_0 kt} d\sigma\, \hat{C}_{ij}(\mathbf{k}) \times \exp\left[-\left(\frac{\gamma_k}{v_0 k}\right)\sigma - \frac{1}{2}\sigma^2\right] \tag{4.73}$$

Thus, for $t \ll 1/v_0 k$,

$$\hat{D}_{ij}(\mathbf{k},t) \sim \hat{C}_{ij}(\mathbf{k})t. \tag{4.74}$$

This implies by inverse Fourier transform that

$$K_{ij}(\mathbf{r},t) \sim S_{ij}(\mathbf{r})t, \quad t \ll r/v_0. \tag{4.75}$$

On the other hand, consider fixed t and large k. Note that the convection time is smaller than the correlation time, or $v_0 k > \gamma_k$, for $k > k_* = (D_3/v_0)^{\frac{1}{1-\beta}}$ when $\beta < 1$. Thus, for $k \gg k_*$, (4.73) gives

$$\hat{D}_{ij}(\mathbf{k},t) \sim \frac{1}{v_0 k}\hat{C}_{ij}(\mathbf{k}) \cdot \sqrt{\frac{\pi}{2}}\mathrm{erf}\left(\frac{v_0 kt}{\sqrt{2}}\right). \tag{4.76}$$

This formula is exact in the case of frozen turbulence ($D_3 = 0$) when $k_* = 0$. If furthermore $k \gg 1/v_0 t$, then

$$\hat{D}_{ij}(\mathbf{k},t) \sim \sqrt{\frac{\pi}{2}} \cdot \frac{1}{v_0 k}\hat{C}_{ij}(\mathbf{k}) \tag{4.77}$$

becomes independent of t and scales as a power $k^{-(d+\alpha+1)}$. For $\alpha < 1$, we thus obtain by inverse Fourier transform that for $r \ll \min\{v_0 t, L_*\}$

$$K_{ij}(\mathbf{r},t) \sim \sqrt{\frac{\pi}{2}}\frac{D_1^{(\alpha+1)}}{v_0} r^{\alpha+1}\left[(d+\alpha)\delta_{ij} - (\alpha+1)\hat{r}_i\hat{r}_j\right]. \tag{4.78}$$

It follows that the essential behavior of the frozen field case carries over to the finite time-correlated velocity with $\alpha < 1$ and $\beta < 1$. Just as for the frozen

velocity, $K_L(r,t) = S_L(r)\tau(r,t)$ and the correlation time satisfies (4.66) and (4.68) with $J_\infty = \sqrt{\frac{\pi}{2}}\frac{D_1^{(\alpha+1)}}{D_1^{(\alpha)}}$[3].

If, however, $\beta > 1$, then the behavior is quite different. Under this assumption $\gamma_k > v_0 k$ for $k > k_*$, so that we now make the change of variables $\sigma = \gamma_k(t-s)$ to obtain

$$\hat{D}_{ij}(\mathbf{k},t) = \frac{1}{\gamma_k}\int_0^{\gamma_k t} d\sigma\, \hat{C}_{ij}(\mathbf{k}) \times \exp\left[-\sigma - \frac{1}{2}\left(\frac{v_0 k}{\gamma_k}\right)^2 \sigma^2\right] \tag{4.79}$$

Equations (4.74) and (4.75) again hold, now for $t \ll 1/\gamma_k$ and $t \ll 1/\gamma_{1/r}$, respectively. On the other hand, for fixed t and $k \gg k_* = 1/L_*$,

$$\hat{D}_{ij}(\mathbf{k},t) \sim \frac{1}{\gamma_k}\hat{C}_{ij}(\mathbf{k})\left[1 - \exp(-\gamma_k t)\right]. \tag{4.80}$$

If furthermore $k \gg 1/L_\beta(t)$, then

$$\hat{D}_{ij}(\mathbf{k},t) \sim \frac{1}{\gamma_k}\hat{C}_{ij}(\mathbf{k}) \tag{4.81}$$

becomes independent of t and scales as a power $k^{-(d+\alpha+\beta)}$. When $\alpha+\beta<2$, we then obtain by inverse Fourier transform that for $r \ll \min\{L_\beta(t), L_*\}$

$$K_{ij}(\mathbf{r},t) \sim \frac{D_1^{(\alpha+\beta)}}{D_3} r^{\alpha+\beta}\left[(d+\alpha+\beta)\delta_{ij} - (\alpha+\beta+1)\hat{r}_i\hat{r}_j\right]. \tag{4.82}$$

We can again write $K_L(r,t) = S_L(r)\tau(r,t)$ but now

$$\tau(r,t) \sim \begin{cases} t & t \ll r^\beta/D_3 \\ (const.)\frac{r^\beta}{D_3} & t \gg r^\beta/D_3,\ r \ll L_* \end{cases}. \tag{4.83}$$

[3]Here the superscript in $D_1^{(\alpha)}$ is used to indicate the spatial scaling exponent α for which the constant in (4.3) is calculated. Using eqs. (2.14) and (2.16) in [39] to calculate $D_1^{(\alpha)}$ gives

$$J_\infty = \sqrt{\frac{\pi}{8}}\frac{\alpha}{\alpha+1}\frac{\Gamma\left(\frac{1-\alpha}{2}\right)}{\Gamma\left(\frac{2-\alpha}{2}\right)}\frac{\Gamma\left(\frac{d+\alpha+2}{2}\right)}{\Gamma\left(\frac{d+\alpha+3}{2}\right)}$$

Thus, the sweeping decorrelation effect is absent at sufficiently small scales when $\beta > 1$ and $\alpha + \beta < 2$.

4.3 Consequences of Diffusion Model

In the previous section we have derived a diffusion model which, for homogeneous and isotropic statistics, takes the form (4.60). For the Gaussian velocity ensemble having covariance (4.2) with Kolmogorov scaling exponent $\alpha = 2/3$, the diffusivity takes the form

$$\begin{aligned} K_L(r,t) &= \frac{C_L \varepsilon^{2/3} r^{5/3}}{v_0} J\left(\frac{v_0 t}{r}\right) \\ &\sim \begin{cases} C_L(\varepsilon r)^{2/3} t & t \ll r/v_0 \\ C_L' \frac{\varepsilon^{2/3} r^{5/3}}{v_0} & t \gg r/v_0 \end{cases} \end{aligned} \tag{4.84}$$

both in the frozen case and in the temporally fluctuating case with $\beta = 2/3$. Here C_L is the Kolmogorov constant in the longitudinal velocity structure function, $S_L(r) \sim C_L(\varepsilon r)^{2/3}$, and $C_L' = C_L J_\infty$. J is defined by (4.67). In this section we shall attempt to determine the growth law for the mean-square separation $\langle r^2(t) \rangle$ predicted by the model (4.60),(4.84).

Does this model lead to the $t^{9/2}$-law of Thomson-Devenish [94]? To answer this question, we must briefly review the argument for the 9/2-law. The key idea in [94] is that the mean-square separation pointwise in space depends on the local value v' of the fluctuating velocity. The sweeping effect occurs at points where $\tau_{sw}(r) = r/v'$ is smaller than the intrinsic correlation time, $\tau_{int}(r,t) = \varepsilon^{-1/3} r^{2/3}$ for finite-correlated velocity ($\beta = 2/3$) and $\tau_{int}(r,t) = t$ for "frozen" velocity. The local correlation time is argued to be the smallest of these:

$$\tau(r,t) = \min\{\tau_{sw}(r), \tau_{int}(r,t)\}. \tag{4.85}$$

Hence, when $v' > (\varepsilon r)^{1/3}$ (fluctuating) or r/t (frozen), then the mean-square separation conditioned on v' is affected by sweeping and shows the slow growth

$$\langle r^2(t)\rangle_{v'} \sim \frac{\varepsilon^4 t^6}{v'^6} \tag{4.86}$$

but in the opposite case exhibits the faster growth

$$\langle r^2(t)\rangle_{v'} \sim \varepsilon t^3. \tag{4.87}$$

Using these growth laws to evaluate τ_{sw} and τ_{int} in (4.85), it is easily checked that the t^6-law holds for points with $v' > (\varepsilon t)^{1/2}$ and the t^3-law for points with $v' < (\varepsilon t)^{1/2}$. The probability for the latter condition to hold is small but growing in time:

$$\mathrm{Prob}\Big(v' < (\varepsilon t)^{1/2}\Big) \sim \frac{(\varepsilon t)^{3/2}}{v_0^3}. \tag{4.88}$$

This formula holds for a Gaussian distribution of 3D velocities $\mathbf{v}'$, or for any similar distribution $p(\mathbf{v}') = (1/v_0^3) f(\mathbf{v}'/v_0)$ with variance v_0^2 and non-vanishing density at the origin. The unconditional mean-square separation can then be estimated from (4.87) and (4.88) as

$$\langle r^2\rangle \sim \varepsilon t^3 \cdot \frac{(\varepsilon t)^{3/2}}{v_0^3} = \frac{\varepsilon^{5/2} t^{9/2}}{v_0^3}. \tag{4.89}$$

The same result can be obtained from the t^6 dispersion law (4.86) by noting that it is a rapidly decreasing function of v', so that the dominant contribution is obtained from the points with $v' \gtrsim (\varepsilon t)^{1/2}$ which also occur with probability $\sim (\varepsilon t)^{3/2}/v_0^3$.

At first sight, it appears that the model (4.60),(4.84) may embody these ideas of [94]. The diffusion model implies the exact equation

$$\frac{d}{dt}\langle r^2(t)\rangle = 2\int K_T(r,t) P(r,t) r^{d-1} dr, \tag{4.90}$$

where $K_T = K_L + (d-1)K_N$ is the trace of the diffusion tensor. The average over r in (4.90) can thus play the same role as did the average over v' in the argument of [94]. The eddy-diffusivity (4.84) is equivalent to the correlation time (4.70). The population of particle pairs with separations $r > v_0 t$ should exhibit a growth law $\langle r^2(t)\rangle_> \sim \varepsilon t^3$, while the pairs with $r < v_0 t$ should exhibit $\langle r^2(t)\rangle_< \sim \frac{\varepsilon^4 t^6}{v_0^6}$. It appears possible that averaging over the entire range of pair separations could give rise to the 9/2-law (4.89) with an intermediate growth rate.

The above reasoning is, however, essentially wrong. The diffusion model (4.60),(4.84) does possess a t^3 regime, but only in an unphysical way. To see this, note that for both the t^3 and the t^6 growth laws the condition $r > v_0 t$ is first satisfied only at such long times that $t > v_0^2/\varepsilon$. Substituting the standard relation $\varepsilon \sim v_0^3/L$ (which follows from the assumed Kolmogorov scaling of the energy spectrum) implies that the t^3 law can be self-consistently satisfied only for times greater than a large-eddy turnover time, $t > L/v_0$. In that case, $\langle r^2(t)\rangle$ exceeds L^2 and the particle pairs have left the inertial range. As we shall verify below, the model (4.60),(4.84) does indeed possess a t^3 range when $t > v_0^2/\varepsilon$ but this exceeds the validity of the model, which was derived only for the range $r < L$. In the range $r > L$ the two particles should instead execute independent Brownian motions with a constant diffusivity D_T and the mean-square separation grow diffusively as $\langle r^2\rangle \sim 4D_T t$. Thus, the t^3 range is an unphysical artefact of the model (4.60),(4.84).

The argument for the asymptotic $t^{9/2}$ law by Thomson & Devenish [94] thus fails for the model (4.60),(4.84). We shall show below that our diffusion model can produce an apparent $t^{9/2}$ law over a finite range of scales at relatively low

Reynolds numbers, for similar choices of parameters with which such growth laws have been observed in kinematic simulations [94, 29, 78]. In this case, the eddy-diffusivity in the equation (4.60) is not given by the formula (4.84), which is asymptotically valid only for $L \gg r$, but instead directly from the expression (4.73), which holds in general. This suggests that the 9/2 growth law observed in several kinematic simulations could be a finite-Reynolds-number effect and may not represent the asymptotic behavior that would be observed with very long inertial ranges.

We argue that the true high-Reynolds-number behavior in our diffusion model is essentially the same as that found by Thomson & Devenish for the situation of large *mean* velocity $\overline{u}$ ([94], section 3.1). The principal difference is that we obtain also an early-time Batchelor ballistic range [4, 3] with t^2 growth. This is followed, as argued in [94], by ranges of diffusive t^1 growth, t^6 growth and finally by a range of t^1 or t^3 growth, depending upon whether the correct diffusivity (4.73) is used for that range or whether the $r \ll L$ approximation (4.84) is used (inappropriately, since $r \gg L$). We have not been able to find an analytical solution of our model (4.60),(4.84) which exhibits all of the above ranges. In this section we shall instead argue using a simple mean-field approximation

$$\frac{d}{dt}r^2 = 2K_T(r,t), \quad r(0) = r_0 \tag{4.91}$$

which ignores fluctuations in the random separation r. In the following section 4.4 we shall verify our theoretical conclusions by a numerical Monte Carlo solution of the diffusion model.

The Batchelor t^2 regime is the only one which we can derive directly from

our diffusion model (4.60) without any approximation. We take as our initial condition for the diffusion equation the spherical delta function

$$P_0(r) = \frac{\delta(r - r_0)}{r_0^{d-1}} \tag{4.92}$$

with all pairs initially at separation r_0. If this is substituted into the exact equation (4.90), it yields

$$\left.\frac{d}{dt}\langle r^2(t)\rangle\right|_{t=0} = 0, \quad \left.\frac{d^2}{dt^2}\langle r^2(t)\rangle\right|_{t=0} = 2S_T(r_0) \tag{4.93}$$

where the trace of the short-time result (4.75) was used,

$$K_T(r,t) \sim 2S_T(r)t, \tag{4.94}$$

for $t \ll r_0/v_0$. Taylor series expansion then gives

$$\langle r^2(t)\rangle - r_0^2 = S_T(r_0)t^2 + O(t^3), \tag{4.95}$$

which is the well-known result of Batchelor [4, 3]. The mean-field approximation (4.91) is exact in this regime, since sufficient time has not passed to change r substantially from its initial (deterministic) value r_0.

As noted in [94], there is an interval of times $t > r_0/v_0$ when r has still not changed substantially from its initial value r_0. For $r \approx r_0$ but $t \gg r_0/v_0$, the result (4.94) is replaced with

$$K_T(r_0,t) \sim K_T(r_0,\infty) = C_T' \frac{\varepsilon^{2/3} r_0^{5/3}}{v_0} \tag{4.96}$$

where $C_T' = \frac{14}{3} C_L'$ as a consequence of incompressibility. The growth law then becomes diffusive

$$\langle r^2(t)\rangle - r_0^2 \sim 2K_T(r_0,\infty)t, \tag{4.97}$$

this period lasting until the "takeoff time" t_{to} when $K_T(r_0, \infty)t_{to} \sim r_0^2$, or

$$t_{to} \sim \frac{v_0 r_0^{1/3}}{\varepsilon^{2/3}}. \tag{4.98}$$

See [94]. Together with the previous Batchelor regime, this diffusive range is obtained from the mean-field model (4.91) simplified to $dr^2/dt = 2K_T(r_0, t)$. It is interesting that the diffusive behavior (4.97) at early times is the analogue in the Kraichnan white-noise advection model [62, 41] of the Batchelor ballistic range (e.g. see [36], section II.B). This is not an accident. The large-scale sweeping of particle pairs through stationary eddies produces an effective small correlation time r_0/v_0 which makes the velocity field appear to be temporally white-noise for times $t \gg r_0/v_0$. This is closely connected with previous attempts to simulate the Kraichnan white-noise ensemble by sweeping fixed large-scale velocity fields rapidly across the computational domain [24, 45].

For times greater than the "takeoff time" t_{to} but smaller than the "end-of-sweeping time" $t_{es} = v_0^2/\varepsilon$, one must solve the mean-field equation (4.91) with

$$dr^2/dt = 2C_T' \frac{\varepsilon^{2/3} r^{5/3}}{v_0}, \tag{4.99}$$

which leads to the t^6-law (4.1). Instead for $t > t_{es}$ one must solve

$$dr^2/dt = 2C_T(\varepsilon r)^{2/3} t, \quad C_T = \frac{11}{3} C_L \tag{4.100}$$

at least for the model (4.84). As previously discussed, this leads to the Richardson t^3-law but in an unphysical way, since $r > L$ lies outside the validity of the model (4.84). For $t > t_{es}$ and $r > L$ in reality $K_T(r, t) \sim 2D_T$, where D_T is the 1-particle diffusivity of Taylor [92]. Thus, one must solve

$$dr^2/dt = 4D_T \tag{4.101}$$

which yields the very long-time diffusive range.

Our diffusion model of particle dispersion in the zero-mean synthetic turbulence ensembles thus yields a picture very close to that in the large mean-velocity ensembles. This is in contrast to Thomson & Devenish [94], who obtain a distinct behavior of particle dispersion in the two cases. To understand better why the model shows a different behavior, it is useful to rederive our results for the eddy-diffusivity in a slightly different way. For convenience we consider only the case of frozen velocity fields. Taking the longitudinal component of the formula (4.54) yields

$$K_L(r,t) = \int_{-t}^{0} d\tau \int d^d y \, S_L(\mathbf{r};\mathbf{y}) P(\mathbf{y},\tau|\mathbf{0},0). \tag{4.102}$$

As discussed in section 4.2.3 the factor $P(\mathbf{y},\tau|\mathbf{0},0)$ arises as the density of the Gaussian large-scale velocity $\mathbf{v} = \mathbf{y}/\tau$. Changing to this variable in the above integral yields

$$K_L(r,t) = \int K_L(r,t|v) \exp\left(-\frac{v^2}{2v_0^2}\right) \frac{d^d v}{(2\pi v_0^2)^{d/2}} \tag{4.103}$$

with

$$K_L(r,t|v) = S_L(r)\tau(r,t|v) \tag{4.104}$$

and

$$\tau(r,t|v) = \int_{-t}^{0} d\tau \, F\left(\frac{v|\tau|}{r}\right) \sim \begin{cases} t & t \ll r/v \\ I_\infty \frac{r}{v} & t \gg r/v \end{cases} \tag{4.105}$$

for $I_\infty = \int_0^\infty dw \, F(w)$. Since $F(v|\tau|/r)$ is the correlation coefficient of increments $\delta u(r)$ at distance $v|\tau|$ apart, $K_L(r,t|v)$ and $\tau(r,t|v)$ can be interpreted as pair diffusivity and correlation time for given large-scale velocity magnitude v. It is easy to average these quantities over v and recover the previous results for $K_L(r,t)$ and $\tau(r,t)$, in particular formula (4.70), and the results in this section

for $\langle r^2(t)\rangle$. It was already observed in [94] (section 3.2, p. 292) that averaging the pair-diffusivity over the large-scale sweeping velocity would lead to the t^6-law also for the zero-mean velocity ensembles and the above results are consistent with this conclusion. Thomson & Devenish argued, however, that correct results should be obtained by averaging $\langle r^2(t)\rangle_v$ rather than by averaging $K_L(r,t|v)$. We should return to this point below.

4.4 Numerical Simulations

We now present numerical results for the diffusion models derived in the previous sections, both to confirm our theoretical predictions of their behavior and to obtain new conclusions where no analytical results are available.

4.4.1 Methods and Tests

As in [94], we shall solve the diffusion equation (4.38) using a Monte Carlo method for the equivalent (Ito) stochastic differential equation

$$dr_i = b_{ij}(\mathbf{r},t)dW_j(t), \quad i,j = 1,...,d \tag{4.106}$$

where Einstein summation convention is used, $W_j(t)$ is a vector Wiener process and $2K_{ij} = b_{ik}b_{jk}$, with lower-triangular square-root b_{ij} calculated by Cholesky decomposition. We can integrate the stochastic equations (4.106) using the standard Euler-Maruyama scheme:

$$\begin{aligned} r_i(t_k) &= r_i(t_{k-1}) + b_{ij}(\mathbf{r},t_{k-1})\sqrt{\Delta t}\, N_{k,j} \quad i,j = 1,...,d \\ t_k &= t_{k-1} + \Delta t \end{aligned} \tag{4.107}$$

where $N_{k,j}$ for $j = 1,..,d$, $k = 1,2,3,...$ is an independent, identically distributed sequence of standard normal random variables. The normal random variables

are obtained from uniform pseudorandom numbers generated by the Mersenne Twister algorithm [71] which are then transformed to normal by the Box-Muller method [17].

Unfortunately, the ranges of time that we must cover are so large that it is completely impossible for us to use a constant timestep Δt. Instead we use an adaptive scheme similar to that of [94]. The stepsize is determined over geometric intervals $T(m) < t < T(m+1)$ with

$$T(m) = A\exp(Bm) \qquad \text{for } m = 1, 2, ..., M. \tag{4.108}$$

The choice for A, B and M is explained in Appendix A.1. In each such interval we have

$$\Delta t = C_\Delta \min\left(\frac{r^2}{K_T(r,t)}, \Delta T\right) \tag{4.109}$$

where K_T is the trace of K_{ij}. C_Δ is the main parameter accounting for the size of the time step within the intervals $T(m) < t < T(m+1)$. We performed convergence tests for values of C_Δ ranging from 1 to 10^{-6} to insure the quality of the timesteping. The results of these tests are presented in Appendix A.2. A large number S of independent samples of the process (4.106) are generated with initial separations $\mathbf{r}(t=0) = \mathbf{r}_0$ uniformly distributed over a sphere of radius $|\mathbf{r}_0|$, and statistics obtained by averaging over realizations. Most of the results presented below used $S = 10^4$.

There is considerable debate in the literature, however, whether such adaptive time-stepping schemes lead to converged, unbiased results for the statistics [94, 81, 29, 78]. To test our numerical methods, we found it useful to consider somewhat simpler diffusion models where exact analytical results are available

for comparison. The models with a power-law diffusivity

$$K_L(r) = Dr^\zeta, \quad 0 < \zeta < 2 \tag{4.110}$$

have been very well studied. It has been shown that the long-time evolution is self-similar, with a dispersion law

$$\langle r^2(t) \rangle \sim g(Dt)^{2/\gamma}, \quad g = \frac{\gamma^{4/\gamma} \Gamma\left(\frac{d+2}{\gamma}\right)}{\Gamma\left(\frac{d}{\gamma}\right)} \tag{4.111}$$

and a stretched-exponential PDF

$$P(r,t) = \frac{1}{\langle r^2(t) \rangle^{d/2}} \exp\left[-\alpha\Big(\frac{r}{\langle r^2(t) \rangle^{1/2}}\Big)^\gamma + \beta\right] \tag{4.112}$$

where $\gamma = 2 - \zeta$,

$$\alpha = \left[\frac{\Gamma((d+2)/\gamma)}{\Gamma(d/\gamma)}\right]^{\gamma/2}, \tag{4.113}$$

$$\beta = \ln\left[\frac{\gamma(\Gamma((d+2)/\gamma))^{d/2}}{(\Gamma(d/\gamma))^{(d+2)/2}}\right], \tag{4.114}$$

with the normalization condition $\int_0^\infty r^{d-1} P(r,t) dr = 1$. See [52], eqs.(3.14),(3.22) and the general, self-similar solutions found in [39] for the case $\ell = 0$ [4]. Incidentally, note that the mean-field equation (4.91) leads to power-law growth with the same exponent $2/\gamma$ as in (4.111) but with a different prefactor $g^{MF} = (\gamma(d+\zeta))^{2/\gamma}$ than g. It is not hard to show that $g^{MF} > g$, with $g^{MF} \to g$ as $d \to \infty$ from Stirling's approximation.

Notice that the inertial-range model (4.84) reduces to the time-independent diffusivity

$$K_L(r, \infty) = C_L' \varepsilon^{2/3} r^{5/3} / v_0, \tag{4.115}$$

[4]The equations of [52] are unfortunately marred by several misprints

as long as $r \ll v_0 t$. This is a special case of the power-law diffusivity (4.110) with $\zeta = 5/3$, or $\gamma = 1/3$, so that the mean-square separation grows as t^6. This case is thus most suitable to test our numerical methods. For the purposes of comparison in the next section with the more complex model (4.84), we take $D = C'_L \varepsilon^{2/3}/v_0$ with $C'_L = 1.262$ and $d = 3$ so that

$$\langle r^2(t) \rangle \sim g_6^{PD} \frac{\varepsilon^4 t^6}{v_0^6} \tag{4.116}$$

with the power-law diffusion model predicting $g_6^{PD} \doteq 15.968$. This model also has the self-similar PDF of form (4.112) with $d = 3$, $\gamma = \frac{1}{3}$, so $\alpha \doteq 11.3714$, $\beta \doteq 10.1767$.

We now employ the numerical scheme discussed earlier to see which of these exact results we can successfully reproduce. As we see in Fig. 4.1, long ranges of perfect t^6 power-laws can be obtained in log-log plots. Furthermore, Fig. 4.2 is a semilog plot of the dispersion compensated by the analytical result (4.116). It shows that the prefactor g_6^{PD} is reasonably well calculated by our Monte Carlo for choices of the constant C_Δ equal or smaller than 0.1. Finally, Fig. 4.3 shows the logarithm of the PDF of pair separations r plotted versus $r^{1/3}$ at 14 different times in the long t^6-range. Self-similarity is well confirmed by the collapse of rescaled curves for different times, and the analytical result (4.112) is accurately reproduced up to almost 16 rms values of the separation.

Our conclusion from these exercises is that the adaptive time-stepping scheme should be adequate for exponents of dispersion power-laws, and even for prefactors and PDF's with good accuracy. Since the primary issue in this work is the exponents, we shall employ the adaptive schemes when necessary to cover extensive ranges where constant time-steps are unfeasible. As additional checks on

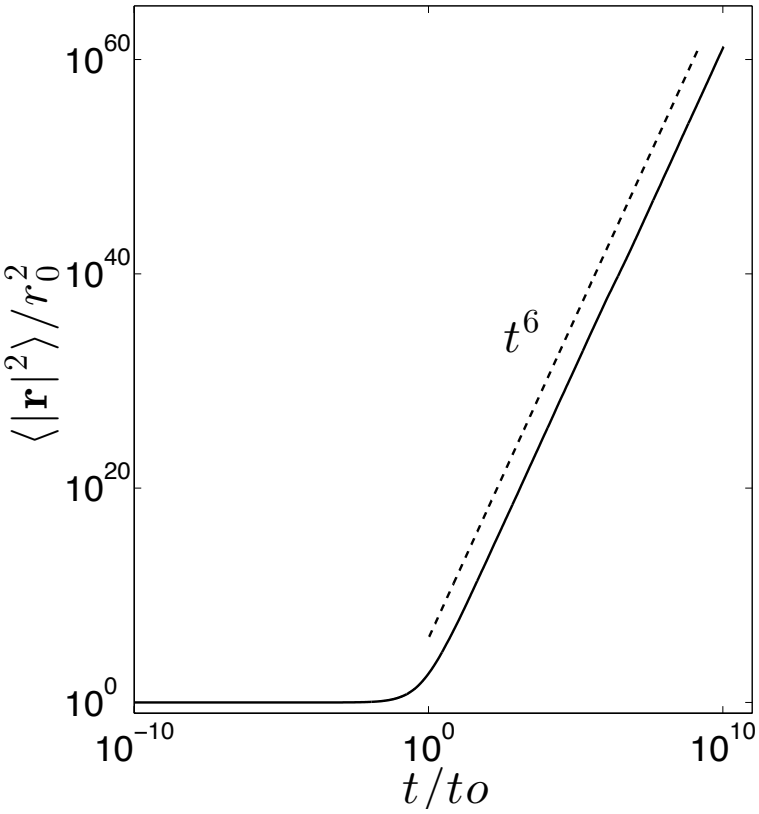

Figure 4.1: Monte Carlo results for $\langle |\mathbf{r}(t)|^2 \rangle$ in the power-law diffusion model (4.115) with $S = 10^4$ and $C_\Delta = 1$.

our numerical results for exponents from adaptive schemes, we test for convergence using constants C_Δ ranging from 1 to 10^{-6}. We also compare our Monte Carlo results for the diffusion equation with a separate numerical solution of the mean-field equation (4.91), integrated with a Fortran 90 implementation of the Watt and Shampine RKF45 ODE solver [19, 90]. This standard ODE integration method is also adaptive, but with variable time-step determined by preselected error tolerances. We therefore can have confidence that the numerical results for the mean-field theory are well converged.

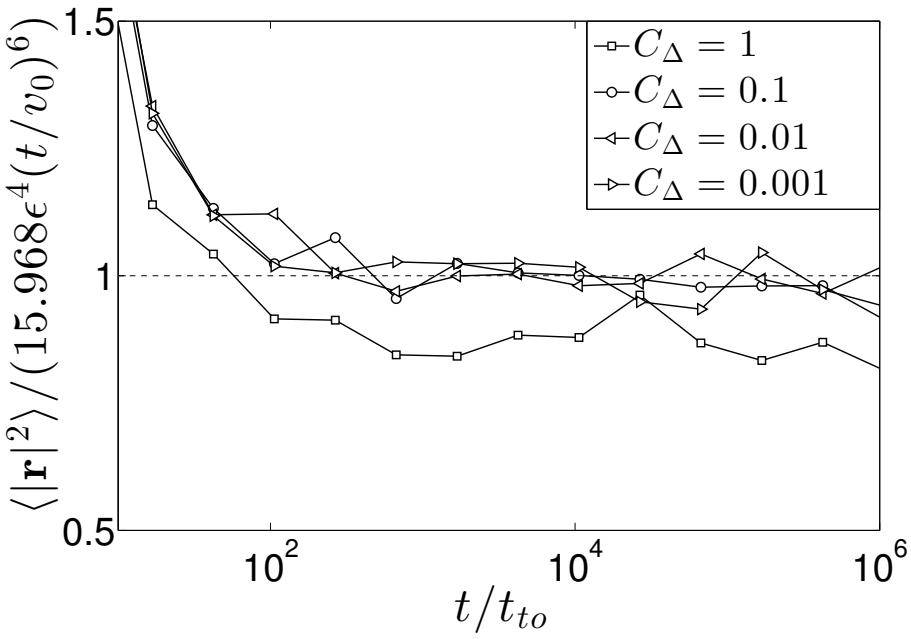

Figure 4.2: Monte Carlo results for $\langle|\mathbf{r}(t)|^2\rangle$ in the power-law diffusion model (4.115) with $S = 10^4$ and various C_Δ, compensated by the analytical result (4.116).

4.4.2 The Inertial-Range Model

We consider first the model (4.84) obtained for Kolmogorov scaling exponents in the limit $L \gg 1$ and thus physically applicable only for separations r in the inertial range of scales. This diffusion model applies for both the frozen velocity case and the finite-time correlated case (since $\beta = 2/3 < 1$). For the purpose of simplifying the numerical work, we opted not to use the exact scaling function $J(x)$ given by integral (4.67), which in three dimensions yields a complicated expression in terms of generalized hypergeometric functions. Instead, we built a function with the same asymptotic behaviors (4.68) as the true $J(x)$. We took

$$J(x) = J_\infty \mathrm{erf}(\lambda x) \quad = \quad \begin{cases} x & x \ll 1 \\ J_\infty & x \gg 1 \end{cases} \tag{4.117}$$

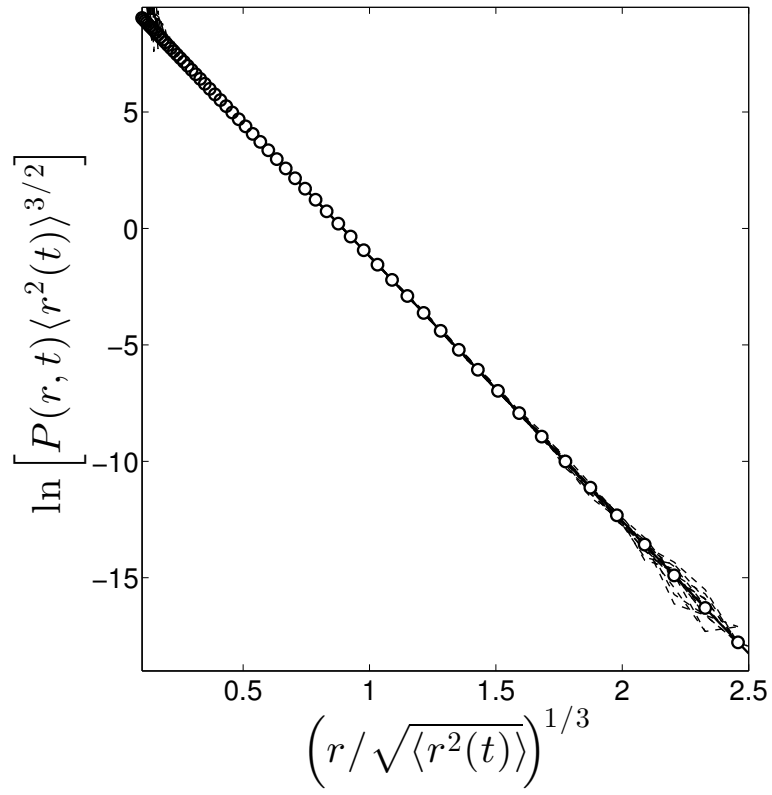

Figure 4.3: Logarithm of the rescaled PDF of pair-separations at 14 different times in the t^6 range, for the power-law diffusion model (4.115). Monte Carlo results for $S = 10^5$ and $C_\Delta = 1$. The straight line marked with circles ($\circ$) is the analytical result (4.112) for $d = 3$ and $\gamma = 1/3$.

with $\lambda = \frac{\sqrt{\pi}}{2J_\infty}$ and $J_\infty = \sqrt{\frac{\pi}{2}}\frac{D_1^{(5/3)}}{D_1^{(2/3)}} \doteq 0.6396$. Our expectation was that only these general features should be sufficient to observe the scaling regimes predicted in the previous section. This idea was borne out by the numerical results. In Fig. 4.4 we plot $\langle|\mathbf{r}(t) - \mathbf{r}_0|^2\rangle$ for the inertial-range diffusion model with $r_0 = 10^{-20}$. On the same graph we plot for comparison the numerical solution $r^2(t) - r_0^2$ of the mean-field equation (4.91). The two agree very well, and clearly exhibit the four predicted regimes with power-laws $\propto t^2, t^1, t^6$ and t^3, successively. A convergence analysis of our adaptive scheme for these results

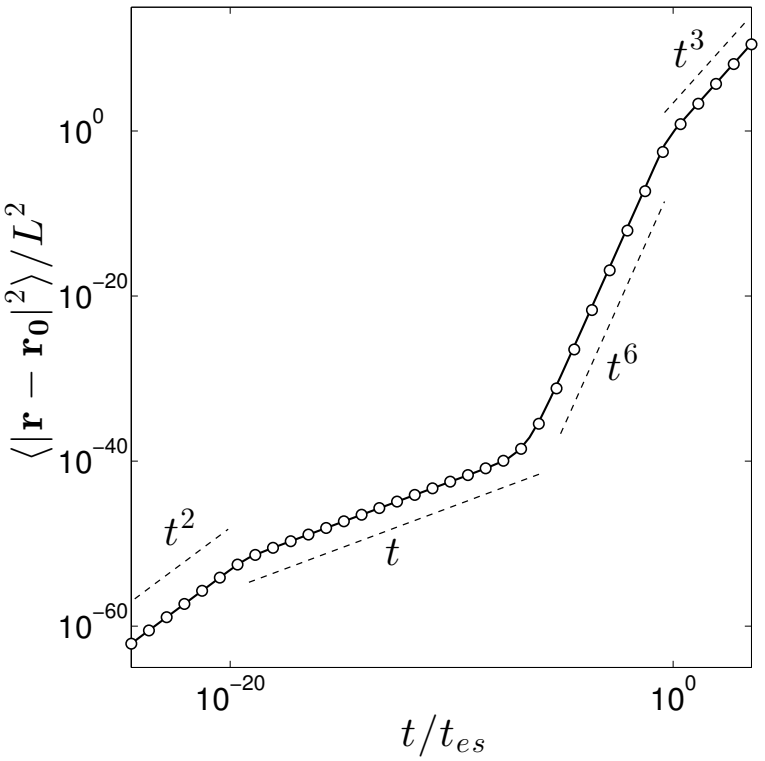

Figure 4.4: Numerical results for $\langle|\mathbf{r}(t)-\mathbf{r}_0|^2\rangle$ in the inertial-range model (4.84): Monte Carlo solution of the diffusion equation ($\circ$) with $C_\Delta = 1, S = 10^4$ and mean-field approximation ($-$).

is presented in Appendix A.

To further test the theoretical predictions, we investigate the crossover times between the different regimes and the prefactors of the scaling laws. For example, in Fig. 4.5(a) we show for various values of r_0/L the quantity $\langle|\mathbf{r}(t)-\mathbf{r}_0|^2\rangle$ compensated by the Batchelor-range prediction $\frac{11}{3}C_L(\epsilon r_0)^{2/3}t^2$ plotted versus the time t/τ_{sw} rescaled with the sweeping time $\tau_{sw} = r_0/v_0$. The Batchelor prediction fits the Monte Carlo data to within 0.13% relative error and the end of this regime is very close to $t/\tau_{sw} = 1$. We similarly show in Fig. 4.5(b) for the same choices of r_0/L the mean-square separation $\langle|\mathbf{r}(t)-\mathbf{r}_0|^2\rangle$ compensated

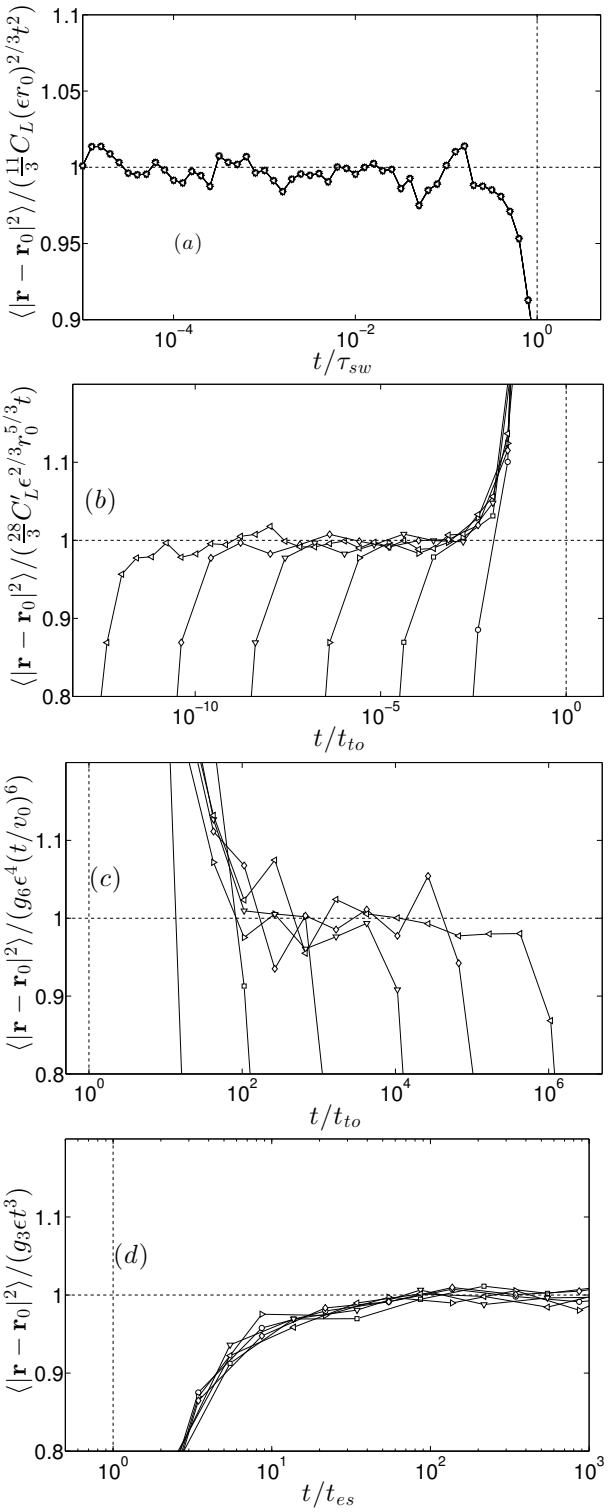

Figure 4.5: Monte Carlo results for $\langle|\mathbf{r}(t)-\mathbf{r}_0|^2\rangle$, $C_\Delta = 0.1$, $S = 10^4$. Each panel shows the same curves with different scalings. (a) Batchelor regime. (b) Kraichnan regime. (c) t^6 regime. (d) Richardson regime. The initial separations are $r_0/L = 10^{-5}(\circ)$, $10^{-8}(\square)$, $10^{-11}(\triangleright)$, $10^{-14}(\triangledown)$, $10^{-17}(\diamond)$, $10^{-20}(\triangleleft)$.

by the Kraichnan-like "diffusive-range" prediction $\frac{14}{3}C'_L\epsilon^{2/3}r_0^{5/3}t$ plotted versus t/t_{to} with the "takeoff time" t_{to} given by equation (4.98). The diffusive-range prediction is verified with a 1.8% error and the end of this regime quite convincing scales as $\sim 10^{-2}t_{to}$. In Fig. 4.5(c) we show the corresponding plot of mean-square separation compensated by $\varepsilon^4 t^6/v_0^6$ versus t/t_{to}. We see that a t^6 range begins at time $\sim 10^2 t_{to}$ and extends to the end-of-sweeping time $t_{es} = v_0^2/\varepsilon$ with a prefactor $g_6^{MC} \simeq 15.97$ of the t^6-law. This Monte Carlo value is equal within numerical errors to the exact value g_6^{PD} for the power-law diffusion model (4.115). It is interesting that the transition between the t^1 and t^6 scaling ranges is quite broad, covering about four decades. We show finally in Fig. 4.5(d) the mean-square separation compensated by the Richardson prediction εt^3 plotted versus t/t_{es}. For $t > t_{es}$ there is a clear t^3 regime with Richardson constant $g_3^{MC} \simeq 9.00$. This value agrees very well with the exact constant for a self-similar diffusion model with diffusivity $K_L(r,t) = C_L(\varepsilon r)^{2/3}t$ and $C_L = 1.9636$. Of course, as emphasized earlier, this entire regime of the inertial-range diffusion model is unphysical and will not be observed in KS model simulations.

4.4.3 Comparison with KS Models

Our derivation of diffusion model approximations was sufficiently general that we can consider cases of more direct relevance for KS simulations, with any energy spectrum and without the approximation of large L. Using the formula (4.76), which is exact for frozen turbulence, one obtains by inverse Fourier transform in 3D that

$$D_{ij}(\mathbf{r},t) = \sqrt{\frac{\pi}{2}} \int \frac{\widehat{C}_{ij}(\mathbf{k})}{v_0 k} \mathrm{erf}\left(\frac{v_0 k t}{\sqrt{2}}\right) e^{i\mathbf{k}\bullet\mathbf{r}}\, d^3k. \tag{4.118}$$

It is convenient to assume statistical isotropy, so that

$$\widehat{C}_{ij}(\mathbf{k}) = \frac{E(k)}{4\pi k^2} P_{ij}(\mathbf{k}), \tag{4.119}$$

where $P_{ij}(\mathbf{k})$ is the projection operator onto the subspace orthogonal to $\mathbf{k}$. The trace of the diffusivity tensor becomes

$$D_T(r,t) = \frac{\sqrt{2\pi}}{v_0} \int_0^\infty \frac{dk}{k} E(k) \mathrm{erf}\left(\frac{v_0 k t}{\sqrt{2}}\right) \frac{\sin(kr)}{kr} \tag{4.120}$$

and $D_L(r,t)$ can be recovered from

$$D_L(r,t) = \frac{1}{r^d} \int_0^r D_T(\rho,t)\, \rho^{d-1} d\rho.$$

Finally, the diffusivity that appears in equation (4.60) is

$$K_L(r,t) = 2(D_L(0,t) - D_L(r,t)).$$

To apply these results to the KS models [94, 81, 29, 78], let us recall that those models have a discrete set of wavenumbers distributed as

$$k_n = k_1 \left(\frac{k_N}{k_1}\right)^{\frac{n-1}{N-1}}, \tag{4.121}$$

for $n = 1, ..., N$ where $k_1 = 2\pi/L$, $k_N = 2\pi/\eta$ and η is the analogue of the Kolmogorov dissipation length. The energy spectrum generally adopted in these models is

$$E(k) = C_K \varepsilon^{2/3} \sum_{n=1}^{N} k_n^{-5/3} \delta(k - k_n) \Delta k_n \tag{4.122}$$

where $\Delta k_n = (k_{n+1} - k_{n-1})/2$ and $C_K = 1.5$ is the Kolmogorov constant, so that $C_L \doteq 1.973$ [5]. Here ε is a constant with dimensions of energy dissipation

[5] The standard formula $C_L = \frac{2\pi}{(3+\alpha)\Gamma(2+\alpha)\sin(\pi\alpha/2)} C_K$ relates the constants C_L, C_K for a $k^{-(1+\alpha)}$ power-law spectrum; e.g. see [73], eq.(13.100). This leads to $C_L \doteq 1.9727$ and $C'_L = C_L J_\infty \doteq 1.262$, the choice of the previous two subsections.

per mass chosen to prescribe values of the rms velocity:

$$v_0 = \sqrt{\frac{2}{3}\int_{k_1}^{k_N} E(k)dk}. \tag{4.123}$$

The formula (4.120) with the KS spectrum (4.122) yields

$$D_T(r,t) = \frac{C_K\epsilon^{2/3}}{v_0 r}\sqrt{2\pi}\sum_{n=1}^{N}\frac{\mathrm{erf}\left(\frac{v_0 k_n t}{\sqrt{2}}\right)}{k_n^{11/3}}\sin\left(k_n r\right)\Delta k_n \tag{4.124}$$

The assumption of isotropy in this formula is only approximately valid for KS simulations. It would be possible to use the general result (4.118), without assuming isotropy, which would lead to a discrete sum over wavevectors rather than wavevector magnitudes. However, this would make numerical implementation a bit more difficult, without essentially different physics.

We now present simulation results for diffusion models based on Gaussian velocity fields with the spectra of KS models, or, to be brief, "KS diffusion models" . The same Monte Carlo method was employed as for the inertial-range model. In all of our numerical studies we take $v_0 = L = 1$. We tried various values for the number of modes N and we found that the numerical results on dispersion laws in log-log plots for $N \gtrsim 100$ are not significantly different (see Appendix B). All of our presented results are for $N = 500$, a comparable number to that in the KS studies [94, 81, 29, 78]. We have also followed the practice in the KS literature of choosing the smallest length-scale $\eta = r_0/10$, for initial separation r_0. We have checked that taking $\eta < r_0/10$ leads to identical results. We have done no systematic study of the opposite case $\eta > r_0/10$, with particles starting in the "dissipation range", when an initial regime of exponentially rapid separation would be expected.

Our first set of numerical experiments investigated whether these more realistic models would exhibit the power-law scaling ranges predicted in section 4.3, with a k_N/k_1 sufficiently large. In Fig. 4.6 we plot the numerical results for the mean-square separation $\langle|\mathbf{r}(t) - \mathbf{r}_0|^2\rangle$ obtained from the KS diffusion model with $r_0 = 10^{-20}$. We observe very clearly the predicted ranges with power-laws t^2, t^1, t^6 and, lastly, the diffusive t^1 range at long times expected for a model with finite L. For comparison, we also plot numerical solutions of the mean-field equation (4.91) using the diffusivity (4.124). As before, the mean-field theory predictions are quite close to the full Monte Carlo solution of the diffusion model. Lastly, we plot the solution of the mean-field equation for the inertial-range large-L diffusivity, with the same choice of constants L, v_0 and ε. As expected, the dispersion law from this approximation agrees quite well with that of the KS diffusion model for $r < L$, but predicts a spurious t^3 power-law range for $r > L$. The good agreement justifies *a posteriori* our simplification of the scaling function $J(x)$ in section 4.4.2. Our general conclusion from this set of experiments is that the KS diffusion models should exhibit the above four scaling ranges with successive power-laws t^2, t^1, t^6 and then t^1 again, whenever the scale ratio k_N/k_1 is sufficiently large.

In order to discriminate between various alternative theories, it is useful to compare predictions not only for mean-square separations but also for the full probability density $P(r, t)$. In Fig. 4.7 we plot the Monte Carlo probability distribution calculated for 23 different times spread within the t^6 range. These are rescaled to test for self-similarity and collapse quite well. It should be emphasized that the overall evolution of our IR and KS diffusion models

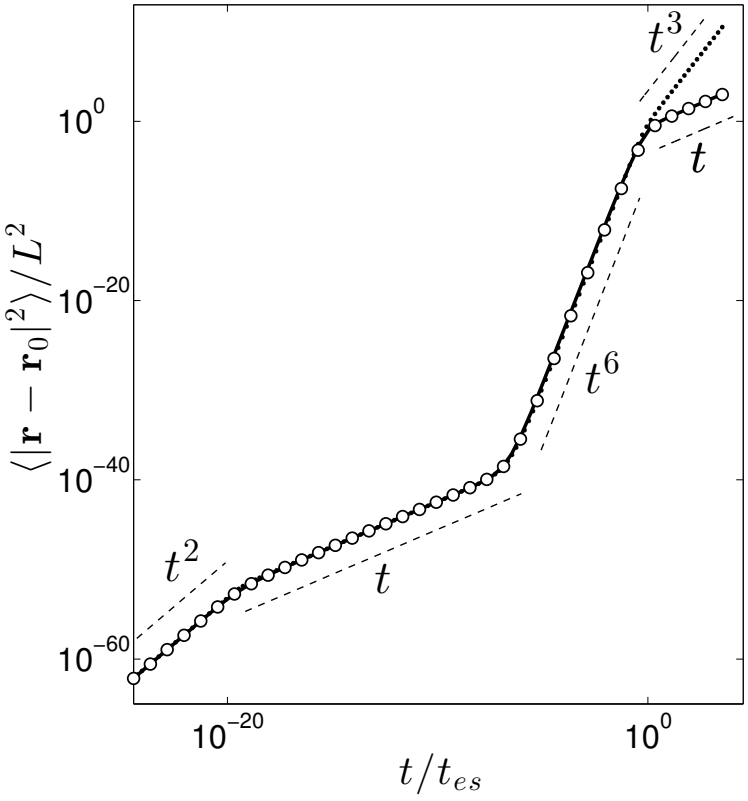

Figure 4.6: Numerical results for $\langle|\mathbf{r}(t)-\mathbf{r}_0|^2\rangle$ in the KS diffusion model (4.124), $k_N/k_1 = 10^{21}$: Monte Carlo solution of the diffusion equation ($\circ$) with $C_\Delta = 1, S = 10^4$ and mean-field ($-$). Also MC results ($\cdots$) for inertial-range model (4.84).

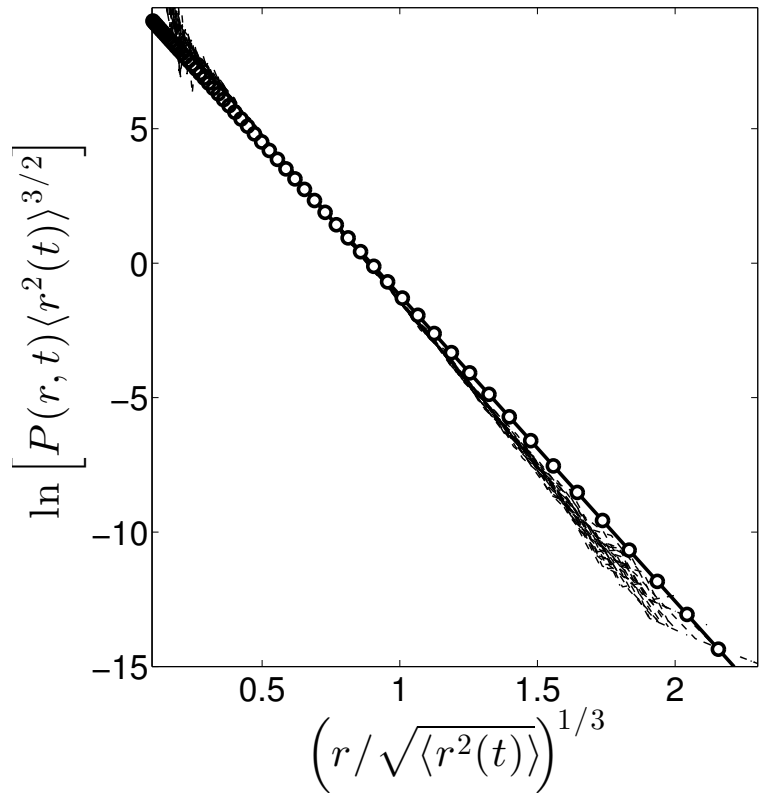

Figure 4.7: Logarithm of the rescaled PDF of pair-separations at 23 different times in the t^6 range, for KS diffusion model with $k_N/k_1 = 10^{21}$. Monte Carlo results for $S = 10^4$ and $C_\Delta = 1$. The straight line marked with circles ($\circ$) is the analytical result (4.112) for $d = 3$ and $\gamma = 1/3$.

is *not* self-similar, globally in time. This can be seen most clearly in the existence of time ranges with distinct power-law growth laws, whereas a truly self-similar evolution should have just one power-law. In a sufficiently long t^6 range, however, one should expect a self-similar evolution. For example, the inertial-range model (4.84) in the t^6 range reduces to the time-independent diffusivity $K_L(r,\infty) = C_L'\varepsilon^{2/3}r^{5/3}/v_0$, except for $r \gg v_0 t$. Since $r \sim v_0 t$ is nearly the maximum particle separation that can be achieved in the time t, only a very tiny large-r tail will experience a different eddy-diffusivity than this. In Fig. 4.7 we also compare the Monte Carlo results for the KS diffusion model with the exact parameter-free predictions (4.113),(4.114) of the power-law diffusion model (4.110) for $d = 3$ and $\zeta = 5/3$. The agreement is reasonably good. The curves collapse to a straight line with the stretching exponent 1/3 but with a slightly steeper slope than the power-law diffusion model. This suggests that if our Monte Carlo could be carried out for a sufficiently long t^6-range, then the PDF would approach the exact self-similar form of the power-law diffusion model.

We have speculated that the growth laws of the KS models themselves, asymptotically for $k_N/k_1 \gg 1$, may be the t^2, t^1, t^6 and t^1 powers that we have found in the KS diffusion models. Can this be reconciled with the $t^{9/2}$ law predicted in [94] and verified to greater or lesser extent in subsequent KS simulations [94, 29, 78]? It is possible that the observed $t^{9/2}$ is an artifact of the modest k_N/k_1 ratios achieved in these simulations, which tends to "blend" the distinct scaling ranges, in particular the early-time t^1 and t^6 ranges, between which lies a broad transition zone. In support of this argument, we have performed a sequence of Monte Carlo simulations of the KS diffusion model with

scale ratios $k_N/k_1 = 10^3, 10^4, 10^5, 10^6$. The last ratio is chosen to correspond roughly to that employed in the previous KS simulations [94, 29, 78]. Because the range of time-scales is not so great, we have been able to carry out the time-integration not only with the adaptive algorithm employed up until now, but also with a constant time step $\Delta t = 0.1\frac{\eta}{v_0}$ which resolves the effects of even the smallest eddies, equivalent to that used in recent KS simulations [29, 78]. The results of the two time-advancement schemes for the dispersion curves are identical when plotted in log-log. As illustrated in Fig. 4.8, a $t^{9/2}$ regime seems to appear as we increase the ratio k_N/k_1. This figure should be compared with Fig. 2 of [29] and Fig. 1 of [78], which it matches very closely. Although we see a similar "$t^{9/2}$-range" at the values of k_N/k_1 used in previous KS simulations, covering 1-2 decades in time, it is clear from our results in Fig. 4.6 that this is only a transitional regime of the KS diffusion model. In fact, for the case $k_N/k_1 = 10^6$ which shows the long "$t^{9/2}$-range" we find $t_{to} \doteq 10^{-2}$ and thus the broad transition zone between the t^1 and t^6 laws covers the interval from 10^{-4} to 10^0. This includes all of the apparent "$t^{9/2}$-range". If we go to $k_N/k_1 = 10^8$, the power-law steepens into a t^5-law. At still larger values of k_N/k_1 four asymptotic scaling ranges emerge, with distinct power-law scalings of t^2, t^1, t^6 and t^1. It is conceivable that the same is true of the KS models themselves at sufficiently large k_N/k_1, but we shall argue for a different resolution below.

Finally, we note that for $k_N/k_1 < 10^4$, the short range of superdiffusive growth of dispersion approximates a t^3-law. This agrees with the observations of [81, 78] for KS models. Note, however, that the physics is completely different from turbulent Richardson diffusion, which would allow t^3 ranges of arbitrary extent. In fact, the narrow range of such a power-law in our KS diffusion model

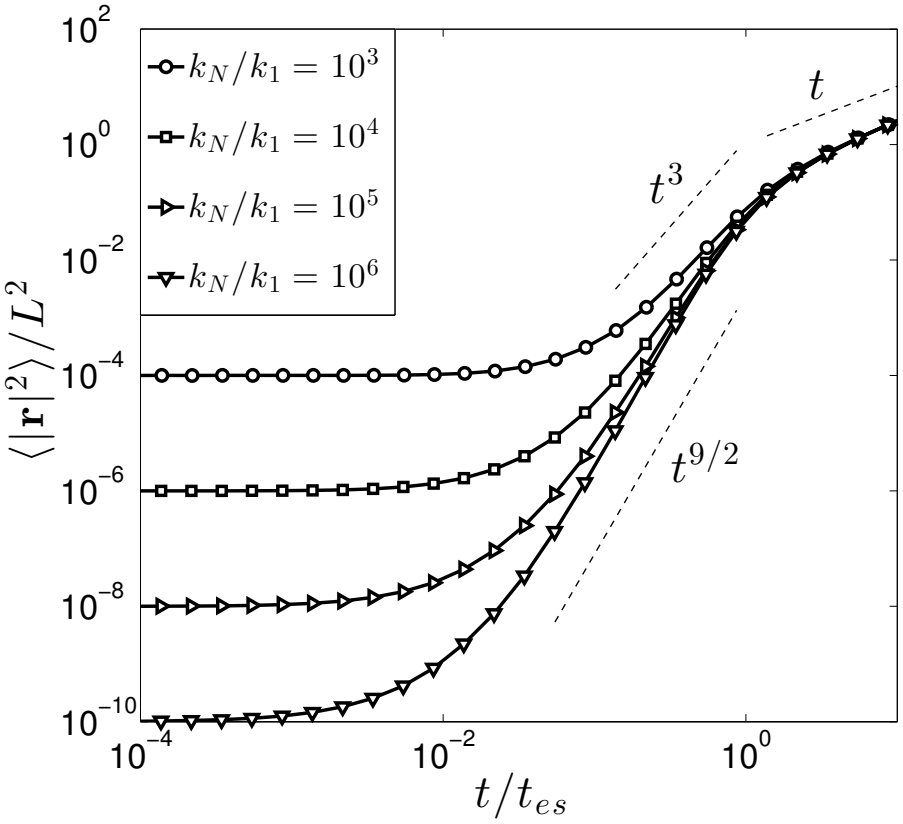

Figure 4.8: Monte Carlo results for $\langle |\mathbf{r}(t)|^2 \rangle$ in KS diffusion model for various values of k_N/k_1, with $\Delta t = 0.1\frac{r}{v_0}$, $S = 10^4$.

arises only because of the "merging" of many distinct ranges. In particular, the exponent of the apparent power-law must decrease with decreasing k_N/k_1 to match the t^1-law starting at $r = L$, until finally the superdiffusive range disappears entirely when $k_N/k_1 \approx 1$.

4.5 Discussion

We have derived in this chapter a diffusion equation for particle-pair dispersion in synthetic Eulerian turbulence modelled by Gaussian velocity ensembles. The

main analytical result is the formula (4.54) for the 2-particle diffusivity and its special cases (4.66) for frozen velocities and (4.76) for finite time-correlated velocities. Although the description of pair-dispersion as a diffusion process is not exact (except in certain limiting cases), it arises from a well-motivated set of analytical approximations. Most importantly, our results confirm the physical argument of Thomson & Devenish [94] that pair-dispersion in such models is fundamentally altered by sweeping decorrelation effects, not experienced by particle pairs in hydrodynamic turbulence. Thus, the t^3-law observed in previous simulations with synthetic turbulence [34, 47, 70, 28, 76] is quite likely an artefact either of the numerical approximations employed or of the shortness of the inertial ranges.

It may that there is a similar origin of the $t^{9/2}$-law proposed by Thomson & Devenish [94] for synthetic turbulence ensembles with zero mean velocities. Solutions of our diffusion model for such ensembles at Reynolds numbers comparable to those employed in KS simulations that show a $t^{9/2}$-law range reproduce that finding, but our model yields instead distinct t^2, t^1, t^6 and t^1-ranges at higher Reynolds numbers. Our results for our model thus illustrate the extreme difficulty of determining asymptotic power-law ranges in Kinematic Simulations are currently achievable resolutions.

It might more plausibly argued, however, that the t^6 range that we observe in our diffusion model is a consequence of the Markovian approximation which underlies it. As pointed out to us by David J. Thomson (private communication) the Markovian approximation is questionable for the conditional probability $P(\mathbf{y}_m, s|\mathbf{x}_2, \mathbf{x}_1, t; \mathbf{a}_2, \mathbf{a}_1, t_0)$ in the exact diffusivity formula (4.20). Lagrangian particles move, to leading order, along straight lines at constant

vector velocity and conditioning on the locations $\mathbf{x}_m$, $\mathbf{a}_m$ of particle m at times t, t_0 fixes its velocity as $\mathbf{v}_m = (\mathbf{x}_m - \mathbf{a}_m)/(t - t_0)$ Thus, a good approximation to $P(\mathbf{y}_m, s|\mathbf{x}_2, \mathbf{x}_1, t; \mathbf{a}_2, \mathbf{a}_1, t_0)$ is the delta function $\delta^3(\mathbf{y}_m - \mathbf{x}_m - \mathbf{v}_m(s-t))$ and not the Markov approximation $P(\mathbf{y}_m, s|\mathbf{x}_m, t) = \frac{\exp(-|\mathbf{y}_m - \mathbf{x}_m|^2/2v_0^2|s-t|^2)}{(2\pi v_0^2|s-t|^2)^{3/2}}$ in which $\mathbf{v}_m$ is taken effectively to be a normal random variable with variance v_0^2. When velocity correlation times are not very short, the approximation proposed by Thomson implies a non-Markovian evolution of the transition probability in which particles located at position $\mathbf{x}$ at time t will experience different effective diffusivities depending upon their initial location a at time t_0, or, equivalently, depending upon their initial velocities $\mathbf{v}(\mathbf{a}, t_0)$. It is plausible that using this better approximation in our formula (4.20) will lead to the Thomson-Devenish $t^{9/2}$-law rather than the t^6-law obtained from the Markovian approximation employed.

Whether the correct scaling is t^6, $t^{9/2}$ or some other power, our analytical results give strong support to the "sweeping effect on particle dispersion in synthetic models of Eulerian turbulence. Synthetic models of turbulence such as Kinematic Simulations have been used to investigate turbulent transport of passive objects (particles, lines, etc.) in such varied problems as environmental flow, aeroacoustics, kinematic magnetic dynamo, and superfluids [1, 77]. However, such numerical studies must clearly be employed with utmost caution, especially to derive conclusions about turbulent transport at very high Reynolds numbers. The difference in sweeping effects in synthetic Eulerian turbulence and in real hydrodynamic turbulence could imply substantially different physics even at relatively low Reynolds numbers.

It is noteworthy that several numerical simulations of pair dispersion in hydrodynamic turbulence have observed not only the t^3-law but also the stretched-exponential probability density function (PDF) of separations or "distance-neighbor graph" predicted by Richardson, already at modestly high Reynolds numbers [51, 9, 36]. None of the KS simulations which have observed a t^3-law of which we are aware [46, 34, 47, 28, 75, 76, 21] have also reported observing Richardson's prediction for the self-similar PDF. The paper [75] observed stretched-exponential PDFs of pair separation distances in two-dimensional KS that are in good agreement with low Reynolds-number experiments in quasi-2D stratified layers [72, 84], but which do not have the 2/3 stretching exponent in Richardson's PDF as observed in the higher Reynolds-number simulations [51, 9, 36].This is another indication that the "t^3-law" observed in those KS is a non-asymptotic and non-Richardson effect arising from rather different physics.

For engineering or environmental modeling purposes it may frequently not matter what is the precise origin of the t^3-law. However, in cases where knowledge of extreme or tail events is important (e.g. the range of dispersal of trace amounts of a dangerous contaminant), KS could lead to erroneous predictions. Discrepancies in particle dispersion properties between KS and hydrodynamic turbulence will grow even larger as the Reynolds numbers increase. There are flows with very extended inertial ranges in astrophysics (e.g. over eleven decades of Kolmogorov spectrum in the interstellar medium [25]), where actual particle dispersion properties must be quite different than what is predicted by KS at the corresponding Reynolds numbers.

Conclusion

The goal of this dissertation has been to develop a better understanding of the physics of the particle separation in a turbulent flow. We approached the problem from three very different angles. We first studied dispersion itself using DNS, analytical results and stochastic models. We then built on the common idea of diffusion models for this physics by deriving an exact diffusion equation for the first time. We finally developed an diffusion model that we studied numerically for non Navier-Stokes models (kinematic simulations) for turbulent flows.

We now emphasize on the main ways in which this thesis has helped to improve in the field of particle pair dispersion in turbulence.

Backward dispersion

An exact t^3 term

In chapter 2, we developed the most convincing attempt so far to "derive" the Richardson t^3 law from first principles and obtain the prefactor (Richardson constant). This is not a proof and is semi-empirical, but it gives a strong argument that the leading contribution in the t^3-law for backward turbulent dispersion of stochastic Lagrangian trajectories arises from an explicitly calculable term. We

computed the backward Richardson constant to be $g = 4/3$. The formalism for stochastic tracers developed in this chapter is relatively simple and opens the door to many other possible research works. Moreover, this t^3 term emerges from the analysis as a true viscosity independent term present at all times. It is therefore is good evidence for spontaneous separation of particle trajectories emanating from a single point in the zero viscosity limit. This shows the t^3-law as a true asymptotic behavior of turbulent flows in the infinite Reynolds number limit and suggests the concept of spontaneous stochasticity as an underlying mechanism for dispersion in turbulence. Spontaneous stochasticity can be seen as an analogy to spontaneous symmetry breaking in condensed matter physics and quantum field theory. It carries the idea that the particle trajectories which solve a deterministic ODE with a rough (nonsmooth, singular) velocity field can become random.

First systematic study of backward dispersion for the highest Reynolds numbers to this date

We made the first systematic study of backward dispersion for different final separations by looking at the rms separation distances between particle pairs but also by measuring the probability distribution. We clearly showed for quantitative differences between backward and forward dispersion. Whereas the Richardson constant for forward dispersion is usually measured to be $\sim 0.5-0.6$, we measured Richardson constants for backward dispersion to be $\sim 4/3$. We, for the first time, confirmed analytically and numerically a short time t^4-law for the separation statistics. This is the highest Reynolds number study of backward dispersion to this date.

Another view on the Batchelor regime

To our knowledge, it is the first time that an exact equation highlighting the Batchelor regime is derived. The Batchelor regime is commonly believed to occur as a short time expansion for the dispersion.

Diffusion models

Exact diffusion equation for the separation statistic: the inverse problem

The second chapter has addressed the old idea to cast the study of dispersion in a Turbulent flow into a diffusion problem, making the evolution of the probability distribution of the system a more central issue. We derived a "conditional diffusion" formulation for PDF's of general smooth flows with averaging over the random velocity vector fields. The statistics are given by a stochastic diffusion equation but with a conditional diffusivity that depends upon the initial state of the system. We proved wrong the old concept of the necessity of delta correlated velocities to obtain a diffusion physics. We understood that any dynamical systems (following $dx/dt = u$ type time evolution) could be cast into a diffusion problem and is not bounded only to the turbulence problem. We solved the inverse problem: given the probability distribution, we can infer the diffusion equation that it solves. The diffusivity gives more physical insight than the PDF alone and can be used as a basis of subsequent approximations.

The assumptions that leads to Kraichnan and Lundgren formula

Using our exact diffusion equation, we gave a justification for the validity of Richardson's diffusion approximation, while explaining how the short correlation-time assumption led to quantitative errors in previous approximations of Kraichnan & Lundgren. It is the first time that a diffusion model has been able to preserve the non-Markovian feature observed in real turbulence. The exact diffusion equation gave us a reference to quantify the effects of the different approximations that can be made. More importantly we understood what assumptions did not need to be made (e.g. imcompressibility assumption) to derive the Kraichnan and Lundgren formula and related improved formulas.

An exact diffusion equation for the joint probability distribution of separations and velocity differences statistics

The short correlation-time approximation that led to the Kraichnan and Lundgren formula makes the computation of the diffusivity considerably simpler regardless how quantitatively wrong it may be. A Markovian approximation relaxes the constraint on tracking each particle in the flow from their initial position. That has been a motivation for looking for a diffusion model where the short correlation-time approximation would be more valid. We derived an exact diffusion equation for the joint transition probability of both the relative position r and the relative velocity v of two Lagrangian particles. The short time correlation of the acceleration field is more compatible with a Markovian approximation.

Diffusion model for Gaussian random fields

The sweeping effect or why kinematic simulations capture a different physics than that of real turbulence

The last chapter built on the idea to describe turbulence through non Navier-Stokes models, the so-called synthetic turbulence models. We add strong argument that these models cannot capture the features of real turbulence as the particles are advected in a very different fashion than for real turbulence. For the first time, we gave an analytical, first-principles argument for the existence of the "sweeping effect" proposed by Devenish & Thomson for 2-particle dispersion dispersion in synthetic models of Eulerian turbulent velocities. The concrete model obtained by a Markovian approximation illustrates the effect of sweeping and also demonstrates the extreme difficulty of probing asymptotic scaling regimes by numerical solutions, even for the synthetic models, such as Kinematic Simulations, which have been attractive because of their relatively low computational cost.

The success of the diffusion model

We strongly criticized our Markovian approximation for being seriously deficient, although the model developed in that chapter has considerable similitude in behavior with kinematic simulations. The short time Batchelor regime is exact up to the sweeping time. The t^6-law in the inertial range of our model qualitatively and quantitatively agrees with the time evolution of the dispersion measured by Thomson and Devenish in the non zero mean velocity case. The model is simple to manipulate we can explore the asymptotic limits that the

kinematic simulations cannot.

Going beyond this diffusion model

We laid the ground for diffusion models for Gaussian random fields and we understood the strengths and weaknesses of the current model. David J. Thomson in a private communication opened new perspectives for improving this model by suggesting a simple approximation of constant-velocity particle motion due to large-scale sweeping. This is the exact leading-order asymptotics of single-particle motion in synthetic Gaussian turbulence and can be systematically improved with corrections for relative advection and time-evolution of eddies [23]. This simple approximation (instead of the Markovian one) could dramatically change the behavior of our model and help explain the $t^{9/2}$-law observed by Thomson and Devenish in 2005.

Conclusion of the conclusion

This thesis material is mostly based on three articles published during my Ph.D. with Pr. Greg L. Eyink and Theodore D. Drivas [38, 37, 5]. This thesis laid down many new concepts and principles and I hope it can help generate many future works in the field of relative dispersion in turbulent flows!

Appendix A

Technical details for the numerical studies of chapter 4

A.1 Details for the choice of the time step

We build the vector $T(m)$

$$T(m) = A\exp(Bm) \qquad \text{for } m = 1, 2, ..., M. \tag{A.1}$$

such that $T(1) = 10^{-5}\tau_{sw} = 10^{-5}r_0/v_0 \ll \tau_{sw}$ and $T(M) \simeq 34200t_{es} = 34200v_0^2/\epsilon \gg t_{es}$ to be sure that the numerical experiments capture the physics associated to these time scales τ_{sw} and t_{es}. As a consequence we have for $v_0 = 1$

$$B = \frac{\ln(\frac{10^9}{r_0})}{M-1} \tag{A.2}$$

$$A = 10^{-5}r_0\exp(-B) \tag{A.3}$$

For each $T(m)$ we compute the value of $\langle|\mathbf{r}(T(m))|\rangle$ or $\langle|\mathbf{r}(T(m)) - \mathbf{r}_0|\rangle$ using linear interpolation. We choose M such that the spacing between the $T(m)$ remain constant on a log-scale. We have

$$\ln(T(m+1)) - \ln(T(m)) = B \tag{A.4}$$

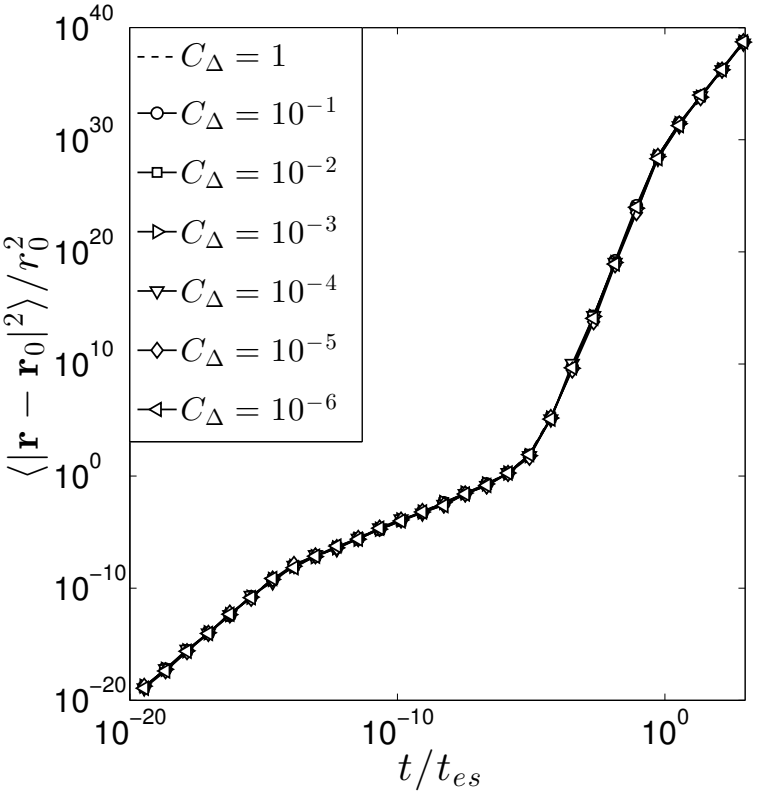

Figure A.1: Monte Carlo results for $\langle|\mathbf{r}(t)-\mathbf{r}_0|^2\rangle$ in the inertial-range diffusion model calculated with $S = 10^2$ samples and varying $C_\Delta = 1$ to $C_\Delta = 10^{-6}$.

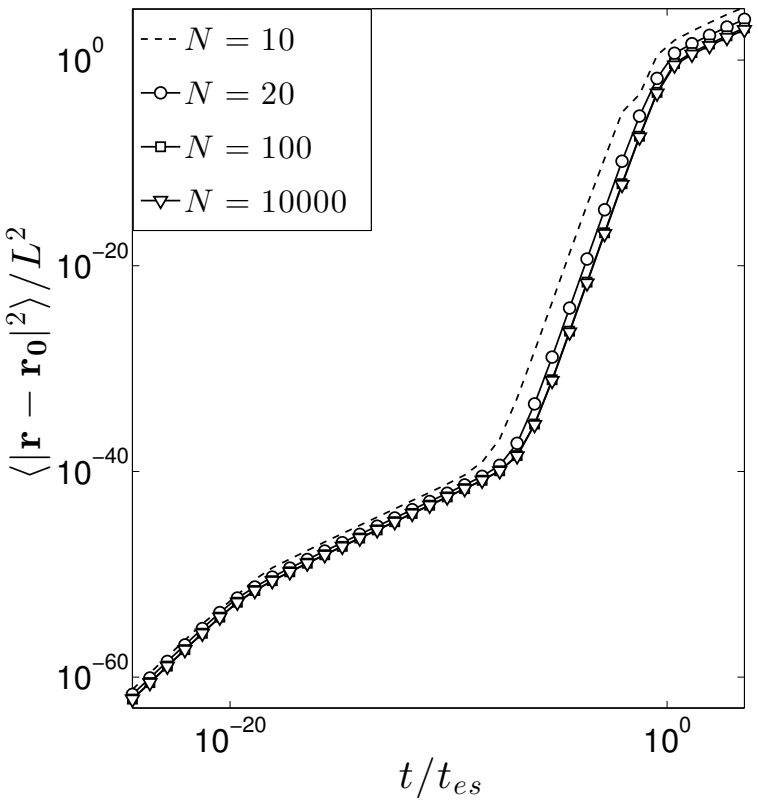

Figure A.2: Monte Carlo results for $\langle|\mathbf{r}(t) - \mathbf{r}_0|^2\rangle$ in the KS diffusion model calculated with $C_\Delta = 1$, $S = 10^4$ samples, varying number of Fourier modes from $N = 10$ to $N = 10^4$.

giving

$$M = \frac{\ln(\frac{10^9}{r_0})}{B} + 1 \tag{A.5}$$

Convergence analysis showed that $B \simeq 9.2 \times 10^{-3}$ is the limiting value leading to a converged simulation for $C_\Delta = 1$ (see Appendix A.2).

A.2 Monte Carlo Time-Step

We tested the dependence of the log-log plots of dispersion on the value of C_Δ. We plot in Fig. A.1 the Monte Carlo results for values of C_Δ ranging from 1 to

10^{-6}. There is no observable change in the behavior.

A.3 Number of Fourier Modes

We also tested the dependence of our dispersion results for the KS diffusion models on the number of Fourier modes N. We show in Fig. A.2 log-log plots of the dispersion curves for different values of N, obtained from Monte Carlo calculations with $C_\Delta = 1$ and $S = 10^4$. The results are nearly indistinguishable for $N \gtrsim 100$. All of our simulations in the text used $N = 500$.

Bibliography

[1] A. W. Baggaley, C. F. Barenghi, A. Shukurov, and K. Subramanian. Reconnecting flux-rope dynamo. *Phys. Rev. E*, 80(5):055301, November 2009.

[2] A. M. Balk. Anomalous behaviour of a passive tracer in wave turbulence. *J. Fluid Mech.*, 467:163–203, September 2002.

[3] G. K. Batchelor. Diffusion in a field of homogeneous turbulence ii. the relative motion of particles. *Proc. Camb. Philos. Soc.*, 48, 1952.

[4] G. K. Batchelor. *Q. J. Royal Met. Soc.*, 76:133–146, 2007.

[5] D. Benveniste and T. D. Drivas. Asymptotic results for backwards two-particle dispersion in a turbulent flow. *Phys. Rev. E*, 89:041003, Apr 2014.

[6] J. Berg, B. Luthi, J. Mann, and S. Ott. *Phys. Rev. E*, 74:016304, 2006.

[7] D. Bernard, K. Gawędzki, and A. Kupiainen. Slow modes in passive advection. *J. Stat. Phys.*, 90:519–569, 1998.

[8] D. Bernard, K. Gawedzki, and A. Kupiainen. *J. Stat. Phys.*, 90:519, 1998.

[9] L. Biferale, G. Boffetta, A. Celani, B. J. Devenish, A. Lanotte, and F. Toschi. Lagrangian statistics of particle pairs in homogeneous isotropic turbulence. *Phys. Fluids*, 17(11):115101, 2005.

[10] R. Bitane, H. Homann, and J. Bec. *Phys. Rev. E*, 86:045302, 2012.

[11] R. Bitane, H. Homann, and J. Bec. Geometry and violent events in turbulent pair dispersion. *ArXiv e-prints*, 2012.

[12] R. Bitane, H. Homann, and J. Bec. Time scales of turbulent relative dispersion. *Phys. Rev. E*, 86(4):045302, 2012.

[13] R. Bitane, H. Homann, and J. Bec. *J. Turb.*, 14:23–45, 2013.

[14] E. Bodenschatz, S. P. Malinowski, R. A. Shaw, , and F. Stratmann. *Science*, 327:970–971, 2010.

[15] Sokolov IM. Boffetta G. Relative dispersion in fully developed turbulence: the richardson?s law and intermittency corrections. *Phys. Rev. Lett.*, 88, 2002.

[16] M. Bourgoin, N. T. Ouellette, H. Xu, J. Berg, and E. Bodenschatz. *Science*, 311:835–838, 2006.

[17] G. E. P. Box and Mervin E. Muller. A note on the generation of random normal deviates. *Ann. Math. Statist.*, 29(2):610–611, 1958.

[18] B.K. Brunk, D.L. Koch, and L.W. Lion. Hydrodynamic pair diffusion in isotropic random velocity fields with application to turbulent coagulation. *Phys. Fluids*, 9:2670–2691, May 1997.

[19] J. Burkhardt, 2012. Florida State University website, `http://people.sc.fsu.edu/~jburkardt/f_src/rkf45`.

[20] A. Celani, M. Cencini, A. Mazzino, and M. Vergassola. *New J. Phys.*, 6, 2004.

[21] S. Chakraborty, M. H. Jensen, and B. S. Madsen. Three-dimensional turbulent relative dispersion by the Gledzer-Ohkitani-Yamada shell model. *Phys. Rev. E*, 81(1):017301, January 2010.

[22] M. Chaves, K. Gawędzki, P. Horvai, A. Kupiainen, and M. Vergassola. Lagrangian dispersion in gaussian self-similar velocity ensembles. *J. Stat. Phys.*, 113:643–692, 2003.

[23] M. Chaves, K. Gawedzki, P. Horvai, A. Kupiainen, and M. Vergassola. *J. Stat. Phys.*, 113:643, 2003.

[24] S. Chen and R. H. Kraichnan. Simulations of a randomly advected passive scalar field. *Physics of Fluids*, 10:2867–2884, November 1998.

[25] A. Chepurnov and A. Lazarian. Extending the Big Power Law in the Sky with Turbulence Spectra from Wisconsin Hα Mapper Data. *The Astrophysical Journal*, 710:853–858, February 2010.

[26] JHU Turbulence Database Cluster. Forced isotropic turbulence dataset. *http://turbulence.pha.jhu.edu*, 2008.

[27] P. Constantin and G. Iyer. *Ann. Appl. Probab.*, 21:1466–1492, 2011.

[28] J. Dávila and J. C. Vassilicos. Richardson's Pair Diffusion and the Stagnation Point Structure of Turbulence. *Phys. Rev. Lett.*, 91(14):144501, October 2003.

[29] B. J. Devenish and D. J. Thomson. Comment on "Fundamentals of pair diffusion in kinematic simulations of turbulence". *Phys. Rev. E*, 80(4):048301, October 2009.

[30] A. Durbin. *J. Fluid Mech.*, 100, 1980.

[31] W. M. Durham, E. Climent, M. Barry, F. De Lillo, G. Boffetta, M. Cencini, and R. Stocker. *Nature Comm.*, 4, 2013.

[32] W. E and E. Vanden Eijnden. *Proc. Natl. Acad. Sci. USA*, 97:8200, 2000.

[33] W. E and E. Vanden Eijnden. *Phys. D (Amsterdam)*, 636:152–153,, 2001.

[34] F. W. Elliott, Jr. and A. J. Majda. Pair dispersion over an inertial range spanning many decades. *Phys. Fluids*, 8:1052–1060, April 1996.

[35] G. Eyink, E. Vishniac, C. Lalescu, H. Aluie, K. Kanov, K. Burger, R. Burns, C. Meneveau, and A. Szalay. *Nature*, 497:466–469, 2013.

[36] G. L. Eyink. Stochastic flux freezing and magnetic dynamo. *Phys. Rev. E*, 83(5):056405, May 2011.

[37] G. L. Eyink and D. Benveniste. Diffusion approximation in turbulent two-particle dispersion. *Phys. Rev. E*, 88:041001, Oct 2013.

[38] G. L. Eyink and D. Benveniste. Suppression of particle dispersion by sweeping effects in synthetic turbulence. *Phys. Rev. E*, 87:023011, Feb 2013.

[39] G. L. Eyink and J. Xin. Self-similar decay in the kraichnan model of a passive scalar. *J. Stat.Phys.*, 100:679–741, 2000.

[40] G.L. Eyink. *Phys. Rev. E*, 83:056405, 2011.

[41] G. Falkovich, K. Gawędzki, and M. Vergassola. Particles and fields in fluid turbulence. *Rev. Mod. Phys.*, 73:913–975, October 2001.

[42] G. Falkovich, K. Gawedzki, and M. Vergassola. *Rev. Mod. Phys.*, 73:913, 2001.

[43] U. Frisch. *Turbulence. The Legacy of A. N. Kolmogorov*. Cambridge University Press, 1995.

[44] U. Frisch, A. Mazzino, A. Noullez, and M. Vergassola. *Phys. Fluids*, 11, 1999.

[45] U. Frisch and A. Wirth. Inertial-diffusive range for a passive scalar advected by a white-in-time velocity field. *EPL (Europhysics Letters)*, 35:683–688, September 1996.

[46] J. C. H. Fung, J. C. R. Hunt, N. A. Malik, and R. J. Perkins. Kinematic simulation of homogeneous turbulence by unsteady random Fourier modes. *J. Fluid Mech.*, 236:281–318, March 1992.

[47] J. C. H. Fung and J. C. Vassilicos. Two-particle dispersion in turbulentlike flows. *Phys. Rev. E*, 57:1677–1690, February 1998.

[48] A. C. Naveira Garabato, K. L. Polzin, B. A. King, K. J. Heywood, and M. Visbeck. *Science*, 303:210–213, 2004.

[49] C. Garrett. *Science*, 301:1858–1859, 2003.

[50] K. Gawedzki and M. Vergassola. *Phys. D (Amsterdam)*, 138:63, 2000.

[51] S. Goto and J. C. Vassilicos. Particle pair diffusion and persistent streamline topology in two-dimensional turbulence. *New Journal of Physics*, 6:65, June 2004.

[52] H. G. E. Hentschel and I. Procaccia. Relative diffusion in turbulent media: The fractal dimension of clouds. *Phys. Rev. A*, 29(3):1461–1471, 1984.

[53] R. M. Humphreys and K. Davidson. *Science*, 223:243–249, 1984.

[54] JHU Turbulence Database Cluster. Forced Isotropic Turbulence Dataset. http://turbulence.pha.jhu.edu, 2008.

[55] Shlesinger M.F. Klafter J., Blumen A. Stochastic pathway to anomalous diffusion. *Phys. Rev. A*, 35, 1987.

[56] AN Kolmogorov. Dissipation of energy in locally isotropic turbulence. *Dokl. Akad. Nauk. SSSR*, 32, 1941.

[57] AN Kolmogorov. The local structure of turbulence in incompressible viscous fluid for very large reynolds number. *Dokl. Akad. Nauk. SSSR*, 30, 1941.

[58] AN Kolmogorov. On degeneration (decay) of isotropic turbulence in an incompressible viscous liquid. *Dokl. Akad. Nauk. SSSR*, 31, 1941.

[59] R. G. Kraichnan. *Phys. Fluids*, 9, 1966.

[60] R. H. Kraichnan. Lagrangian-History Closure Approximation for Turbulence. *Phys. Fluids*, 8:575–598, 1965.

[61] R. H. Kraichnan. Isotropic Turbulence and Inertial Range Structure. *Phys. Fluids*, 9:1728, 1966.

[62] R. H. Kraichnan. Small-scale structure of a scalar field convected by turbulence. *Phys. Fluids*, 11:945–953, 1968.

[63] H. Kunita. *Stochastic Flows and Stochastic Differential Equations*. Cambridge Univ. Press, Cambridge, 1990.

[64] A. Kupiainen. *Ann. Henri Poincare*, 4:S713, 2003.

[65] A. Lazarian, G. Eyink, and E. Vishniac. *Phys. Plasm.*, 19:01210, 2012.

[66] Y. Li, E. Perlman, Y. Yang M.Wan, C. Meneveau, and R. Burns. *J. Turb.*, 9, 2008.

[67] Y. Li, E. Perlman, M.P. Wan, Y. Yang, C. Meneveau, and R. Burns. A public turbulence database cluster and applications to study Lagrangian evolution of velocity increments in turbulence. *J. Turbulence*, 9:31, 2008.

[68] C. C. Lin. On a Theory of Dispersion by Continuous Movements. *Proc. Nat. Acad. Sci. (USA)*, 46:566–570, April 1960.

[69] T. S. Lundgren. Turbulent pair dispersion and scalar diffusion. *J. Fluid Mech.*, 111:27–57, October 1981.

[70] N. A. Malik and J. C. Vassilicos. A lagrangian model for turbulent dispersion with turbulent-like flow structure: Comparison with direct numerical simulation for two-particle statistics. *Phys. Fluids*, 11:1572–1580, June 1999.

[71] M. Matsumoto and T. Nishimura. Mersenne twister: a 623-dimensionally equidistributed uniform pseudo-random number generator. *ACM Trans. Model. Comput. Simul.*, 8(1):3–30, 1998.

[72] P. Tabeling M.C. Jullien, J. Paret. *Phys Rev. Lett.*, 82, 1999.

[73] A. S. Monin and A. M. Yaglom. *Statistical Fluid Mechanics*, volume II. MIT Press, 1975.

[74] Mickael Bourgoin Nicholas T. Ouellette, Haitao Xu and Eberhard Bodenschatz. *New Journal of Physics*, 8(109), 2006.

[75] F. Nicolleau and J. C. Vassilicos. Turbulent Pair Diffusion. *Physical Review Letters*, 90(2):024503, January 2003.

[76] F. Nicolleau and G. Yu. Two-particle diffusion and locality assumption. *Phys. Fluids*, 16:2309–2321, July 2004.

[77] F. C. G. A. Nicolleau, C. Cambon, J. M. Redondo, J.C. Vassilicos, M. Reeks, and A.F. Nowakowski, editors. *New Approaches in Modeling Multiphase Flows and Dispersion in Turbulence, Fractal Methods and Synthetic Turbulence*. Springer, New York, 2011.

[78] F. C. G. A. Nicolleau and A. F. Nowakowski. Presence of a Richardson's regime in kinematic simulations. *Phys. Rev. E*, 83(5):056317, 2011.

[79] A. M. Obukhov. Description of turbulence in terms of Lagrangian variables. In *Advances in Geophysics*, volume 6, pages 113–116, New York, 1959. Academic Press.

[80] A.M. Obukhov. *Izv. Akad. Nauk SSSR, Ser. Geogr. Geofiz.*, 5:453–466, 1941.

[81] D. R. Osborne, J. C. Vassilicos, K. Sung, and J. D. Haigh. Fundamentals of pair diffusion in kinematic simulations of turbulence. *Phys. Rev. E*, 74(3):036309, 2006.

[82] S. Ott and J. Mann. *J. Fluid Mech.*, 422:207, 2000.

[83] L. F. Richardson. *Proc. R. Soc. Lond. Ser. A*, 110, 1926.

[84] M. K. Rivera and R. E. Ecke. Pair Dispersion and Doubling Time Statistics in Two-Dimensional Turbulence. *Physical Review Letters*, 95(19):194503, November 2005.

[85] D. Ryu, H. Kang, J. Cho, and S. Das. *Science*, 320:909–912, 2008.

[86] J. Salazar and L. Collins. *Annu. Rev. Fluid Mech.*, 41, 2009.

[87] B. Sawford. *Annu. Rev. Fluid Mech.*, 33:289, 2001.

[88] B. L. Sawford, P. K. Yeung, and M. S. Borgas. *Phys. Fluids*, 17:095109, 2005.

[89] R. Scatamacchia, L. Biferale, and F. Toschi. Extreme Events in the Dispersions of Two Neighboring Particles Under the Influence of Fluid Turbulence. *Phys. Rev. Lett.*, 109(14):144501, 2012.

[90] L. Shampine, H. Watts, and S. Davenport. Solving non-stiff ordinary differential equations - the state of the art. *SIAM Review*, 18:376–411, 1976.

[91] B. I. Shraiman and E. D. Siggia. *Nature*, 405:639–646, 2000.

[92] G. I. Taylor. *Proceedings of the London Mathematical Society*, 196, 1921.

[93] D. J. Thomson. *Phys. Fluids*, 15, 2003.

[94] D. J. Thomson and B. J. Devenish. Particle pair separation in kinematic simulations. *J. Fluid Mech.*, 526:277–302, March 2005.

[95] A. W. Visser. *Science*, 316:838–839, 2007.

[96] D. Ward-Thompson. *Science*, 295:76–81, 2002.

[97] M. F. Yassin and M. Ohba. *JESEE*, 22:502–515, 2012.

[98] H. Yu, K. Kanov, E. Perlman, J. Graham, E. Frederix, R. Burns, A. Szalay, G. Eyink, and C. Meneveau. *J. Turb.*, 13, 2012.

[99] H. Yu, K. Kanov, E. Perlman, J. Graham, E. Frederix, R. Burns, A. Szalay, G. Eyink, and C. Meneveau. Studying Lagrangian dynamics of turbulence using on-demand fluid particle tracking in a public turbulence database. *J. Turbulence*, 13:12, January 2012.

Vitae

Damien was born is 1981 in Paris, France. In 2004 he received a B.Sc. in Physics and a M.S. in Physics in 2006 from the University Pierre et Marie Curie. He then enrolled in the Physics and Astronomy Ph.D. program at the Johns Hopkins University.

In 2013, he worked as quantitative analyst at Constellation Energy and started to work in 2014 for Transfuse Solutions, Inc. as a data scientist.